

**BOUNDARY LAYER DEVELOPMENT
BEHIND A DOCTOR BLADE RESTING
ON THE SURFACE OF A
CYLINDER ROTATING
IN STILL AIR**

By


WILLIAM GARY DEWAR

**Bachelor of Engineering
University of Glasgow
Glasgow, Scotland
1994**

**Submitted to the Faculty of the
Graduate College of the
Oklahoma State University
in partial fulfillment of
the requirements for
the Degree of
MASTER OF SCIENCE
May, 1996**

**BOUNDARY LAYER DEVELOPMENT
BEHIND A DOCTOR BLADE RESTING
ON THE SURFACE OF A
CYLINDER ROTATING
IN STILL AIR**


Thesis Approved:



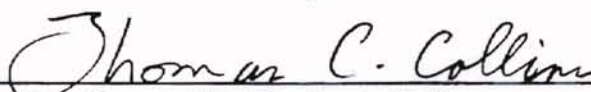
Thesis Advisor



Ronald L. Dougherty



Thomas C. Collins



Dean of the Graduate College

PREFACE

The control of air entrained between a revolving drive roller and moving web can be of great importance in the web handling process, where an excess of air drawn between a web and drive roller can reduce traction and result in a number of handling problems. The insertion of a doctor blade into the flow is a common technique for reducing the boundary layer on the surface of a roller rotating in still air, with the doctor blade rested against the roller surface in order to remove the surface boundary layer prior to contact between roller and web.

The purpose of this project was to investigate the effectiveness of a model doctor blade in reducing the amount of air carried along with a rotating roller and analyze the speed at which the boundary layer flow re-establishes behind the doctor blade. Boundary layer velocity profiles were measured above the surface of a smooth 5.1 cm radius roller rotating in still air (at 2000 rpm) using a hot-wire anemometer. A doctor blade was placed against the surface of the cylinder to remove the boundary layer, and profiles were measured at a number of locations downstream of the blade. These results were compared to a profile for the roller without a blade, with the comparison between these results giving an indication of the speed at which the boundary layer re-develops on the roller surface. It was found that the profile was initially laminar, with transition to a turbulent profile occurring at a Reynolds number (based on distance from blade) of about 80000.

ACKNOWLEDGEMENTS

I wish to express my gratitude to my major advisor, Dr Frank Chambers, for his guidance and input in all aspects of this report. My thanks also to Dr. A. Arena and Dr. R. L. Dougherty, my other committee members, for their assistance and encouragement in my graduate studies.

Thanks must also go to those who helped with the practical aspects of this study: Rod Brackage, James Davis, Satyanarayan Kothari and Wayne Gimlin.

Finally, I would like to express my sincere thanks to the Oklahoma State University Web Handling Center for their support of this work.

TABLE OF CONTENTS

Chapter	Page
I. INTRODUCTION.....	1
II. THEORY.....	7
a: Derivation of δ^* and θ	7
b: Kings' Law and Velocity Equations.....	10
III. EXPERIMENTAL APPARATUS AND PROCEDURE.....	15
IV. RESULTS.....	22
V. DISCUSSION.....	34
VI. CONCLUSIONS AND RECOMMENDATIONS.....	43
REFERENCES.....	46
APPENDICES.....	49
APPENDIX I - GWBASIC COMPUTER PROGRAM FOR DATA ACQUISITION.....	49
APPENDIX II - CALIBRATION DATA.....	58
APPENDIX III - FULLY DEVELOPED BOUNDARY LAYER (I.E. NO DOCTOR BLADE) DATA.....	72
APPENDIX IV - BOUNDARY LAYER DATA BEHIND DOCTOR BLADE.....	76

APPENDIX V -	BOUNDARY LAYER PROFILES OVER	
	WIDTH OF ROLLER.....	96

LIST OF TABLES

Table	Page
3.1. Position of Doctor Blade for Experiments.....	20
4.1. Boundary Layer Characteristics for Experimental Data.....	25
4.2. Mass Flow Rate Behind Doctor Blade.....	33
Appendix II: Calibration Data.	
1. Calibration Data for Experiment without Doctor Blade.....	59
2. Calibration Data for Experiment with Doctor Blade at 17 Degrees.....	61
3. Calibration Data for Experiment with Doctor Blade at 36 Degrees.....	63
4. Calibration Data for Experiment with Doctor Blade at 69 Degrees.....	65
5. Calibration Data for Experiment with Doctor Blade at 93 Degrees.....	67
6. Calibration Data for Experiment with Doctor Blade at 119 Degrees.....	69
7 Kings' Law Calibration Equations for Experiments.....	71
Appendix III: Fully Developed Boundary Layer (i.e. No Doctor Blade) Data.	
1. Data for Fully Developed Boundary Layer.....	73
Appendix IV: Boundary Layer Data Behind Doctor Blade.	
1. Boundary Layer Data 17 Degrees Behind Doctor Blade.....	77
2. Boundary Layer Data 36 Degrees Behind Doctor Blade.....	79
3. Boundary Layer Data 69 Degrees Behind Doctor Blade.....	81

Table	Page
4. Boundary Layer Data 93 Degrees Behind Doctor Blade.....	83
5. Boundary Layer Data 119 Degrees Behind Doctor Blade.....	85
6. Boundary Layer Characteristics for All Experiments.....	94
Appendix V: Boundary Layer Data Over Width of Roller.	
1. Boundary Layer Data for Central Position.....	97
2. Boundary Layer Data for Left Position.....	100
3. Boundary Layer Data for Right Position.....	103

LIST OF FIGURES

Figure	Page
1.1. Positioning of Doctor Blade on Drive Roller.....	5
2.1. Representation of Velocity Profile on Roller Surface.....	8
3.1. Schematic Diagram of Instrumentation.....	16
3.2. Experimental Apparatus for the Boundary Layer Measurements Without Doctor Blade.....	18
3.3. Experimental Apparatus for Doctor Blade Investigation.....	19
3.4. Positioning of Doctor Blade and Hot-Wire Probe.....	20
4.1. Calibration Data for Fully Developed Boundary Layer Measurements.....	22
4.2. Kings' Law Curve Fit to Calibration Data for Fully Developed Boundary Layer Measurements.....	23
4.3. Measured Velocity Profiles For Experiments.....	24
4.4. Boundary Layer Characteristics Behind Doctor Blade.....	27
4.5. Dimensionless Velocity Profiles Behind Doctor Blade.....	28
4.6. Dimensionless Velocity Profiles Behind Doctor Blade for Laminar Results.....	29
4.7. Comparison with Theoretical Estimates of Velocity Profiles.....	30
4.8. Comparison Between Experimental Transition Region and Flat Plate Laminar and Turbulent Velocity Profiles.....	31

Figure	Page
4.9. Comparison Between Fully Developed and Theoretical Turbulent Velocity Profiles.....	31
4.10. Turbulent Intensity Profiles Before, During and After Transition.....	32
Appendix II: Calibration Data.	
1. Kings' Law Curve Fit to Calibration Data Without Doctor Blade.....	60
2. Kings' Law Curve Fit to Calibration Data 17 degs from Doctor Blade.....	62
3. Kings' Law Curve Fit to Calibration Data 36 degrees from Doctor Blade.....	64
4. Kings' Law Curve Fit to Calibration Data 69 degrees from Doctor Blade.....	66
5. Kings' Law Curve Fit to Calibration Data 93 Degrees from Doctor Blade.....	68
6. Kings' Law Curve Fit to Calibration Data 119 Degrees from Doctor Blade....	70
Appendix III: Fully Developed Boundary Layer (i.e. No Doctor Blade) Data.	
1. Velocity Profiles for Fully Developed Flow.....	75
Appendix IV: Boundary Layer Data Behind Doctor Blade.	
1. Velocity Profiles 17 Degrees from Doctor Blade.....	78
2. Velocity Profiles 36 Degrees from Doctor Blade.....	80
3. Velocity Profiles 69 Degrees from Doctor Blade.....	82
4. Velocity Profiles 93 Degrees from Doctor Blade.....	84
5. Velocity Profiles 119 Degrees from Doctor Blade.....	86
6. Velocity Profiles for All Experiments.....	87
7. Dimensionless Velocity Profiles Behind Doctor Blade.....	88
8. Dimensionless Velocity Profiles for Laminar Region.....	89

9. Comparison with Theoretical Estimations of Velocity Profiles in Laminar Region.....	90
10. Comparison Between Experimental Transition Region and Flat Plate Laminar and Turbulent Velocity Profiles.....	91
11. Comparison Between Fully Developed Experimental and 1/7 Power Law Turbulent Profiles.....	92
12. Turbulent Intensity Profiles Before, During and After Transition.....	93
13. Boundary Layer Characteristics Behind Doctor Blade.....	95
Appendix V: Boundary Layer Data Over Width of Roller.	
1. Velocity Profiles for Central Position.....	99
2. Velocity Profiles for Left Position.....	102
3. Velocity Profiles for Right Position.....	105
4. Velocity Profiles over Width of Roller.....	106

NOMENCLATURE

A, B	-	constants
E	-	mean voltage from hot-wire anemometer (volts)
E_{rms}	-	r.m.s. voltage from hot-wire anemometer (volts)
f	-	function.
g	-	gravitational acceleration (m/s^2)
h	-	manometer reading height (m)
h_0	-	air film thickness (m)
H	-	Shape Factor , height (m)
Q	-	flow rate (m^2/s)
r, R	-	radius of roller (m)
RPM	-	roller revolutions per second
Re_x	-	Reynolds number scaled with x-distance
Turb. Int	-	turbulent intensity (U_{rms}/U_{bar})
T	-	Web Tension (N/m)
u	-	local velocity (m/s)
U	-	velocity of air at exit of calibration jet (m/s)
U, U_{bar}	-	mean velocity (m/s)

U_{rms}	-	r.m.s. velocity (m/s)
U_{roller}	-	roller surface velocity (m/s)
U_w	-	velocity of roller surface (m/s)
U_{web}	-	web velocity (m/s)
x	-	surface distance from doctor blade (m)
Y	-	height above roller surface (m)
β	-	angle from doctor blade to measurement point (degrees)
δ	-	boundary layer thickness (m)
δ^*	-	boundary layer displacement thickness (m)
ϕ	-	angle between doctor blade and roller (degrees)
η	-	dimensionless similarity variable
μ	-	kinematic viscosity (kg/ms)
ν	-	dynamic viscosity (m ² /s)
θ	-	boundary layer momentum thickness (m)
ρ_{air}	-	air density (kg/m ³)
ρ_{H2O}	-	water density (kg/m ³)
ψ	-	Stream function

CHAPTER I: INTRODUCTION

The flow over the surface of a rotating cylinder can be of great interest in a number of engineering applications. Circulatory flow about a cylinder in a uniform inviscid stream is one of the basic tools for describing the lifting process in an inviscid fluid, and in a viscous fluid the resultant flow on a rotating cylinder is important to the windage drag on a shaft.

The properties of the flow above the surface of a cylinder rotating in still air are also of major importance in the web handling process, where revolving rollers are used in the handling of rapidly moving paper and plastic webs. The development of the boundary layers on these rotating rollers can result in an excess of air being drawn between the roller and a moving web passing over this roller, which could in turn result in a loss of traction between web and roller, reducing the ability of the roller to drive and steer the web. Problems can also occur in a winding roll, where a sufficiently large volume of air trapped in the wound roll can result in a number of mechanical defects in the web and also cause problems with the unwinding and further processing of the material.

However, despite the practical importance and seemingly elementary nature of this flow surprisingly little research has been documented on the properties of the boundary layer on the surface of a cylinder or roller rotating in still air. Much of the work carried out in the field of circulating flows has concentrated on the flow around both cones, discs and spheres rotating in still air. Nigam¹ carried out a study into the behavior of the flow around a rotating sphere using the Von Karman-Momentum Integral Method

in power series form. It was shown for this problem that the boundary layers originate at the poles of the sphere, before developing towards the equator and impinging on each other. However, these equations were insufficient for modeling the flow near the equator, where the boundary layers impinge on each other and disturb the flow.

Koosinlin, Launder and Sharma² carried out predictions for the momentum, heat transfer and mass transfer properties of the flow above cones and discs, as well as for axisymmetric flow along a spinning cylinder. This work was carried out using finite-difference methods with a version of the mixing-length hypothesis. The predictions gave good agreement with the experimental data for the heat transfer properties, but the rates of mass transfer at high swirl rates were underpredicted for the disc and cone analyses.

The flow between concentric rotating cylinders, which lends itself well to mathematical analysis, has also been extensively investigated. Taylor^{3,4,5} carried out a number of experiments on the properties of the fluid layer between two concentric cylinders, with both the inner and outer cylinder being rotated. This work has shown that a large portion of the flow is irrotational when the inner of the two cylinders is rotated. Mathematical predictions of this problem are also well documented. Kinney⁶ proposed a universal velocity similarity hypothesis in fully turbulent rotating flows by extending Von Karman's similarity hypothesis to a cylindrical geometry, with the use of a characteristic mixing length proportional to the radial coordinate. The work concluded that the equilibrium velocity profile which exists in a fully turbulent rotating flow is that which corresponds to a constant mean vorticity, with this result holding for both laminar and

turbulent flows. The results also verified the vorticity transport theory predicted by Taylor³ in his rotating cylinder investigations.

This investigation will however concentrate on the boundary layer velocity profile on the surface of a smooth isothermal cylinder rotating in still air. Theodorsen and Regier⁷ carried out a number of experiments on the skin friction and drag properties of a rotating cylinder, with the experimental results comparing favorably with the theoretical predictions of Prandtl and Von Karman. The experiments were carried out on revolving discs, cylinders and streamline rods up to high Mach numbers and Reynolds numbers. The results from these experiments were then compared to formulas based on the Von Karman-Prandtl logarithmic resistance law for skin friction. The results gave good agreement with the theoretical predictions and also determined the effect of surface roughness on the boundary layer, with the effects of surface roughness dependent upon the particle size and particle unit density. The work, which has become a standard reference on the skin friction coefficients, also concluded that the flow over the surface of a rotating cylinder is essentially turbulent down to the smallest values of Reynolds number (based on angular velocity and diameter of the cylinder).

The majority of the research into this problem has in the past concentrated mainly on the convection heat transfer and mass transport to a rotating cylinder. Anderson and Saunders⁸ carried out experiments to measure the convection heat transfer from an isolated heated cylinder rotating about its axis, with Kappesser, Cornet and Greif⁹ carrying out comparable mass transfer experiments for both smooth and rough rotating cylinders over a wide range of Reynolds numbers. Smith and Greif¹⁰ solved the

conservation equations with a modified mixing length to model this flow. This model gave good agreement with the experimental results, but the results were limited to high Prandtl or Schmidt numbers, and it was recommended that further work should be carried out to extend the theory to lower Prandtl or Schmidt numbers, and to the viscous sublayer within the flow.

The only available velocity profile information coming from the work of Chambers & Gadapa¹¹. Their investigation gave a number of insights into the properties of the boundary layer, with the work showing considerable differences between the velocity profiles on the surface of a rotating cylinder and a comparable flow over a planar wall. The experimental results were also compared to the predicted profiles using Kinney's⁶ similarity hypothesis. It was shown that Kinney's predictions only gave good agreement to the experimental data over a limited range near the wall, with a rapid divergence between experimental and predicted results further out. It was concluded from this that the rotating flow similarity hypothesis may resemble the application of the Von Karman similarity hypothesis to the planar boundary layer, where it is applicable only in the fully turbulent segment of the near wall region.

Thus, as the mathematical models for the rotating flow problem are inaccurate, it was deemed appropriate for this investigation to use versions of the planar wall models to help in the analysis of the experimental results.

The purpose of this research was to investigate the development of the boundary layer velocity profile on the surface of a cylinder rotating in still air behind a 'doctor blade' inserted into the flow. The use of a doctor blade is common in industry for

reducing the volume of air carried along with the rotating roller, with the doctor blade removing the boundary layer air flow prior to the surface coming into contact with a web.

The placement of the doctor blade on the surface of a drive roller can be seen in Figure 1.1.

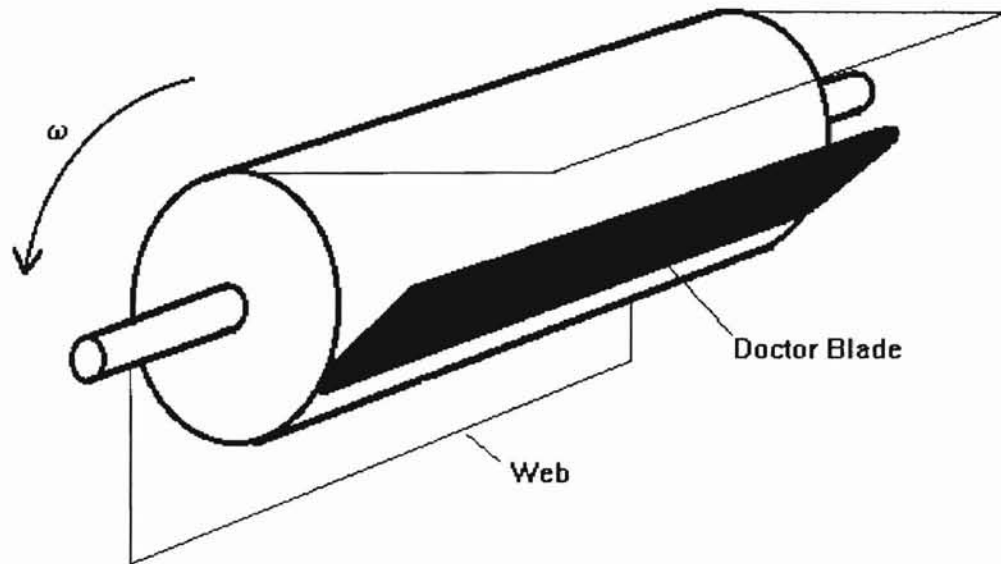


Figure 1.1: Positioning of Doctor Blade on Drive Roller

For the purposes of this experiment the roller was assumed to be smooth, allowing application of foil bearing theory to predict the flow rate between the roller and a stationary web. The effects of surface roughness on the air entrained between a roller and web were investigated by King, Funk and Chambers¹², with the experimental results showing surface roughness to have a large effect on the air film thickness. It was shown that the results for roughened cylinders differ to that of foil bearing theory, especially at high web speeds and low web tensions, with the roughened cylinders reducing the air film thickness from that found for a smooth cylinder.

The doctor blade can be thought of as a simple scraper rested on the surface of a roller with a light load, thus removing the boundary layer air flow as the roller passes under the surface of the doctor blade. The doctor blade also has the effect of removing any dust or loose impediments from the surface of the roller, which reduces the chance of the roller surface damaging the passing web. This does however mean that the doctor blade must be placed at a reasonably shallow angle to the oncoming roller to allow the debris to be lifted away from the roller surface.

Measurements were carried out using a hot-wire anemometer system, allowing readings of the mean velocity and turbulent fluctuations above the surface of a rotating aluminum cylinder. A doctor blade was placed at a number of locations away from the hot-wire probe with the results giving an indication of the development of the boundary layer velocity profile for a distance behind the blade.

CHAPTER II: THEORY

The work in this section will concentrate on the definitions of the equations necessary for the analysis of the experimental data, including the development of the boundary layer displacement and momentum thickness equations used throughout this study.

a: Derivation of δ^* and θ

Due to the nature of the flow in the boundary layer (with $u=U_w$ at $y=0$, and $u=0$ as $y \rightarrow \infty$), modified versions of the boundary layer displacement thickness and momentum thickness definitions must be derived.

Here, we define δ^* as the distance in the 'y' direction such that the product $U_w \delta^*$ is equal to the volumetric flow rate per unit width carried by the entire velocity profile, for any position $x=x_1$. Note, the volumetric flow rate at any position is found from:

$$Q = \int_0^{\infty} u(y) dy \quad (1)$$

An example of the resulting velocity profile above the surface of the roller at any point $x = x_1$ is shown in Figure 2.1:

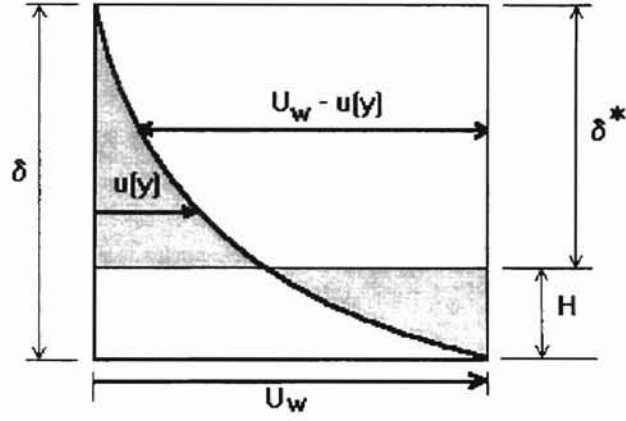


Figure 2.1: Representation of Velocity Profile on Roller Surface

For a regular boundary layer, the displacement thickness can be thought of as the distance which the wall would have to be moved up from the surface to produce a uniform flow with equivalent flow rate to the actual flow profile. This results in an amount of uniform flow, $U_w \delta^*$, being lost due to the non-uniform boundary layer velocity profile.

By using the same arguments for the flow in this investigation, i.e., a moving wall flow with $U = 0$ where $y = \delta$, the displacement thickness can be defined as the distance the moving wall could be displaced outward to produce an equivalent uniform flow, giving:

$$U_w \delta^* = \int_0^{\infty} u(y) dy \quad (2)$$

Thus:

$$\delta^* = \int_0^{\infty} \frac{u(y)}{U_w} dy \quad (3)$$

or:

$$\delta^* = \int_0^{\infty} 1 - \frac{(U_w - u(y))}{U_w} dy \quad (4)$$

Note: δ , the boundary layer thickness, is represented by the value where:

$$\frac{(U_w - u(y))}{U_w} = 0.99 \quad (5)$$

Now, it can be found that using the same arguments for the momentum displacement equation for this flow, the following equation can be obtained:

$$\theta = \int_0^{\infty} \frac{(U_w - u(y))}{U_w} \left[1 - \frac{(U_w - u(y))}{U_w} \right] dy \quad (6)$$

i.e.

$$\theta = \int_0^{\infty} \frac{u(y)}{U_w} \left(\frac{U_w - u(y)}{U_w} \right) dy \quad (7)$$

Note:

$$\text{Shape Factor, } H = \frac{\delta^*}{\theta} \quad (8)$$

For the actual calculations of δ^* and θ , the following numerical approximations to the above integrals were used, with the measured values extrapolated to $u=U_w$ at $y=0$:

$$\delta^* = \sum_{n=0}^{\delta} (y_n - y_{n-1}) 0.5 \left(\frac{u_n}{U_w} + \frac{u_{n-1}}{U_w} \right) \quad (9)$$

$$\theta = \sum_{n=0}^{\delta} (y_n - y_{n-1}) \frac{1}{2} \left[\frac{u_n}{U_w} \left(\frac{U_w - u_n}{U_w} \right) + \frac{u_{n-1}}{U_w} \left(\frac{U_w - u_{n-1}}{U_w} \right) \right] \quad (10)$$

b: Kings' Law and Velocity Equations

For the calibration of the hot-wire anemometer using the compressed air calibration jet, the following equations were used. For the velocity of the air at the exit of the calibration jet:

$$U = \sqrt{\left(\frac{2\rho_{H_2O} g \Delta h}{\rho_{air}} \right)} \quad (11)$$

The hot-wire probe was placed at the exit nozzle of the jet to measure this velocity. The anemometer kept the temperature of the hot-wire constant, with the current

needed to keep the hot-wire at constant temperature related to the velocity seen by the probe. These velocities were then used in conjunction with the output voltage from the hot-wire anemometer to produce a linear relationship between output voltage and velocity, derived from the modified Kings' Law:

$$\bar{E}^2 = A + B \times \bar{U}^{0.45} \quad (12)$$

Where A & B are constants dependant on the calibration curve fit.

Values for the r.m.s. velocities and the turbulent intensities were also found, with the following equations used in the calculations. It was assumed that the velocity fluctuations were small, so that the mean and rms voltages were found first and then converted into mean and rms velocities with the equations shown here (from Hinze¹³):

$$U_{rms} = E_{rms} (dU/dE) \quad (13)$$

$$\text{Turbulent Intensity} = U_{rms}/U_{bar} \quad (14)$$

The Reynolds number used in the results were calculated from the equation:

$$Re_x = \frac{U_w x}{\nu} \quad (15)$$

Where U_w was taken to be the velocity of the surface of the roller.

The experimental boundary layer velocity profiles found in this investigation could then be compared to empirical estimates from the literature. An approximate formula for a turbulent boundary layer was derived by Prandtl, see White,¹⁴ with the empirical velocity distribution for a turbulent boundary layer in a zero pressure gradient flow given by a simple one-seventh power-law profile:

$$\frac{U_{bar}}{U_{\infty}} = \left(\frac{y}{\delta} \right)^{1/7} \quad (16)$$

Now, re-arranging this equation to fit the boundary conditions for this flow gives:

$$\left(\frac{U_w - u}{U_w} \right) = \left(\frac{y}{\delta} \right)^{1/7} \quad (17)$$

or:

$$\frac{u}{U_w} = 1 - \left(\frac{y}{\delta} \right)^{1/7} \quad (18)$$

Re-arranging this equation in terms of y/δ^* (as an accurate estimation of δ is difficult to find from the experimental data), the equation becomes:

$$\frac{y}{\delta^*} = 6 \left(1 - \frac{u}{U_w} \right)^7 \quad (19)$$

where an estimation for the edge of the boundary layer at $y/\delta^*=6$ was assumed from the experimental results. This value was found by curve fitting the theoretical predictions to the experimental profiles and taking the best match as an estimation of the edge of the boundary layer.

Now, a theoretical estimation of the corresponding laminar profile can be found using the Blasius solution for flat-plate flow, derived in Keuthe and Chow,¹⁵ where:

$$\eta = y \sqrt{\left(\frac{U_w}{2\nu x} \right)} \quad (20)$$

with an appropriate dimensionless similarity variable, η .

With the stream function, ψ , of the flow:

$$\psi = \sqrt{2\nu U_w x} f(\eta) \quad (21)$$

The boundary layer velocity profile for a flat-plate flow thus becomes

$$f' = \frac{u}{U_w} \quad (22)$$

This result can be re-arranged to give an estimated laminar equation for the flow with a moving wall in still air

$$f' = 1 - \frac{u}{U_w} \quad (23)$$

Calculations can also be made to determine the flow rate per unit width travelling between a drive roller and web. The thickness of the central region, i.e. the minimum distance between web and roller, can be estimated from the following foil bearing theory equation for a smooth cylinder (see King et al¹²):

$$h_0 = 0.643R \left(\frac{6\mu(U_{web} + U_{roller})}{T} \right)^{\frac{2}{3}} \quad (24)$$

If it is assumed that the web is stationary (i.e. $U_{web}=0$), then the flow within this region can be compared to a Couette flow. Thus the flow rate per unit width between the roller and web can be calculated from the equation:

$$Q = \frac{h_0 U_w}{2} \quad (25)$$

CHAPTER III: EXPERIMENTAL APPARATUS AND PROCEDURE

The experiments were carried out on a 5.08 cm radius, 35.56 cm width aluminum roller which was driven by a variable speed D.C motor, attached to the roller by a belt and pulley system. The radial speed of the roller was adjusted by varying the output of the motor, with the resulting speed being sensed by a photo-diode facing the end of the roller and sending a signal to the computer for analysis, with the computer converting the signal from the photo-diode into a roller speed in rpm and a roller surface velocity in m/s. For these experiments the roller was driven at a speed of about 2000 rpm, which was the roller speed used for previous testing in this research area.

Measurements of the properties of the boundary layer above the surface of the roller were obtained using a hot-wire anemometer system. This apparatus consisted of a hot-wire probe connected to a constant temperature anemometer which was in turn connected to a 286 personal computer for analysis of results. The output voltage from the constant temperature anemometer was digitized by a high speed 12 bit Metrabyte DAS-16F Data Acquisition Board before being processed through a GWBASIC computer program controlling the data acquisition board through the use of Labtech Notebook software. A schematic of the experimental instrumentation can be seen in Figure 3.1. The system works by passing a current through the hot-wire probe to keep the wire at a constant temperature. When air is passed over the wire surface, it has the effect of cooling the wire. Therefore a larger current is needed to maintain the constant temperature, with a faster air velocity requiring a still higher current. Thus, once the hot-wire anemometer has

been calibrated and an equation relating voltage to velocity has been found, unknown velocities can be calculated from the output voltage of the hot-wire anemometer system.

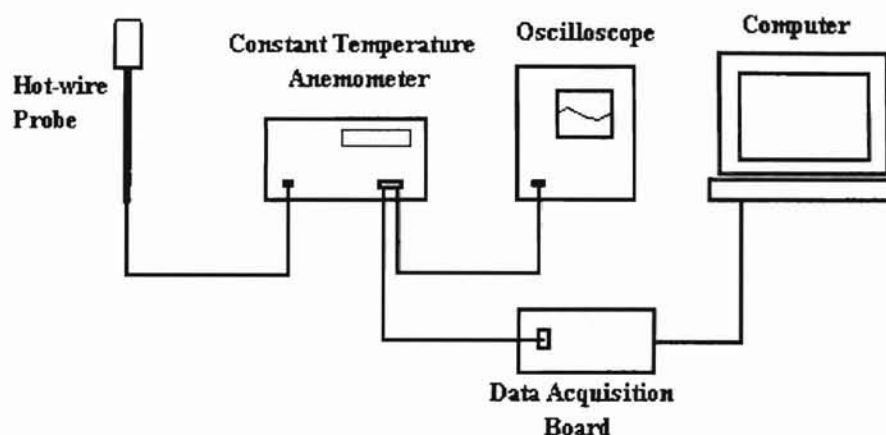


Figure 3.1: Schematic Diagram of Instrumentation.

The calibration of the hot-wire anemometer system, carried out prior to each set of readings, was obtained with the use of a compressed air calibration jet. An inclined manometer was attached to the calibration jet to measure the plenum pressure, with the resulting jet output velocity being calculated from the equation given in the previous chapter. The hot-wire probe was placed at the center of the jet outlet and readings were then taken over a range of plenum pressures with the results being fitted to the modified Kings' Law calibration curve. The calibration range for experiments were from a plenum pressure of 0.0254 to 0.635 cm H₂O, giving a velocity calibration range of about 2 to 10 m/s. The Kings' Law calibration curve was then extrapolated over the full range of results for the experimental data, as velocities far lower than those available from the calibration jet were measured in the experiments.

This calibration equation was then used by the computer in the actual experiments to convert the hot-wire anemometer output voltage into mean and rms voltages, and then into the mean and rms velocities using equations 12,13 and 14 given in Chapter 2b (Note: a full listing of the GWBASIC computer program used in the calibration and experimental data gathering and analysis is shown in Appendix I). The resulting values for the mean and rms velocities therefore give an indication of the average value for the velocity at a certain point, as well as the average fluctuation from this value.

For the experiments themselves, the hot-wire probe was suspended vertically above the surface of the roller with readings being taken over a range from 0 to 3.6 cm above the surface, with the zero height taken to be the closest position of the hot-wire to the roller surface without any contact - this height being estimated by sight. These heights were obtained from a dial indicator attached to the support stand for the hot-wire probe.

The measurements were carried out by first resting the hot-wire probe on the surface of the stationary roller, and then moving the probe up slightly so it is no longer touching the surface. The roller was then driven at the required speed (2000 rpm), with the probe being moved up a set distance for each consecutive reading.

A set of readings were first taken without the doctor blade in order to obtain a profile for the fully developed boundary layer, the set-up for this experiment being shown in figure 3.2, with the results taken up to 3.56 cm above the roller surface.

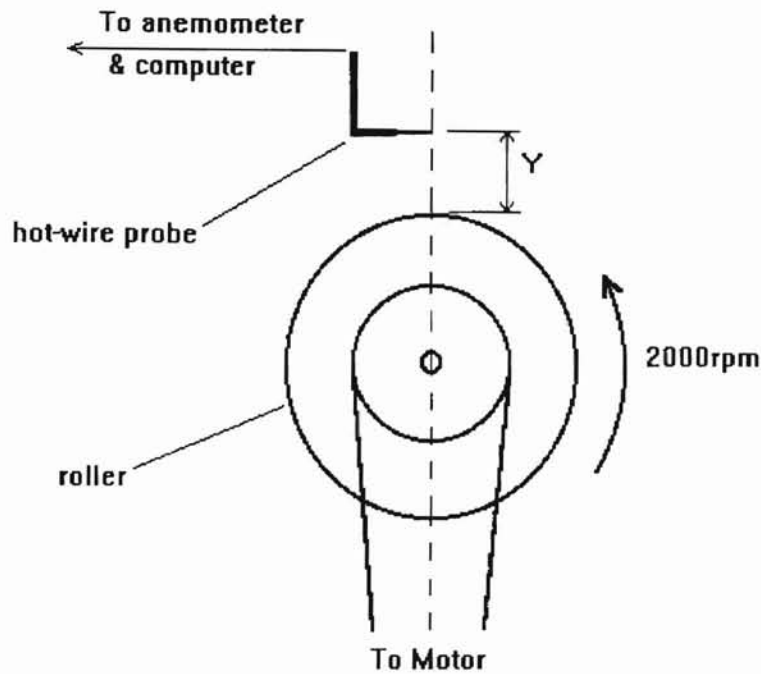


Figure 3.2: Experimental Apparatus for the Boundary Layer Measurements
Without Doctor Blade.

These readings, as with the results obtained with the insertion of a doctor blade into the flow, were taken at the center of the roller width, i.e. 17.8 cm from each end. Within this region the flow is assumed essentially two-dimensional, with no flow across the width of the roller surface. This assumption could be made from previous measurements proving the two-dimensional nature of the flow in the central portion of the roller (see Appendix V).

For the investigation into the effect of a doctor blade on the boundary layer velocities, the experimental set-up shown in Figure 3.3 was used:

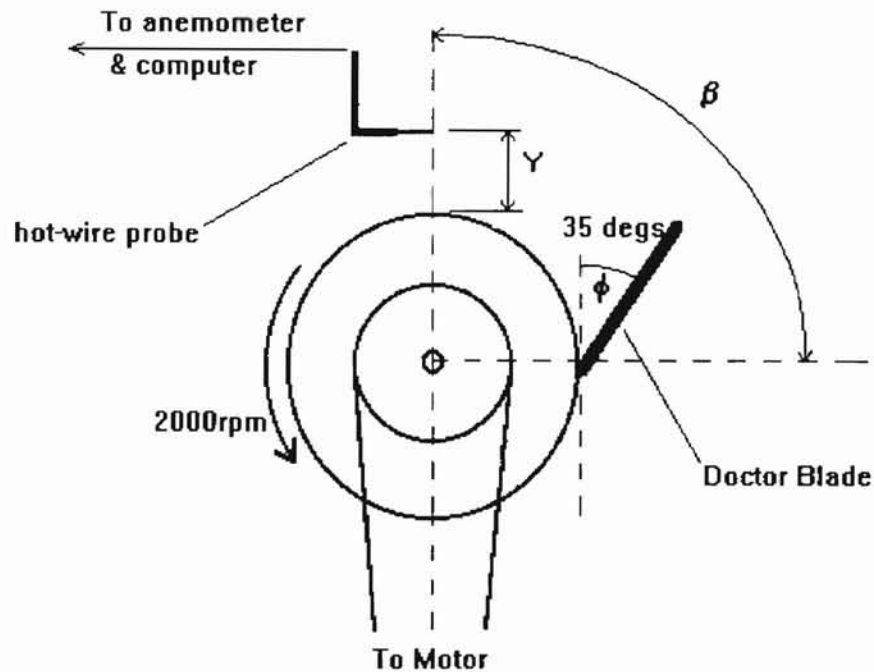


Figure 3.3: Experimental Apparatus for Doctor Blade Investigation.

Here, a plastic doctor blade was rested on the surface of the aluminum roller with a light load, at an angle, ϕ , of 35 degrees to the surface tangent. The doctor blade was held in place by four moveable aluminum rods and could be rested on the roller surface at a number of locations upstream of the hot-wire, up to an angle, β , of 120 degrees from the position of the hot-wire probe (again vertically above the roller surface). The positioning of the hot-wire probe, dial indicator and doctor blade can be seen in Figure 3.4.

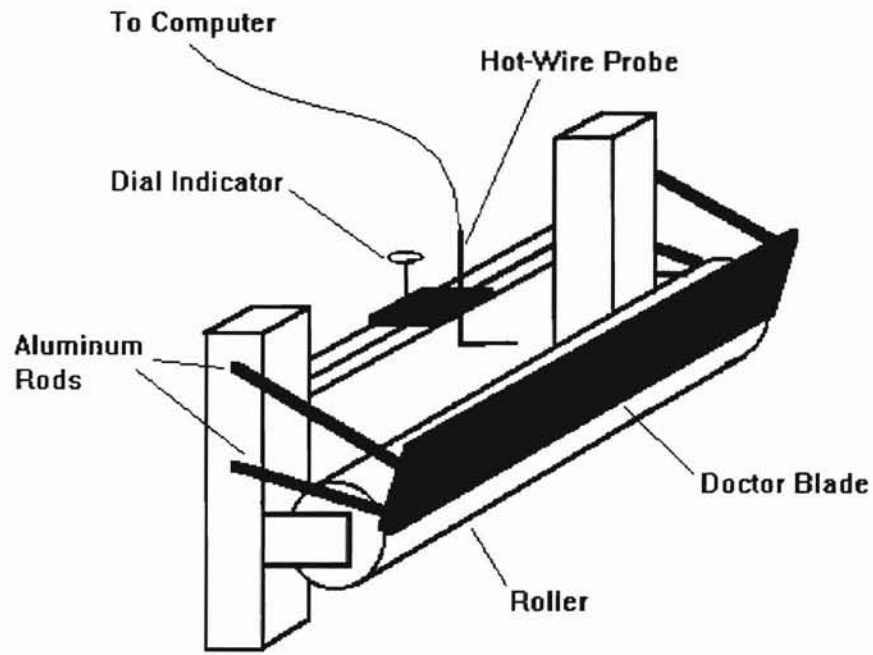


Figure 3.4: Positioning of Doctor Blade and Hot-Wire Probe

For the purposes of these experiments, five doctor blade locations were chosen, these being:

Position Number N	β (degrees)	x (m) (Surface distance from doctor blade to measurement position)
1	17	0.015
2	36	0.032
3	69	0.061
4	93	0.082
5	119	0.105

Table 3.1: Position of Doctor Blade for Experiments.

Measurements were taken up to a height of 2.54 cm above the surface of the roller in these cases to make sure that the full boundary layer was measured.

CHAPTER IV: RESULTS

A number of results can be produced from the measurements made in these experiments. Full tables and plots of these results can be seen in the Appendix section of this report as follows:

Appendix II: Calibration Data.

Appendix III: Fully Developed Boundary Layer Characteristics

Appendix IV: Boundary Layer Characteristics behind Doctor Blade

The main results from this investigation are summarized below. An example of the calibration data (in this case for the fully developed boundary layer) and the relevant Kings' Law curve fit are shown in Figures 4.1 and 4.2:

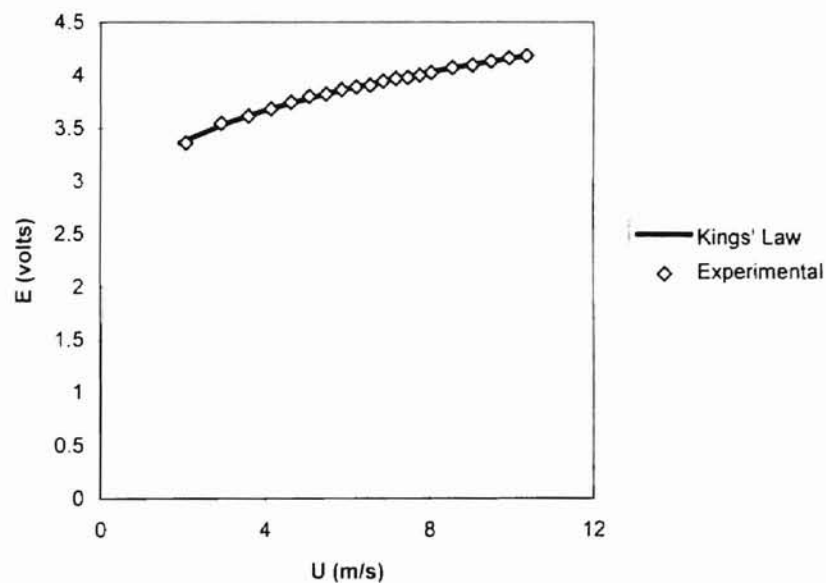


Figure 4.1: Calibration Data for Fully Developed Boundary Layer Measurements.

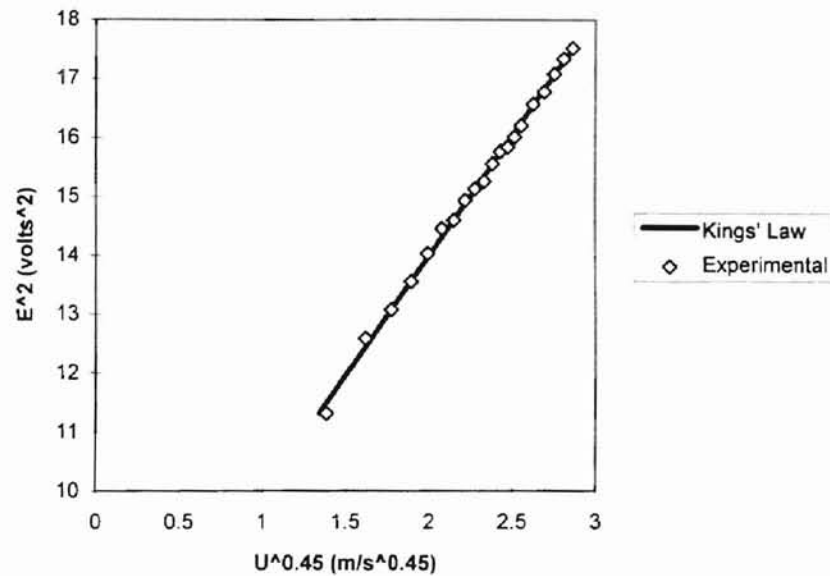


Figure 4.2: Kings' Law Curve Fit to Calibration Data for Fully Developed Boundary Layer Measurements.

The resulting error between the calibration data and the Kings' Law curve fit can be calculated for all the experiments. It was found that for all the calibrations the maximum percentage error between measured and Kings' Law data never exceeded 3%.

The boundary layer thickness behind the doctor blade were then calculated from equations 5, 8, 9 and 10 derived in Chapter 2. These results are given in Table 4.1 below. It should be noted that it was impossible to calculate the boundary layer thickness for the fully developed boundary layer, as the edge of the boundary layer could not be reached with the traverse used in these experiments. However, estimates of the boundary layer displacement and momentum thickness could be found, as the outer edge of the boundary layer has little effect on these values.

Figure 4.3 shows the distribution of the mean velocity (scaled with roller surface velocity) for both the doctor blade and fully developed profiles. Note that the results for the fully developed boundary layer without the doctor blade were taken up to a height of about 3.6 cm above the roller surface, with little decrease in the velocity above the 1 cm position. However, these results have been truncated for Figure 4.3 to allow comparison with the doctor blade results. The full profile for the fully developed flow can be seen in Appendix III.

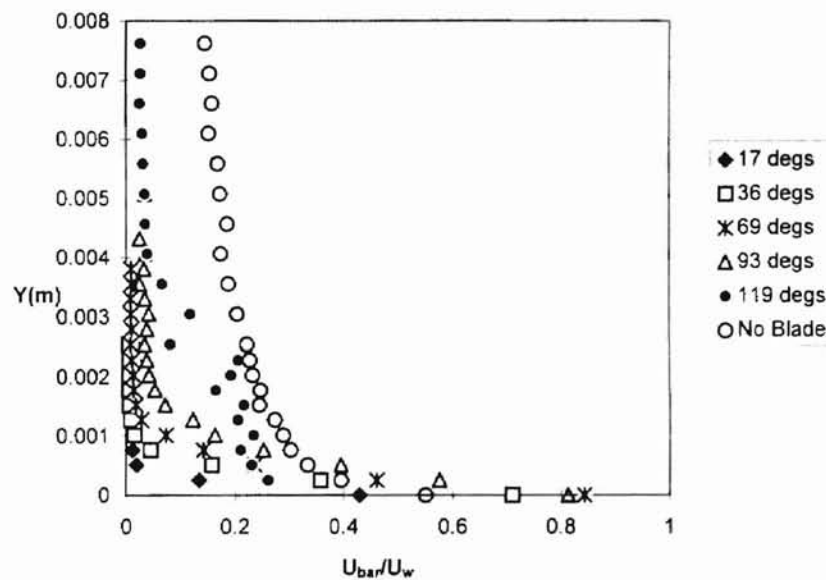


Figure 4.3: Measured Velocity Profiles For Experiments.

N	β (degrees)	x (m)	Re_x	$\delta(\text{est})$ (m)	δ^* (m)	θ (m)	H
1	17	0.015	11163	0.00076	98.1×10^{-6}	76.3×10^{-6}	1.40
2	36	0.032	24433	0.00127	242×10^{-6}	137×10^{-6}	1.77
3	69	0.061	47165	0.00178	359×10^{-6}	196×10^{-6}	1.83
4	93	0.082	60595	0.00254	562×10^{-6}	312×10^{-6}	1.80
5	119	0.105	80069	0.00457	784×10^{-6}	564×10^{-6}	1.39
No Blade	-	-	-	-	4.52×10^{-3}	3.83×10^{-3}	1.18

Table 4.1: Boundary Layer Characteristics for Experimental Data.

It can be seen that the shape factor for positions 2, 3 and 4 are about 1.8, with a shape factor for the fully developed boundary layer without the doctor blade of about 1.2. The error in the calculated shape factor at the 17 degree position can be explained by the fact that due to the very thin boundary layer at this point, only three measurements were taken within this region, which was not enough to give an accurate representation of the boundary layer profile.

The predicted shape factors from flat plate theory are 2.6 for a Blasius laminar boundary layer and 1.3 for a 1/7 law turbulent profile. As can be seen, these values are higher than the shape factors found for this experiment.

For these results, due to the limitations of the readings near the edge of the boundary layer, it is difficult to carry out an accurate analysis of the experimental errors.

However, a rough estimate of the errors near the edge of the boundary layer can be made by comparing the differences between $\delta_{0.99}$ and $\delta_{0.95}$ for the experimental and Blasius theoretical results. For the Blasius profile, it may be found that $\delta_{0.99} / \delta_{0.95} = 1.5$. The corresponding ratios for the experimental results can be found from Equation 5 (see Chapter II) with the edge of the boundary layer calculated for 0.99 and 0.95. The resulting ratios, $\delta_{0.99} / \delta_{0.95}$, were then calculated for all the experimental positions behind the doctor blade, giving ratios from 1.3 to 1.9. By comparing these experimental ratios to that predicted by Blasius, it can be said that the experimental results give a maximum error of about 25% over the laminar region. It can therefore be said that the estimated boundary layer thickness over the experimental range has an error of about 25%.

The results from Table 4.1 were then graphed in Figure 4.4, with the theoretically predicted boundary layer thickness for a Blasius laminar flat plate flow also shown. The displacement thickness, δ^* , was also used to non-dimensionalize the boundary layer velocity profiles behind the doctor blade, as can be seen in Figure 4.5. The displacement thickness was used for the non-dimensionalization of the velocity profiles as these values were subject to a far smaller error than the boundary layer thickness, δ . This was due to the fact that the edge of the boundary layer (where much of the experimental errors occur) has little effect on the δ^* calculations.

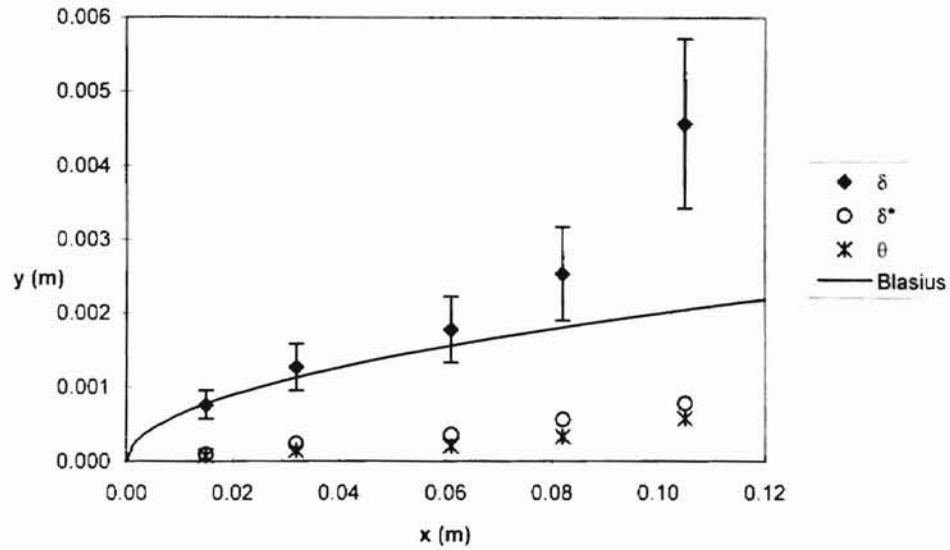


Figure 4.4: Boundary Layer Characteristics Behind Doctor Blade.

It should be noted that the values given for δ were estimated from the experimental results, and due to the limitations of the experimental method near the edge of the boundary layer, these values are subject to significant error.

This error was due to the limitations of the hot-wire at very low velocities, as the hot-wire cannot distinguish between the flow induced by the roller and any air flow from the surrounding atmosphere. This meant that near the edge of the boundary layer the flow from the surrounding atmosphere could be of the same magnitude as the flow from the roller, giving a significant margin for error in the experimental data.

The hot-wire also has the problem of being unable to differentiate between varying flow angles (it measures only the magnitude of the air flow, not the direction). This can also result in significant error in the results near the edge of the boundary layer.

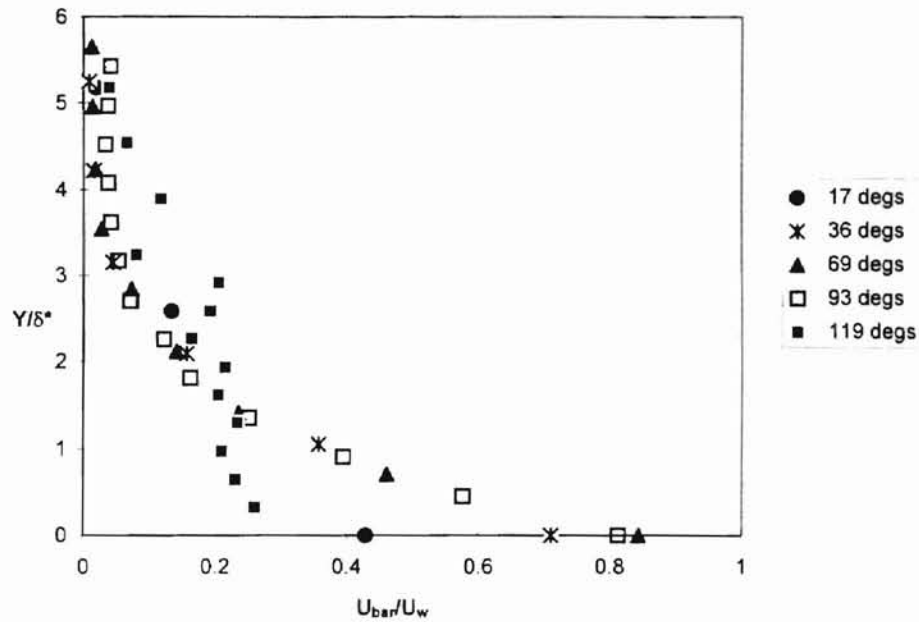


Figure 4.5: Dimensionless Velocity Profiles Behind Doctor Blade.

As the results in this graph appear cluttered, a plot of y/δ^* 'versus' U_{bar}/U_w for only the three central results has been plotted in Figure 4.6, giving a much clearer picture of the boundary layer velocity profile. The reasons for the variations in the results at the higher and lower Reynolds numbers will be discussed later in Chapter V.

The change in the profile shape at the 119 degree position (i.e. $Re_x=80069$), coupled with the rapid increase in boundary layer thickness at this point, leads to the conclusion that the boundary layer is laminar up to $Re_x \approx 80000$, with transition to a turbulent profile occurring at about this point.

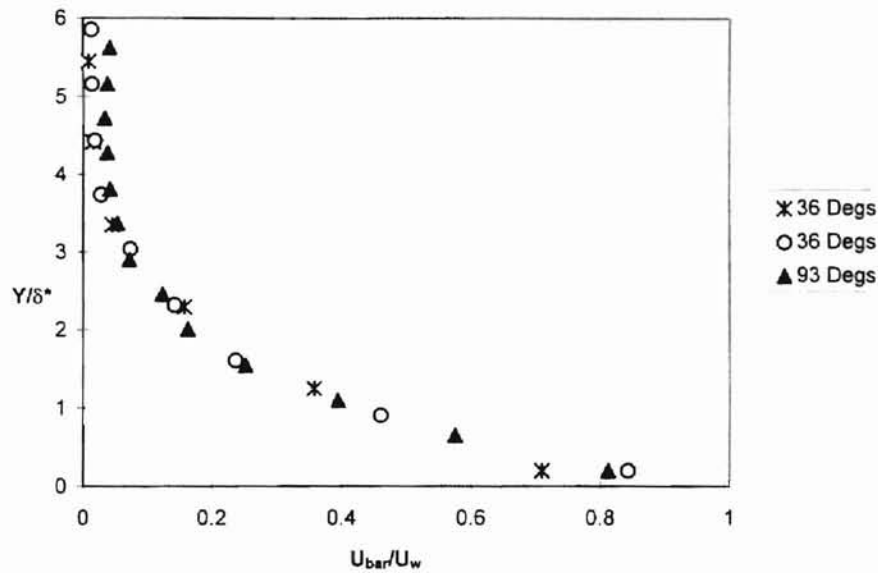


Figure 4.6: Dimensionless Velocity Profiles Behind Doctor Blade for Laminar Results.

These results were also compared to estimated boundary layer velocity profiles for the 1/7 law turbulent profile and Blasius laminar profile as given in Chapter 2, with the comparison being shown in Figure 4.7.

It should be noted that the theoretical profiles given are derived from flat-plate flow - no theoretical estimates of the profiles above the surface of a rotating cylinder were available from the literature. As a result, they can only be used in a limited evaluation of the experimental results. The edge of the boundary layer for these profiles was assumed, from curve fits to the experimental results, to be at $y/\delta^*=6$, with the resulting curve fits shown in Figure 4.7.

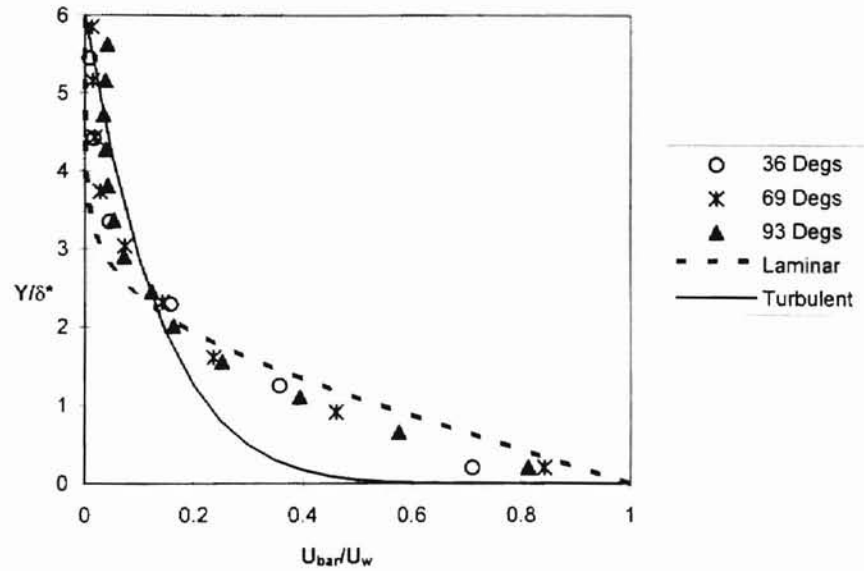


Figure 4.7: Comparison with Theoretical Estimates of Velocity Profiles.

This same comparison can be made for the transition region (i.e. with $Re_x \approx 80000$), with the experimental profile again compared to the dimensionless laminar and turbulent theoretical profiles, as shown in Figure 4.8.

A comparison plot can also be made between the experimental data for the fully developed flow and the $1/7$ power law turbulent profile, as shown in Figure 4.9. Here, the edge of the boundary layer was again assumed at $y/\delta^*=6$ for line “power law, a”, and $y/\delta^*=12$ for line “power law, b”. This allowed an evaluation of the effect of the choice of boundary layer thickness on the relevant curve fit.

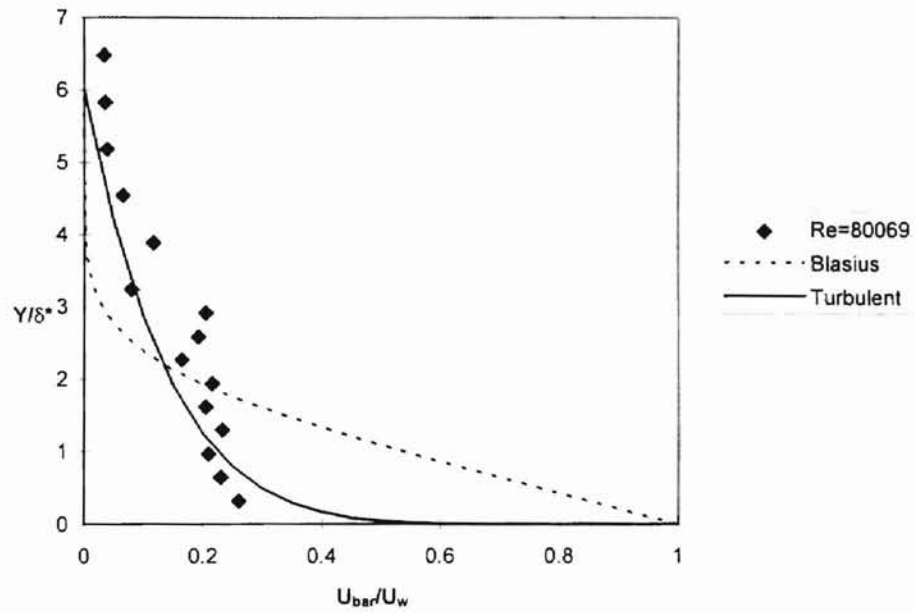


Figure 4.8: Comparison Between Experimental Transition Region and Flat Plate Laminar and Turbulent Velocity Profiles.

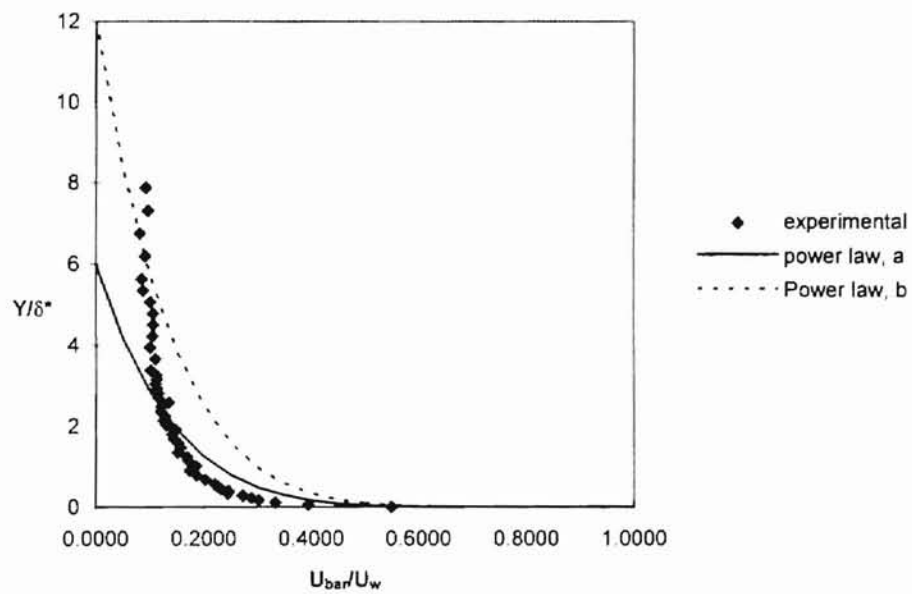


Figure 4.9: Comparison Between Fully Developed and Theoretical Turbulent Velocity Profiles.

Further analysis of the transition region can be carried out by investigating the turbulence intensities within the boundary layer before, during and after transition. The resulting profiles can be seen in Figure 4.10.

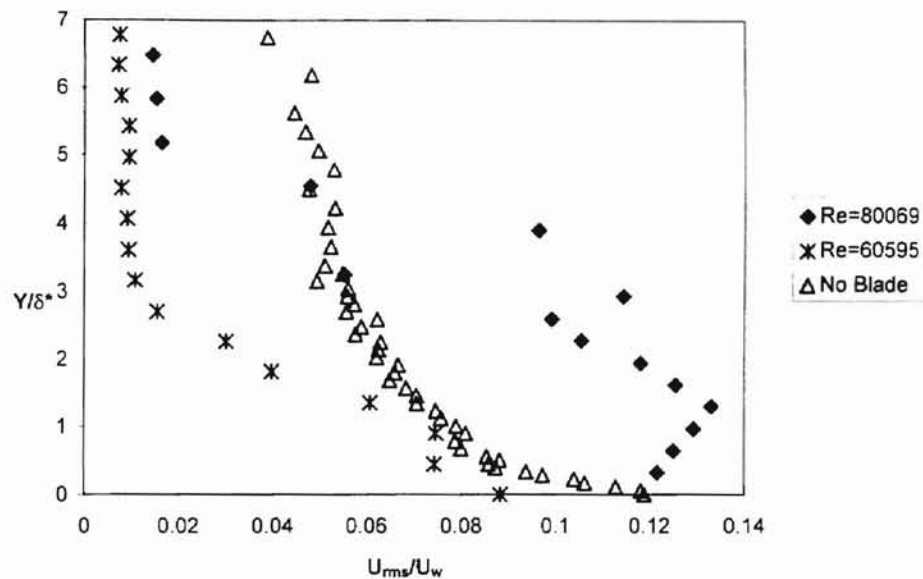


Figure 4.10: Turbulent Intensity Profiles Before, During and After Transition.

It should be noted that the transition area between a laminar and turbulent flow can be estimated from the experimental data to be at about $Re_{x,tr} \approx 80000$. This is far smaller than the transition Reynolds number predicted from flat plate theory (i.e. $Re_{x,tr} \approx 3.5 \times 10^5$ to 10^6), as given in Schlichting.¹⁶

Now, the mass flow rate per unit width between this roller and a stationary web can be found using equations 24 and 25 in Chapter II. These equations give the results:

$$h_0 = 13 \times 10^{-6} m$$

$$Q = 70.8 \times 10^{-6} m^2/s$$

Where h_0 is the predicted minimum thickness for the region between the roller and stationary web, and Q is the calculated flow rate at this point.

This result can then be compared to the flow rates carried along with the roller behind the doctor blade, with these results being calculated from equation 1 in Chapter II.

N	x (m)	Q (m ² /s)
1	0.015	1.24×10^{-3}
2	0.032	2.62×10^{-3}
3	0.061	4.01×10^{-3}
4	0.082	6.29×10^{-3}
5	0.105	9.24×10^{-3}

Table 4.2: Mass Flow Rate Behind Doctor Blade.

As can be seen, the flow rate behind the doctor blade is of the order 10^2 greater than that traveling between the roller and a stationary web.

CHAPTER V: DISCUSSION

Much information can be drawn from the results given in the previous chapter and in the appendices. However, a discussion of the limitations and possible errors in the results must first be made before conclusions can be drawn with regards to the characteristics of the developing boundary layer.

There are a number of limitations in the accuracy of the hot-wire measurements which must be accounted for in the results. First, the calibration technique includes certain possible sources of error. The calibration was carried out over a range of plenum pressures (from 0.01 to 0.25 inches of water), i.e. over a limited velocity range from about 2 to 10 m/s, with the resulting Kings' Law curve fit being extrapolated over the full velocity range for the resulting data gathered in the actual experiments. The minimum velocity obtainable for the calibration was about 2 m/s, but the readings near the edge of the boundary layer were all of a much lower velocity. Thus it can be seen that much of the experimental data comes from an area of the Kings' Law curve which has been extrapolated from the calibration data, which could result in errors for the low velocity readings.

When it is also considered that the curve fit does not fit perfectly the calibration data (with an estimated error of 3% between calibration data and curve fit), it can therefore be seen that the resulting curve fit will have a small but significant error inherent in its form. This is due to the limitations in the calibration jet in producing an

accurate constant output velocity and the limitations in the accuracy of the plenum pressure readings from the attached inclined manometer.

Other sources of error in the use of the hot-wire probe will include the limitations of the hot-wire probe in accurately measuring very low velocities, as is seen near the edge of the boundary layer on the roller surface (see Figure 4.3). This is due to the fact that the hot-wire cannot differentiate between air flow due to the boundary layer and any air currents due to the surrounding atmosphere. Thus, any air flow in the surrounding atmosphere can result in a significant error in the hot-wire readings near the edge of the boundary layer, where the velocity of air currents could be of the same order as the velocity of the boundary layer at this point. There is also a possible source of error due to the hot-wire itself, especially near the surface of the roller. Here the very existence of the hot-wire probe could in fact effect the properties of the flow around the region within which it is measuring, with the heat transfer effects from the hot-wire to cylinder possibly becoming significant.

One final source of error for the results could come from the vertical positioning of the probe above the surface of the roller. It was difficult to accurately position the hot-wire at the surface of the roller with just the human eye as a guide, and as a result it is possible that the heights read from the dial indicator attached to the vertical traverse were slightly in error of the actual distance from roller surface to hot-wire position. The zero height was set by placing the probe in contact with the stationary roller surface, and then moving the the probe upwards slightly to make sure there was no contact between wire

and roller. As a result, the zero reading in the results was estimated, by extending the experimental profiles to $U_{bar}/U_w=1$, to be about 5×10^4 m above the actual roller surface.

However, taking all these possible sources of error into consideration, the results can still give a very good indication of the properties of the flow on the surface of the roller, with significant error only creeping into the results near the outer edge of the boundary layer for each set of experimental data (the simple error analysis in Chapter IV seems to indicate an error of about 25% in the boundary layer thickness calculations). The possibility for error at the edge of the boundary layer can be seen from the still significant turbulent intensity even at and above the estimated edge of the boundary layer (as can be seen from Figure 4.10).

It can be seen from Figure 4.1b that the Kings' Law calibration curve does give a reasonably accurate representation of the relationship between the anemometer voltage output and the air velocity over the calibration range used in these experiments. Thus, although possible errors are expected at the edge of the boundary layer where the velocity is approaching zero, due to the extrapolation of the Kings' Law curve fit for these low velocities and also due to the limitations of the hot-wire method (as described above), it can be said that the results obtained do give an accurate representation of the velocities at each point measured up to the area around the edge of the boundary layer.

It can therefore be seen from Figure 4.2 that the resulting velocity profiles on the surface of the boundary layer follow the shape expected from the theory, with the velocity approaching the roller surface velocity near the wall and then reducing to zero at the edge of the boundary layer with the expected profile. Figure 4.2 also shows a vast difference in

the thickness of the boundary layer for the fully developed profile, i.e. without a doctor blade, and the profiles behind the doctor blade. Using equations 8 and 9 in Chapter 2, values for δ^* and θ were found for the profiles behind the doctor blade as shown in Table 4.1 (an estimated value for the boundary layer thickness, δ , was also calculated although this was subject to far greater error than the other values). As these results show (in Table 4.1 and Figure 4.3), the boundary layer develops very slowly behind the blade with an estimated boundary layer thickness of only about 2.54 millimeters 93 degrees behind the position of the doctor blade (corresponding to a Reynolds number scaled with distance from the doctor blade of $Re_x \approx 60000$). These calculations appear to give a shape factor of roughly 1.7 over the first 90 degrees behind the blade, with the error in the shape factor at the 17 degree point easily attributable to the fact that only 3 readings could be taken within this region (the boundary layer was less than a millimeter thick at that point), which was not enough to give an accurate representation of the flow.

Scaling the height with the displacement thickness δ^* allows direct comparison between the shape of the boundary layer profiles behind the doctor blade, as can be seen in Figures 4.4, 4.5 and 4.6. Figure 4.5 clearly shows that the velocity profiles over the first 90 degrees are of a similar form, with the comparisons between the experimental results and the theoretical laminar and turbulent profiles indicating that the profile behind the doctor blade is initially laminar over the first 90 to 100 degrees.

The profile for the boundary layer at the position 119 degrees behind the blade tends to validate this assumption, as it appears to show transition between a laminar region and the turbulent profile which can be seen for the fully developed flow. This

transition is accompanied by a reduction in the shape factor for the velocity profile, with the calculated shape factor of only 1.39 at the 119 degree position, and also a large increase in the thickness of the boundary layer, as can be seen from Figure 4.4.

It was difficult to estimate results accurately for the fully developed boundary layer with no doctor blade, as the traverse used in the experiments only allowed measurements up to a height of about 3.6 cm above the surface of the roller, which doesn't seem to encompass the entire boundary layer for this case. However, estimations for the boundary layer displacement thickness and momentum thickness were made (as the outer edge of the boundary layer has little effect on these numbers) with a resultant shape factor of about 1.2, which is significantly smaller than the shape factor for the initial laminar profiles. As the shape factor for a turbulent velocity profile is known to be smaller than that of a comparable laminar profile, this again tends to prove that the boundary layer behind the doctor blade is initially laminar before becoming turbulent at a certain circumferential distance from the blade (in this case about 10 cm), after which the boundary layer grows toward the fully developed turbulent profile shown.

It can be seen from Figures 4.6 and 4.7 that the experimental profiles measured over the cylinder surface do not however follow exactly the expected flat plate laminar and turbulent profiles. In the flow over the first 100 or so degrees from the doctor blade the profiles do follow the shape of the Blasius laminar profile to a certain extent.

However there are discrepancies in the profiles, with the experimental profile producing a slightly fuller profile near the edge of the boundary layer coupled with a lower profile near the wall. This is also the case of the turbulent fully developed profile

(see Figure 4.7), with the experimental profile again being fuller near the edge of the boundary layer and lower near the roller surface.

Part of this discrepancy in the profiles in these cases may be attributed to the difficulties in accurately scaling the laminar and turbulent predictions to the experimental data. For this study, a value of $Y/\delta^* = 6$ was assumed for the edge of the boundary layer, with this value simply being estimated from the experimental data. As a result, there is significant room for error in this value due to the already stated limitations of the experimental techniques at the edge of the boundary layer. In Figure 4.7 the turbulent data has been plotted against two different curve fits (with $Y/\delta^* = 6$ and 12 at the boundary layer edge), but both show the same discrepancies with the experimental results.

The reason for these discrepancies between experimental and theoretical data may be the result of the centrifugal forces working on the roller flow, as the theoretical profiles were developed from flat-plate theory and do not take into account the centrifugal effects of the rotating wall. It can be seen from the comparison of the experimental and theoretical profiles that the rotating wall has the effect of transferring mass from the wall region outwards toward the edge of the boundary layer, resulting in lower velocities near the wall but a much fuller profile further from the wall. This tends to validate the conclusions from Koosinlin et. al.⁹, where the theoretical model tended to underestimate the rate of mass transfer towards the edge of the boundary layer. It would therefore appear that the flat-plate estimation, and even the swirling flow models, are inadequate for the modeling of this flow, and thus a more complete theoretical model will have to be produced before any accurate prediction of the properties of this flow can be made.

It can be seen from the experimental results that the transition from a laminar to turbulent boundary layer occurs at a Reynolds number of about $Re_{x,tr} \approx 80000$. This value is much smaller than the predicted transition region for a flow above a flat plate, from Schlichting, of 3.5×10^5 to 10^6 . The experimental Reynolds number for transition is even smaller than the predicted critical Reynolds number for initial instability above a flat plate of $Re_{x,cr} \approx 91000$ (from White).

This result can be explained, to a certain extent, by comparing the boundary layer flow in this experiment to a theoretical Falkner-Skan flow. Using the relationship devised by Wazzan et al, it could be found that the transition Reynolds number for this experiment, i.e. $Re_{x,tr} \approx 80000$, corresponds to a Falkner-Skan parameter of $\beta = -0.2$. This negative Falkner-Skan parameter applies to an adverse pressure gradient flow, with transition occurring earlier for adverse pressure gradient flow.

This argument can be taken further by considering the effect of freestream turbulence on the boundary layer development. It is reasonable to assume that the insertion of the doctor blade into the flow could induce freestream turbulence behind the blade. For the given transition Reynolds number and the deduced Falkner-Skan parameter, a freestream turbulence of $T = 1.7\%$ can be found (see White, Fig 5-34). This freestream turbulence would help to induce transition, again explaining the surprisingly low transition Reynolds number behind the doctor blade. This phenomenon would also go some way to explaining why the velocity and turbulent intensity never returns to zero at the edge of the boundary layer for these experiments.

It was impossible to further compare the experimental data with the Falkner-Skan flows in this case as the velocity profiles predicted for adverse pressure gradients in Falkner-Skan flows cannot be modified to the boundary conditions for this experiment.

It does however appear from the growth of the boundary layer that the positioning of the doctor blade does have a major effect on the volume of air being carried along with the roller surface. The results show that the boundary layer thickness is decreased considerably in the region following the doctor blade with a very thin laminar profile produced immediately behind the blade, which will result in a very low mass flow rate of air in the region behind the doctor blade. However, it can be seen from Table 4.2 that the flow rate behind the doctor blade is still far higher than that being carried between the roller and a stationary web. It can be seen that the flow rate per unit width behind the blade is of the order of 10^2 larger than the estimated flow rate between a stationary web and drive roller (calculated to be about $70.8 \times 10^{-6} \text{ m}^2/\text{s}$). Thus, it is doubtful whether the doctor blade will have a significant effect on the air entrained between web and roller, although an experimental analysis of this effect will be able to better answer this question.

An attempt was made to better understand the effect of the doctor blade on the roller surface and on the resulting air film between web and roller using flow visualization techniques, but problems with the image gathering made it impossible to show the results in this report. The flow visualization work did however tend to support the experimental data taken in this investigation, with the effect of the doctor blade in reducing the boundary layer easily visible, and the rotating flow resulting in a large rate of mass transfer toward the edge of the boundary layer, especially in the turbulent flow

region. The flow visualisation work also tended to show a very intermittent outer region in the boundary layer, especially in the fully developed turbulent flow, with large bulges being produced at the edge of the boundary layer.

CHAPTER VI: CONCLUSIONS AND RECOMMENDATIONS

- 1/ It can be seen that the doctor blade has a significant effect on the boundary layer on the surface of a rotating cylinder.
- 2/ The velocity profile immediately behind the doctor blade is of a laminar form, with transition to a turbulent profile occurring at a certain position downstream of the doctor blade (in this case at a Reynolds number with respect to x-position of about 80000).
- 3/ The Reynolds number for transition in this experiment was far lower than flat plate theory predicts. By comparing this flow to a theoretical Falkner-Skan flow the low $Re_{x,tr}$ can be explained as the result of an adverse pressure gradient on the roller surface, with freestream turbulence also contributing to the early transition.
- 4/ Further manipulation of the Falkner-Skan predictions, taking into account the inverse boundary conditions for this flow, would allow a better comparison with these experimental results.
- 5/ Limitations in the hot-wire method result in boundary layer thickness calculations with large uncertainties.

6/ The theoretical Blasius and $1/7$ law turbulent flat plate predictions are inadequate for modeling the flow over a rotating cylinder. It is recommended that work be carried out to produce a more accurate prediction of the boundary layer velocity profiles, taking into account the rotational aspects of the flow.

7/ The experimental velocity profiles differ from both the Blasius and $1/7$ law turbulent flat plate predictions. The reason for this is that the rotational nature of the flow results in an excess of mass transfer toward the edge of the boundary layer, which the theoretical predictions cannot take into account.

8/ Repeating these experiments for various roller speeds and radii would allow an estimation of the universality of the conclusions made from this investigation.

9/ The use of LDA measurements instead of the hot-wire method could greatly increase the accuracy of the boundary layer measurements, especially near the outer edge of the boundary layer, allowing for a far more in depth study into the properties of the flow.

10/ An experimental investigation into the thickness of the air gap between the roller and a drive web for different doctor blade positions would answer whether or not the doctor blade does reduce the level of air entrainment.

11/ Flow visualization work tended to support the experimental data, although problems with the image gathering techniques made accurate comparison and analysis difficult. The flow visualization work did seem to show a rather intermittent outer region for the roller boundary layer, with a series of large bulges appearing in the boundary layer.

REFERENCES

1. Nigam, S.D., "Note on the Boundary Layer on a Rotating Sphere," ZAMP, Vol. V, 1954, pp. 151-155.
2. Koosinlin, M.L., Launder, B.E. & Sharma, B.I., "Prediction of Momentum, Heat and Mass Transfer in Swirling, Turbulent Boundary Layers," Trans. of ASME, Journal of Heat Transfer, Vol. 96, 1974, pp. 204-209.
3. Taylor, G.I., "Distribution of Velocity and Temperature between Concentric Rotating Cylinders," Scientific Papers of G.I. Taylor, Vol. 2, Cambridge University Press, 1960, pp. 336-350.
4. Taylor, G.I., "Fluid Friction Between Rotating Cylinders, Part I - Torque Measurements," Scientific Papers of G.I. Taylor, Vol. 2, Cambridge University Press, 1960, pp. 380-396.
5. Taylor, G.I., "Fluid Friction Between Rotating Cylinders, Part II - Distribution of Velocity Between Concentric Cylinders When Outer One Is Rotating and Inner One Is at Rest," Scientific Papers of G.I. Taylor, Vol. 2, Cambridge University Press, 1960, pp. 397-408.

6. Kinney, R.B., "Universal Velocity Similarity in Fully Turbulent Rotating Flows," Trans. of ASME, Journal of Applied Mech., Vol. 34, 1967, pp. 437-442.
7. Theodorsen, T. & Regier, A., "Experiments on Drag of Revolving Disks, Cylinders and Streamline Rods at High Speeds," NACA Report No .793, 1944.
8. Anderson, J.T. & Saunders, O.A., "Convection From an Isolated Heated Cylinder Rotating About Its Axis," Proceedings Royal Society London, Series A, Vol. 217, 1953, p. 555.
9. Kappesser, R., Cornet, I. & Greif, R., "Mass Transfer to a Rough Rotating Cylinder," Journal of Electrochemical Society, Vol. 118, No. 12, 1971, p. 1957.
10. Smith, R.N. & Greif, R., "Turbulent Transport of a Rotating Cylinder for Large Prandtl or Schmidt Numbers", Trans. of ASME, Journal of Heat Transfer, Vol. 97, 1975, pp. 594-597.
11. Chambers, F.W. & Gadapa, P.S., "Flow About a Cylinder Spinning in Still Air," Submitted to the AIAA Journal, 1992.

12. King, S.L., Funk, B.A. & Chambers, F.W., "Air Films Between A Moving Tensioned Web And A Stationary Support Cylinder," Proceedings of the Second International Web Handling Conference, Stillwater, Oklahoma, June 1993.
13. Hinze, J.O., "TURBULENCE", 2nd Edition, McGraw-Hill, New York, 1975.
14. White, F.M., "VISCOUS FLUID FLOW," 2nd Edition, McGraw-Hill, New York, 1991.
15. Keuthe, A.H. & Chow, C-Y, "FOUNDATIONS OF AERODYNAMICS," 4th Edition, John Wiley & Sons, New York, 1996.
16. Schlichting, H.S., "BOUNDARY LAYER THEORY," McGraw-Hill, New York, 4th Ed., 1960.

APPENDIX I

GWBASIC Computer Program For Data Acquisition.

```

100 REM: CYLINDER.BAS - PROGRAM TO CALIBRATE A HOT WIRE ANEMOMETER PROBE
110 REM: AND PERFORM VELOCITY PROFILE AND TURBULENCE MEASUREMENTS. THE
120 REM: DATA ACQUISITION IS PERFORMED WITH A METRABYTE MODEL 16F ADC
BOARD
130 REM
140 REM: AIR PROPERTY CALCULATIONS ASSUME IDEAL GAS BEHAVIOR AND USE
150 REM: SUTHERLAND EQUATION FOR TEMPERATURE DEPENDENCE OF VISCOSITY
160 REM
170 DIM
DP(100),E(100),U(100),ES(100),UK(100),US(100),TI(100),V(5001),RPM(100),UWALL(100),TA(5001)
180 REM
190 PI=3.14159265#
200 REM
210 REM: SUTHERLAND COEFFICIENTS
220 B=1.458E-06
230 S=110.4
240 REM
250 REM: AIR GAS CONSTANT AND SPECIFIC HEAT RATIO
260 R=287!
270 GAM=1.4
280 OPEN "O",#1,"C:\NB\DATAFILE\HWCALOUT.DAT"
290 PRINT "CALIBRATION WRITTEN TO FILE C:\NB\DATAFILE\HWCALOUT.DAT"
300 INPUT "CALIBRATION FILE HEADING (< 20 CHARACTERS)";CHEAD$
310 PRINT USING "\          \";CHEAD$
320 PRINT USING "\    \    \    \";DATE$,TIME$
330 PRINT #1,USING "\          \";CHEAD$
340 PRINT #1,USING "\    \    \    \";DATE$,TIME$
350 REM
360 REM: INPUT BAROMETER READING AND CALCULATE ATMOSPHERIC PRESSURE
370 REM
380 PRINT " "
390 INPUT "ATMOSPHERIC PRESSURE IN mm Hg";PMM
400 PATM=101325!*PMM/760!
410 KPATM=PATM/1000!
420 REM
430 REM: INPUT TEMPERATURE AND CALCULATE OTHER TEMPERATURES
440 REM
450 INPUT "TEMPERATURE IN DEGREES C OR 1000+F";TC
460 IF TC<600 THEN 500
470 TF=TC-1000!
480 TC=(TF-32!)*5/9!
490 GOTO 510
500 TF=(TC*9/5)+32!
510 TK=TC+273.15
520 TR=TF+459.7
530 REM
540 REM: CALCULATE DYNAMIC VISCOSITY WITH SUTHERLAND EQUATION
550 REM
560 DVIS=B*SQR(TK)/(1!+(S/TK))
570 DVICE=DVIS/(1.488164)
580 REM
590 REM: CALCULATE AIR DENSITY USING IDEAL GAS EQUATION OF STATE
600 REM
610 RHO=PATM/(R*TK)
620 REM

```

```

630 REM: CALCULATE KINEMATIC VISCOSITY
640 REM
650 KVIS=DVIS/RHO
660 REM
670 REM: PRINT RESULTS
680 REM
690 PRINT " "
700 PRINT USING"ATMOSPHERIC PRESSURE:   ###.### kPa";KPATM
710 PRINT #1,USING" ###.### KPA - ATMOSPHERIC PRESSURE";KPATM
720 PRINT USING"TEMPERATURE:           ###.## deg. C";TC
730 PRINT #1,USING" ###.## DEG. C - TEMPERATURE";TC
740 PRINT USING"ABSOLUTE TEMPERATURE: ###.## deg. K";TK
750 PRINT #1,USING" ###.## DEG. K - ABS. TEMP.";TK
760 PRINT USING"AIR DENSITY:           #.#### kg/m3";RHO
770 PRINT #1,USING" #.#### KG/M3 - AIR DENSITY";RHO
780 PRINT USING"DYNAMIC VISCOSITY (mu): ##.###^ Pa-s";DVIS
790 PRINT #1,USING"##.###^ PA-S - DYNAMIC VISCOSITY";DVIS
800 PRINT USING"KINEMATIC VISCOSITY (nu): ##.###^ m2/s";KVIS
810 PRINT #1,USING"##.###^ M2/S - KINEMATIC VISCOSITY";KVIS
820 REM
830 REM: TEST TO PERFORM CALIBRATION OR READ CAL. FILE
840 INPUT "ENTER 0 TO PERFORM CALIBRATION OR 1 TO READ CAL. FILE";NTOCAL
850 IF NTOCAL>0 THEN 1880
860 CLS
870 REM
880 PRINT "BEGINNING OF CALIBRATION LOOP"
890 REM
900 REM: RAW CALIBRATION DATA WRITTEN TO FILE HWCAL.DAT IN
910 REM: DIRECTORY C:\NB\DATAFILE
920 REM
930 REM *****
940 REM LOADING SETUP FILES NEEDED. THESE FILES ARE PROVIDED BY
950 REM LABTECH NOTEBOOK
960 REM *****
970 REM
980 SHELL "CD\NB"
990 PRINT "LOADING SETUP FILES FOR LABTECH NOTEBOOK"
1000 PRINT " "
1010 SHELL "COPY SETUP\HWCAL"
1020 CLS
1030 REM
1040 REM INITIALIZE VARIABLES
1050 REM
1060 NCAL = 0!
1070 RH2O=998!
1080 G=9.807
1090 UCON=SQR(2!*G*RH2O*.0254/RHO)
1100 FOR I=1 TO 50
1110 INPUT "MANOMETER READING (INCHES H2O)";DELP
1120 NCAL=NCAL+I
1130 DP(NCAL)=DELP
1140 U(NCAL)=UCON*SQR(DP(NCAL))
1150 UK(NCAL)=U(NCAL)^.45
1160 REM
1170 REM *****

```

```

1180 REM BEGINNING OF DATA ACQUISITION AND AVERAGING LOOP
1190 REM THE DATA ACQUISITION IS PERFORMED BY LABTECH
1200 REM NOTEBOOK
1210 REM *****
1220 REM
1230 PRINT "ACQUIRING DATA"
1240 SHELL "GO"
1250 CLS
1260 REM *****
1270 REM END OF DATA ACQUISITION, REOPENING DATA ACQUISITION FILE
1280 REM TO BEGIN COMPUTING AVERAGE OF VOLTAGE OUTPUT.
1290 REM *****
1300 REM
1310 PRINT "OPENING ACQUIRED CALIBRATION DATA FILE"
1320 PRINT "AND COMPUTING AVERAGE OUTPUT VOLTAGE"
1330 OPEN "I", #2, "C:\NB\DATAFILE\HWCAL.DAT"
1340 INPUT #2, A$
1350 INPUT #2, B$
1360 INPUT #2, C$
1370 REM
1380 REM *****
1390 REM BEGINNING OF AVERAGING LOOP
1400 REM
1410 VSUM=0!
1420 JMAX=400
1430 FOR J = 1 TO JMAX
1440 INPUT #2, V(J)
1450 VSUM=VSUM+V(J)
1460 NEXT J
1470 VAVG=VSUM/JMAX
1480 E(NCAL)=VAVG
1490 ES(NCAL)=E(NCAL)*E(NCAL)
1500 PRINT USING "## ##.### ##.### ##.### ##.###
##.###";NCAL,DP(NCAL),U(NCAL),E(NCAL),UK(NCAL),ES(NCAL)
1510 REM
1520 REM
1530 CLOSE #2
1540 INPUT "0 TO WRITE POINT TO FILE OR -1 TO DELETE";NFLAG
1550 IF NFLAG>-1 THEN 1570
1560 NCAL=NCAL-1
1570 INPUT "0 TO CONTINUE OR -1 TO END CALIBRATION";NFLAG
1580 IF NFLAG<0 THEN 1600
1590 NEXT I
1600 PRINT USING "CALIBRATION COMPLETED WITH ## POINTS";NCAL
1610 PRINT #1,USING"##### CALIBRATION POINTS";NCAL
1620 PRINT " "
1630 PRINT " N DP U E U^0.45 E^2"
1640 PRINT #1, " N DP U E U^0.45 E^2"
1650 PRINT " (IN H20) (M/S) (VOLTS)"
1660 PRINT #1, " (IN H20) (M/S) (VOLTS)"
1670 SX=0!
1680 SY=0!
1690 SXY=0!
1700 SX2=0!
1710 FOR M=1 TO NCAL

```

```

1720 SX=SX+UK(M)
1730 SY=SY+ES(M)
1740 SXY=SXY+(UK(M)*ES(M))
1750 SX2=SX2+(UK(M)*UK(M))
1760 PRINT USING "### ##.### ##.### ##.### ##.###"
###.###";M,DP(M),U(M),E(M),UK(M),ES(M)
1770 PRINT #1,USING "### ##.### ##.### ##.### ##.###"
###.###";M,DP(M),U(M),E(M),UK(M),ES(M)
1780 NEXT M
1790 B=(SXY-(SX*SY/NCAL))/(SX2-((SX^2)/NCAL))
1800 A=(SY-(B*SX))/NCAL
1810 PRINT USING " E^2 = ##.### + (##.### * U^0.45)";A,B
1820 PRINT #1,USING "##.###^### ##.###^### :A,B - E^2 = A + BU^0.45)";A,B
1830 CLOSE #1
1840 PRINT "END OF CALIBRATION LOOP"
1850 REM
1860 REM: END OF CALIBRATION LOOP
1870 GOTO 2150
1880 OPEN "I",#2,"C:\NB\DATAFILE\HWCALIN.DAT"
1890 INPUT #2,DHEAD$
1900 PRINT DHEAD$
1910 INPUT #2,DDATE$
1920 PRINT DDATE$
1930 INPUT #2,DKPATM,DUMMY$
1940 INPUT #2,DTC,DUMMY$
1950 PRINT DTC
1960 INPUT #2,DTK,DUMMY$
1970 INPUT #2,DRHO,DUMMY$
1980 PRINT DRHO
1990 INPUT #2,DDVIS,DUMMY$
2000 INPUT #2,DKVIS,DUMMY$
2010 INPUT #2,NCAL,DUMMY$
2020 INPUT #2,DHEADS$
2030 INPUT #2,DHEADS$
2040 PRINT #1,USING"##### CALIBRATION POINTS";NCAL
2050 PRINT #1, " N DP U E U^0.45 E^2"
2060 PRINT #1, " (IN H2O) (M/S) (VOLTS)"
2070 FOR K=1 TO NCAL
2080 INPUT #2,M,DP(M),U(M),E(M),UK(M),ES(M)
2090 PRINT #1,USING "### ##.### ##.### ##.### ##.###"
###.###";M,DP(M),U(M),E(M),UK(M),ES(M)
2100 NEXT K
2110 INPUT #2,A,B
2120 PRINT USING" A = ##.###^### B = ##.###^###";A,B
2130 CLOSE #1
2140 CLOSE #2
2150 OPEN "O",#3,"C:\NB\DATAFILE\PROFILE.DAT"
2160 PRINT "VELOCITY PROFILE DATA WRITTEN TO FILE 'C:\NB\DATAFILE\PROFILE.DAT'"
2170 INPUT "PROFILE MEASUREMENT FILE HEADING (< 20 CHARACTERS)";PHEAD$
2180 PRINT USING "\ \ \ \ \";PHEAD$
2190 PRINT USING "\ \ \ \ \";DATE$,TIME$
2200 PRINT #3,USING "\ \ \ \ \";PHEAD$
2210 PRINT #3,USING "\ \ \ \ \";DATE$,TIME$
2220 REM
2230 REM: RAW PROFILE DATA WRITTEN TO FILE RAWHWT.DAT IN

```

```

2240 REM: DIRECTORY C:\NB\DATAFILE
2250 REM
2260 REM *****
2270 REM LOADING SETUP FILES NEEDED. THESE FILES ARE PROVIDED BY
2280 REM LABTECH NOTEBOOK
2290 REM *****
2300 REM
2310 SHELL "CD\NB"
2320 PRINT "LOADING SETUP FILES FOR LABTECH NOTEBOOK"
2330 PRINT " "
2340 SHELL "COPY SETUP\HWTACH"
2350 CLS
2360 REM
2370 REM INITIALIZE VARIABLES
2380 REM
2390 KEX=1!/.45
2400 SKEX=(1!-.45)/.45
2410 NP = 0!
2420 INPUT "SURFACE POSITION READING (INCHES)";DZERO
2430 FOR I=1 TO 100
2440 INPUT "POSITION READING (INCHES)";DELP
2450 KEY OFF
2460 NP=NP+1
2470 DP(NP)=(DZERO-DELP)*.0254
2480 VBART=0!
2490 VBAR2T=0!
2500 TRPM=0!
2510 TSURF=0!
2520 KMAX=2
2530 FOR K=1 TO KMAX
2540 REM
2550 REM *****
2560 REM BEGINNING OF DATA ACQUISITION AND AVERAGING LOOP
2570 REM THE DATA ACQUISITION IS PERFORMED BY LABTECH
2580 REM NOTEBOOK
2590 REM *****
2600 REM
2610 PRINT USING "BEGINNING BLOCK ## OF ##";K,KMAX
2620 PRINT "ACQUIRING DATA"
2630 SHELL "GO"
2640 CLS
2650 REM *****
2660 KEY OFF
2670 REM END OF DATA ACQUISITION, REOPENING DATA ACQUISITION FILE
2680 REM TO BEGIN COMPUTING AVERAGE OF VOLTAGE OUTPUT.
2690 REM *****
2700 REM
2710 PRINT "OPENING ACQUIRED PROFILE DATA FILE"
2720 PRINT "AND COMPUTING AVERAGE OUTPUT VOLTAGE"
2730 OPEN "I", #1, "C:\NB\DATAFILE\RAWHWT.DAT"
2740 INPUT #1, AHEAD$
2750 INPUT #1, NHEAD$
2760 INPUT #1, VHEAD$
2770 REM
2780 REM *****

```

```

2790 REM BEGINNING OF AVERAGING LOOP
2800 REM
2810 VSUM=0!
2820 TSUM=0!
2830 VSUM2=0!
2840 TSUM2=0!
2850 JMAX=5000
2860 FOR J = 1 TO JMAX
2870 INPUT #1, V(J),TA(J)
2880 VSUM=VSUM+V(J)
2890 TSUM=TSUM+TA(J)
2900 VSUM2=VSUM2+(V(J)*V(J))
2910 TSUM2=TSUM2+(TA(J)*TA(J))
2920 NEXT J
2930 CLOSE #1
2940 VBAR=VSUM/JMAX
2950 UBLOCK=((VBAR*VBAR)-A)/B)^KEX
2960 PRINT USING "E = ###.### volts U = ###.### m/s";VBAR,UBLOCK
2970 TBAR=TSUM/JMAX
2980 VBAR2=VSUM2/JMAX
2990 TBAR2=TSUM2/JMAX
3000 VBART=VBART+VBAR
3010 TAVG=TBAR
3020 VBAR2T=VBAR2T+VBAR2
3030 TRMS=SQR(TBAR2-(TBAR*TBAR))
3040 TRIG=TAVG+(.5*TRMS)
3050 PRINT USING "TAVG = ### TRMS = ### TRIG = ###";TAVG,TRMS,TRIG
3060 PRINT USING "COMPLETED BLOCK ## OF ##";K,KMAX
3070 PRINT USING "EBAR = ###.####, TBAR = ###.#### FOR BLOCK ##";VBAR,TBAR,K
3080 NPER=0
3090 MSTART=0
3100 PLOW=0
3110 FOR M=1 TO JMAX
3120 IF TA(M)>TRIG THEN 3150
3130 PLOW=1
3140 GOTO 3250
3150 IF PLOW<1 THEN 3250
3160 IF MSTART>0 THEN 3210
3170 MSTART=M
3180 PLOW=0
3190 REM PRINT USING "M = #### MSTART = ####";M,MSTART
3200 GOTO 3250
3210 NPER=NPER+1
3220 MEND=M
3230 REM PRINT USING "M = #### MSTART = #### MEND = #### NPER =
###";M,MSTART,MEND,NPER
3240 PLOW=0
3250 NEXT M
3260 TPERIOD=(MEND-MSTART)/(NPER*2000!)
3270 PRINT USING "NPER = #### TPERIOD = ###.###^";NPER,TPERIOD
3280 FREQ=1!/TPERIOD
3290 PRINT USING "FREQUENCY = ###.###";FREQ
3300 USURF=4!*.0254*PI/TPERIOD
3310 PRINT USING "USURF = ###.### M/S";USURF
3320 TRPM=TRPM+(60!/TPERIOD)

```



```

3330 TSURF=TSURF+USURF
3340 NEXT K
3350 VBART=VBART/KMAX
3360 VBAR2T=VBAR2T/KMAX
3370 RPM(NP)=TRPM/KMAX
3380 UWALL(NP)=TSURF/KMAX
3390 E(NP)=VBART
3400 ES(NP)=SQR(VBAR2T-(VBART*VBART))
3410 VTEST=(VBART*VBART)-A
3420 IF VTEST<0! THEN 3480
3430 U(NP)=(((VBART*VBART)-A)/B)^KEX
3440 DUDE=(((VBART*VBART)-A)/B)^SKEX*2!*VBART*KEX/B
3450 US(NP)=ES(NP)*DUDE
3460 TI(NP)=US(NP)/U(NP)
3470 GOTO 3520
3480 U(NP)=-1!
3490 US(NP)=0!
3500 TI(NP)=0!
3510 PRINT " WARNING - VELOCITY BELOW CALIBRATION ZERO!"
3520 PRINT " N Y(IN.) Y(M)  EBAR  ERMS  UBAR  URMS  TURB INT. UWALL
RPM"
3530 PRINT USING "##### ##.### ##.###^~ ##.### ##.###^~ ##.### ##.###^~ ##.###^~ ##.###
#####";NP,DELP,DP(NP),E(NP),ES(NP),U(NP),US(NP),TI(NP),UWALL(NP),RPM(NP)
3540 URATIO=(UWALL(NP)-U(NP))/UWALL(NP)
3550 PRINT USING "(Uw-U)/Uw = ##.###";URATIO
3560 INPUT "0 TO WRITE TO FILE OR -1 TO DELETE POINT";NFLAG
3570 IF NFLAG>-1 THEN 3600
3580 NP=NP-1
3590 GOTO 3610
3600 PRINT #3,USING
"#####tab##.###^~tab##.###^~tab##.###^~tab##.###^~tab##.###^~tab##.###^~ta
b##.###^~tab##.###^~";NP,DELP,DP(NP),E(NP),ES(NP),U(NP),US(NP),TI(NP),UWALL(NP),RPM
(NP)
3610 REM
3620 INPUT "0 TO CONTINUE OR -1 TO END MEASUREMENTS";NFLAG
3630 IF NFLAG<0 THEN 3650
3640 NEXT I
3650 PRINT USING "MEASUREMENTS COMPLETED WITH ## POINTS";NP
3660 MNP=-MNP
3670 PRINT #3,MNP
3680 PRINT " "
3690 PRINT #3," "
3700 PRINT " N Y(M)  EBAR  ERMS  UBAR  URMS  TURB. IN. UWALL RPM"
3710 PRINT " "
3720 PRINT #3, " N Y(M)  EBAR  ERMS  UBAR  URMS  TURB. IN. UWALL
RPM"
3730 FOR M=1 TO NP
3740 PRINT USING "##### ##.###^~ ##.### ##.###^~ ##.### ##.###^~ ##.###^~ ##.###
#####";M,DP(M),E(M),ES(M),U(M),US(M),TI(M),UWALL(M),RPM(M)
3750 PRINT #3,USING
"#####tab##.###^~tab##.###^~tab##.###^~tab##.###^~tab##.###^~tab##.###^~ta
b##.###^~";M,DP(M),E(M),ES(M),U(M),US(M),TI(M),UWALL(M),RPM(M)
3760 NEXT M
3770 PRINT #3,USING" #####.### KPA - ATMOSPHERIC PRESSURE";KPATM
3780 PRINT #3,USING" ###.## DEG. C - TEMPERATURE";TC

```

```
3790 PRINT #3,USING" ###.## DEG. K - ABS. TEMP.";TK
3800 PRINT #3,USING" ##.#### KG/M3 - AIR DENSITY";RHO
3810 PRINT #3,USING"##.###^ M2/S - DYNAMIC VISCOSITY";DVIS
3820 PRINT #3,USING"##.###^ M2/S - KINEMATIC VISCOSITY";KVIS
3830 PRINT #3,USING "##.####^ ##.####^ :A,B - E^2 = A + BU^0.45)";A,B
3840 CLOSE #3
3850 END
```

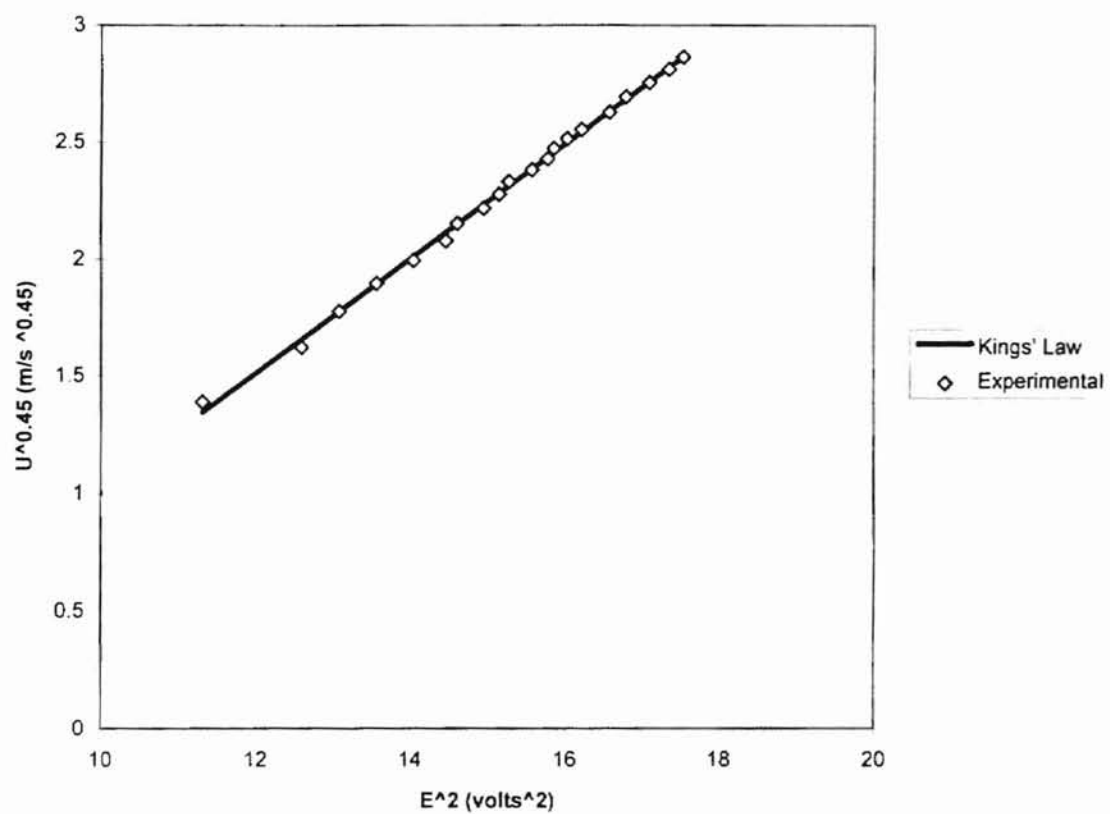
APPENDIX II

Calibration Data.

Appendix II, Table 1: Calibration Data for Experiment Without Doctor Blade.

N	DP (IN H ₂ O)	U (M/S)	E (VOLTS)	U ^{0.45}	E ²
1	0.01	2.072	3.3633	1.3880	11.3118
2	0.02	2.931	3.5484	1.6224	12.5911
3	0.03	3.59	3.6162	1.7774	13.0769
4	0.04	4.145	3.6823	1.8962	13.5593
5	0.05	4.634	3.7467	1.9938	14.0378
6	0.06	5.077	3.8022	2.0774	14.4567
7	0.07	5.483	3.821	2.1506	14.6000
8	0.08	5.862	3.865	2.2163	14.9382
9	0.09	6.217	3.8907	2.2757	15.1375
10	0.1	6.554	3.9068	2.3304	15.2631
11	0.11	6.874	3.9448	2.3809	15.5614
12	0.12	7.179	3.9706	2.4279	15.7657
13	0.13	7.472	3.9808	2.4720	15.8468
14	0.14	7.755	4.0022	2.5137	16.0176
15	0.15	8.027	4.0257	2.5530	16.2063
16	0.17	8.545	4.0704	2.6259	16.5682
17	0.19	9.034	4.0964	2.6924	16.7805
18	0.21	9.497	4.1332	2.7537	17.0833
19	0.23	9.939	4.1644	2.8106	17.3422
20	0.25	10.362	4.1861	2.8638	17.5234

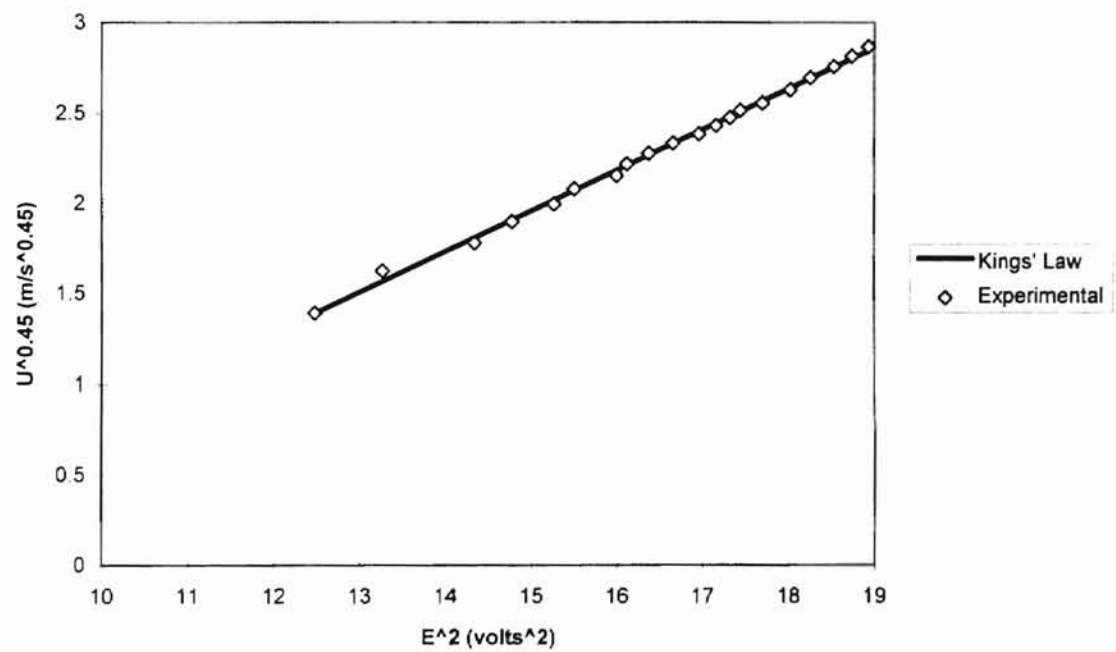
Appendix II, Figure 1: Kings' Law Curve Fit To Calibration Data Without Doctor Blade



Appendix II, Table 2: Calibration Data for Experiment with Doctor Blade at 17 Degrees

N	DP (IN H ₂ O)	U (M/S)	E (VOLTS)	U ^{0.45}	E ²
1	0.01	2.080	3.5322	1.3904	12.4764
2	0.02	2.942	3.6423	1.6251	13.2663
3	0.03	3.603	3.7870	1.7803	14.3414
4	0.04	4.161	3.8444	1.8995	14.7794
5	0.05	4.652	3.9073	1.9973	15.2670
6	0.06	5.096	3.9378	2.0809	15.5063
7	0.07	5.504	4.0001	2.1543	16.0008
8	0.08	5.884	4.0152	2.2200	16.1218
9	0.09	6.241	4.0470	2.2796	16.3782
10	0.10	6.579	4.0818	2.3344	16.6611
11	0.11	6.900	4.1182	2.3850	16.9596
12	0.12	7.206	4.1427	2.4320	17.1620
13	0.13	7.501	4.1623	2.4763	17.3247
14	0.14	7.784	4.1766	2.5179	17.4440
15	0.15	8.057	4.2072	2.5573	17.7005
16	0.17	8.577	4.2455	2.6303	18.0243
17	0.19	9.068	4.2730	2.6970	18.2585
18	0.21	9.533	4.3048	2.7584	18.5313
19	0.23	9.977	4.3288	2.8155	18.7385
20	0.25	10.402	4.3510	2.8688	18.9312

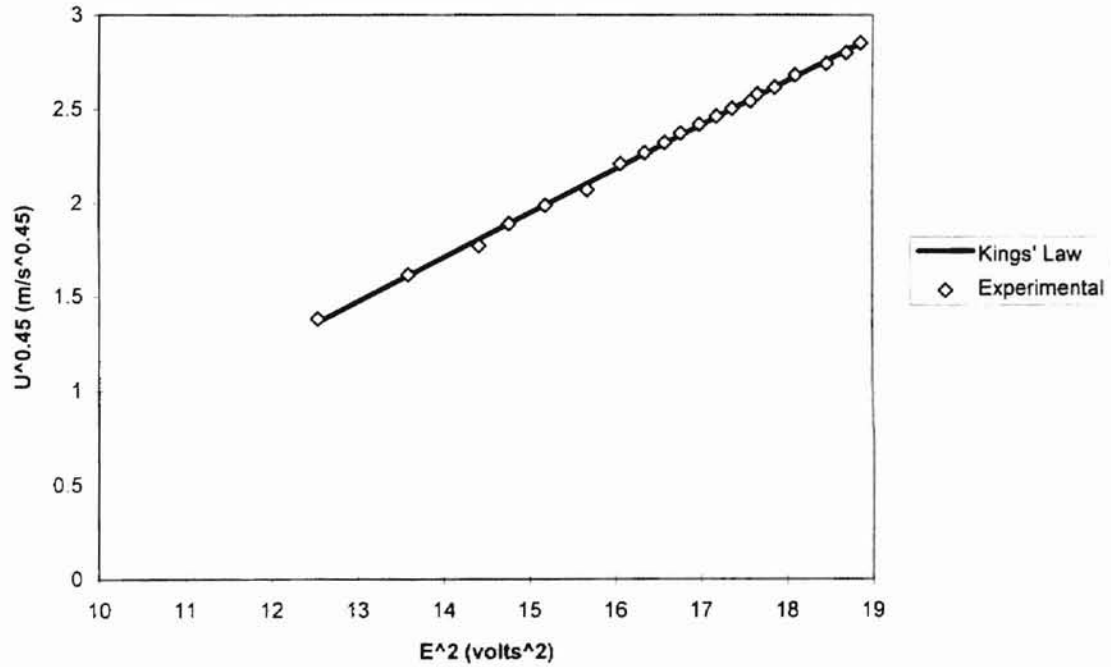
Appendix II, Figure 2: Kings' Law Curve Fit to Calibration Data 17 degs from Doctor Blade



Appendix II, Table 3: Calibration Data for Experiment with Doctor Blade at 36 Degrees

N	DP (IN H2O)	U (M/S)	E (VOLTS)	U ^{0.45}	E ²
1	0.01	2.057	3.5410	1.3834	12.5387
2	0.02	2.909	3.6875	1.6169	13.5977
3	0.03	3.563	3.7972	1.7714	14.4187
4	0.04	4.114	3.8433	1.8898	14.7710
5	0.05	4.600	3.8977	1.9872	15.1921
6	0.06	5.039	3.9599	2.0704	15.6808
7	0.07	5.818	4.0084	2.2088	16.0673
8	0.08	6.171	4.0435	2.2681	16.3499
9	0.09	6.505	4.0723	2.3225	16.5836
10	0.10	6.822	4.0953	2.3728	16.7715
11	0.11	7.126	4.1216	2.4198	16.9876
12	0.12	7.417	4.1458	2.4638	17.1877
13	0.13	7.697	4.1674	2.5052	17.3672
14	0.14	7.967	4.1932	2.5444	17.5829
15	0.15	8.228	4.2026	2.5816	17.6618
16	0.17	8.481	4.2267	2.6170	17.8650
17	0.19	8.966	4.2550	2.6833	18.1050
18	0.21	9.426	4.2971	2.7444	18.4651
19	0.23	9.865	4.3238	2.8012	18.6952
20	0.25	10.285	4.3428	2.8542	18.8599

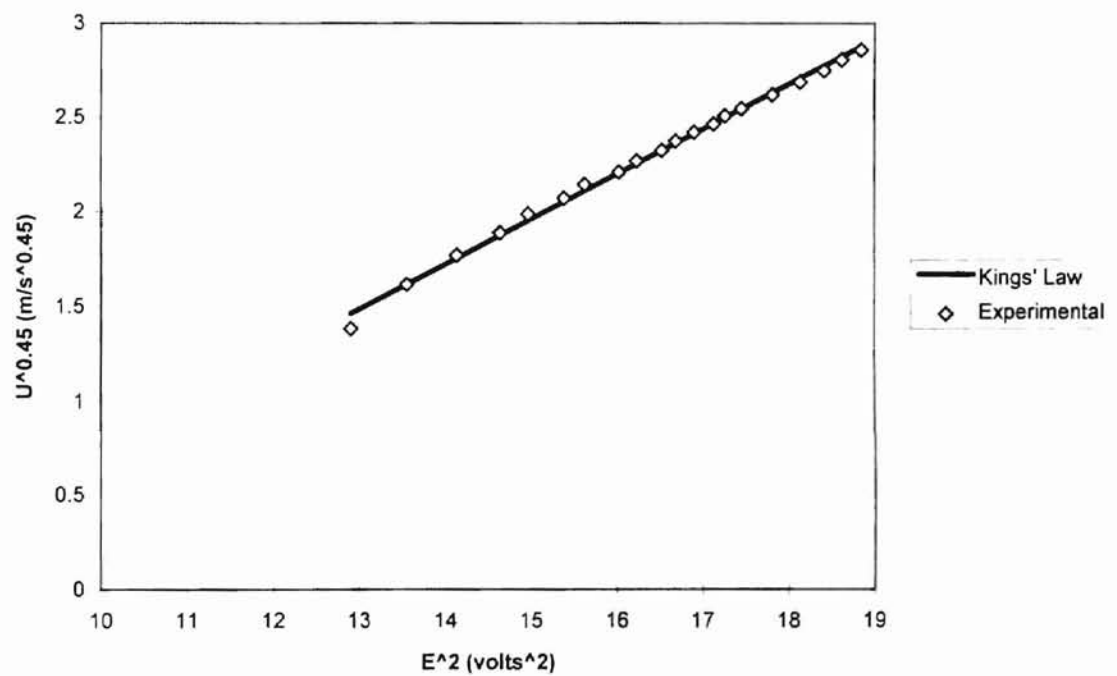
Appendix II, Figure 3: Kings' Law Curve Fit to Calibration Data 36 degrees from Doctor Blade



Appendix II, Table 4: Calibration Data for Experiment with Doctor Blade at 69 Degrees

N	DP (IN H ₂ O)	U (M/S)	E (VOLTS)	U ^{0.45}	E ²
1	0.01	2.059	3.5920	1.3840	12.9025
2	0.02	2.912	3.6821	1.6177	13.5579
3	0.03	3.567	3.7596	1.7723	14.1346
4	0.04	4.118	3.8264	1.8906	14.6413
5	0.05	4.604	3.8690	1.9880	14.9692
6	0.06	5.044	3.9228	2.0713	15.3884
7	0.07	5.448	3.9532	2.1444	15.6278
8	0.08	5.824	4.0033	2.2098	16.0264
9	0.09	6.177	4.0291	2.2691	16.2336
10	0.10	6.512	4.0656	2.3237	16.5291
11	0.11	6.829	4.0854	2.3739	16.6905
12	0.12	7.133	4.1116	2.4209	16.9053
13	0.13	7.424	4.1388	2.4648	17.1297
14	0.14	7.705	4.1550	2.5064	17.2640
15	0.15	7.975	4.1780	2.5455	17.4557
16	0.17	8.490	4.2205	2.6182	17.8126
17	0.19	8.976	4.2590	2.6846	18.1391
18	0.21	9.436	4.2913	2.7457	18.4153
19	0.23	9.875	4.3152	2.8025	18.6210
20	0.25	10.296	4.3412	2.8556	18.8460

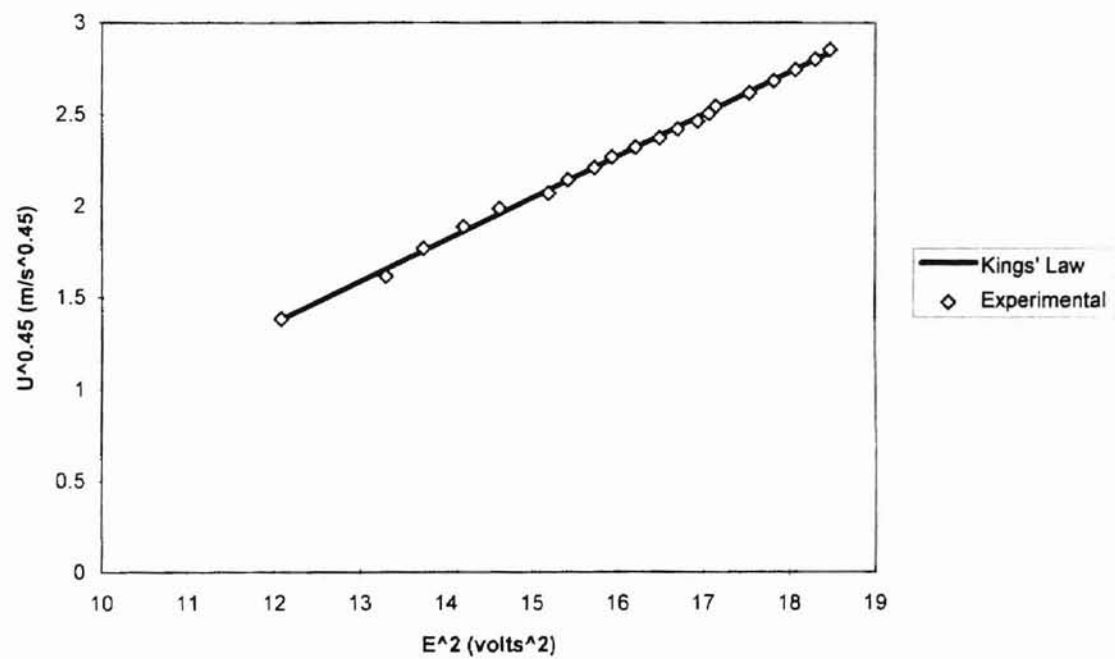
Appendix II, Figure 4: Kings' Law Curve Fit to Calibration Data 69 degrees from Doctor Blade



Appendix II, Table 5: Calibration Data for Experiment with Doctor Blade at 93 Degrees

N	DP (IN H ₂ O)	U (M/S)	E (VOLTS)	U ^{0.45}	E ²
1	0.01	2.055	3.4757	1.3828	12.0805
2	0.02	2.906	3.6471	1.6162	13.3013
3	0.03	3.559	3.7060	1.7705	13.7344
4	0.04	4.110	3.7680	1.8890	14.1978
5	0.05	4.595	3.8230	1.9862	14.6153
6	0.06	5.034	3.8969	2.0695	15.1858
7	0.07	5.437	3.9260	2.1425	15.4135
8	0.08	5.812	3.9649	2.2077	15.7204
9	0.09	6.165	3.9912	2.2671	15.9297
10	0.10	6.498	4.0254	2.3214	16.2038
11	0.11	6.816	4.0601	2.3719	16.4844
12	0.12	7.119	4.0861	2.4187	16.6962
13	0.13	7.409	4.1147	2.4626	16.9308
14	0.14	7.689	4.1308	2.5040	17.0635
15	0.15	7.959	4.1401	2.5432	17.1404
16	0.17	8.473	4.1872	2.6159	17.5326
17	0.19	8.957	4.2213	2.6821	17.8194
18	0.21	9.417	4.2511	2.7432	18.0719
19	0.23	9.855	4.2782	2.7999	18.3030
20	0.25	10.275	4.2978	2.8530	18.4711

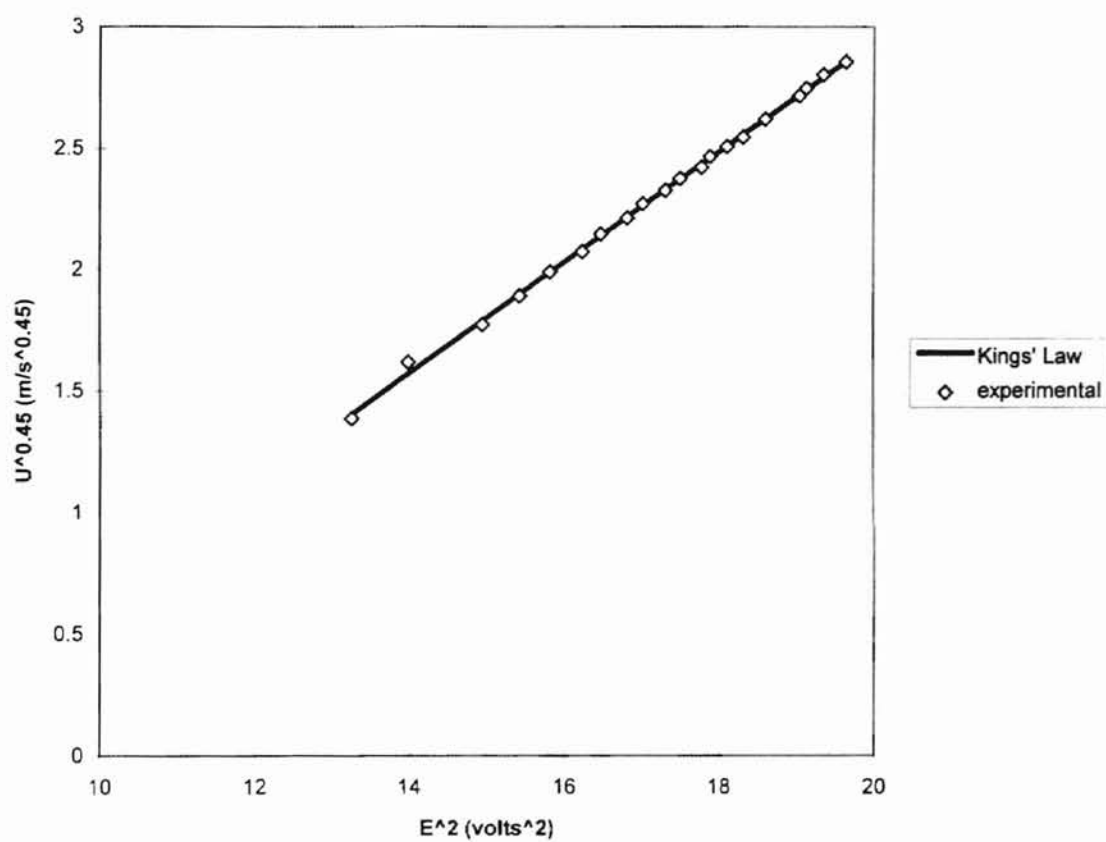
Appendix II, Figure 5: Kings' Law Curve Fit to Calibration Data 93 Degrees from Doctor Blade



Appendix II, Table 6: Calibration Data for Experiment with Doctor Blade at 119 Degrees

N	DP (IN H ₂ O)	U (M/S)	E (VOLTS)	U ^{0.45}	E ²
1	0.01	2.061	3.6405	1.3846	13.2532
2	0.02	2.915	3.7399	1.6184	13.9869
3	0.03	3.570	3.8666	1.7730	14.9506
4	0.04	4.122	3.9283	1.8915	15.4315
5	0.05	4.609	3.9774	1.9889	15.8197
6	0.06	5.049	4.0296	2.0723	16.2377
7	0.07	5.453	4.0591	2.1453	16.4763
8	0.08	5.830	4.1011	2.2108	16.8190
9	0.09	6.184	4.1258	2.2702	17.0222
10	0.1	6.518	4.1612	2.3246	17.3156
11	0.11	6.836	4.1840	2.3750	17.5059
12	0.12	7.140	4.2170	2.4219	17.7831
13	0.13	7.432	4.2299	2.4660	17.8921
14	0.14	7.712	4.2553	2.5074	18.1076
15	0.15	7.983	4.2801	2.5467	18.3193
16	0.17	8.499	4.3132	2.6195	18.6037
17	0.19	9.218	4.3635	2.7170	19.0401
18	0.21	9.446	4.3736	2.7470	19.1284
19	0.23	9.885	4.3991	2.8038	19.3521
20	0.25	10.306	4.4315	2.8569	19.6382

Appendix II, Figure 6: Kings' Law Curve Fit to Calibration Data 119 Degrees from Doctor Blade



Appendix II, Table 7: Kings' Law Calibration Equations for Experiments

Experiment	Calibration Equation
Fully Developed Boundary Layer	$E^2 = 5.8275 + (4.0836 * U^{0.45})$
$Re_x = 11163$	$E^2 = 6.3256 + (4.4305 * U^{0.45})$
$Re_x = 24433$	$E^2 = 6.7513 + (4.2451 * U^{0.45})$
$Re_x = 47165$	$E^2 = 6.7342 + (4.2156 * U^{0.45})$
$Re_x = 60594$	$E^2 = 6.0338 + (4.3862 * U^{0.45})$
$Re_x = 80069$	$E^2 = 7.0905 + (4.3915 * U^{0.45})$

APPENDIX III

Fully Developed Boundary Layer (i.e. No Doctor Blade) Data.

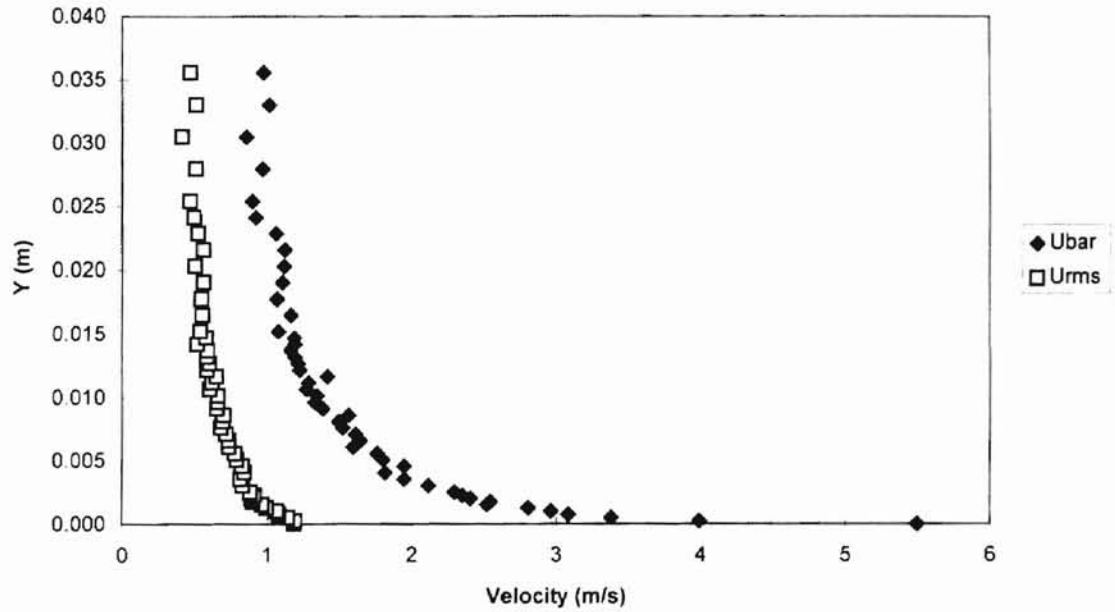
Appendix III, Table 1: Data for Fully Developed Boundary Layer

N	Y (in)	Y (m)	Ebar (volts)	Erms (volts)	Ubar (m/s)	Urms (m/s)	Turb. Int.	Uwall (m/s)	RPM	Ubar/Uwall	Urms/Uwall
1	0.00	0.0000	3.823	0.1117	5.4960	1.1870	0.2160	9.99	1880	0.5502	0.1188
2	0.01	0.0003	3.666	0.1397	3.9900	1.1930	0.2991	10.10	1900	0.3950	0.1181
3	0.02	0.0005	3.591	0.1498	3.3810	1.1440	0.3384	10.14	1910	0.3334	0.1128
4	0.03	0.0008	3.551	0.1508	3.0840	1.0830	0.3511	10.19	1920	0.3026	0.1063
5	0.04	0.0010	3.533	0.1525	2.9620	1.0650	0.3596	10.25	1930	0.2890	0.1039
6	0.05	0.0013	3.511	0.1483	2.8060	0.9992	0.3561	10.27	1930	0.2732	0.0973
7	0.06	0.0015	3.467	0.1538	2.5230	0.9655	0.3827	10.30	1940	0.2450	0.0937
8	0.07	0.0018	3.471	0.1428	2.5460	0.9018	0.3542	10.33	1940	0.2465	0.0873
9	0.08	0.0020	3.449	0.1460	2.4090	0.8888	0.3689	10.36	1950	0.2325	0.0858
10	0.09	0.0023	3.439	0.1522	2.3510	0.9116	0.3877	10.35	1950	0.2271	0.0881
11	0.10	0.0025	3.430	0.1501	2.2960	0.8851	0.3856	10.37	1950	0.2214	0.0854
12	0.12	0.0030	3.399	0.1487	2.1170	0.8309	0.3925	10.39	1950	0.2038	0.0800
13	0.14	0.0036	3.368	0.1545	1.9490	0.8174	0.4194	10.39	1950	0.1876	0.0787
14	0.16	0.0041	3.342	0.1671	1.8170	0.8442	0.4646	10.44	1960	0.1740	0.0809
15	0.18	0.0046	3.368	0.1560	1.9500	0.8256	0.4234	10.47	1970	0.1862	0.0789
16	0.20	0.0051	3.339	0.1571	1.8030	0.7896	0.4380	10.44	1960	0.1727	0.0756
17	0.22	0.0056	3.331	0.1573	1.7620	0.7790	0.4421	10.45	1960	0.1686	0.0745
18	0.24	0.0061	3.297	0.1590	1.5960	0.7380	0.4623	10.48	1970	0.1523	0.0704
19	0.26	0.0066	3.307	0.1558	1.6460	0.7374	0.4480	10.47	1970	0.1572	0.0704
20	0.28	0.0071	3.300	0.1537	1.6110	0.7173	0.4453	10.50	1970	0.1534	0.0683
21	0.30	0.0076	3.281	0.1513	1.5250	0.6814	0.4469	10.52	1980	0.1450	0.0648
22	0.32	0.0081	3.274	0.1559	1.4950	0.6932	0.4636	10.52	1980	0.1421	0.0659
23	0.34	0.0086	3.290	0.1532	1.5650	0.7015	0.4483	10.53	1980	0.1486	0.0666
24	0.36	0.0091	3.249	0.1543	1.3850	0.6527	0.4713	10.52	1980	0.1317	0.0620
25	0.38	0.0097	3.236	0.1594	1.3320	0.6575	0.4935	10.54	1980	0.1264	0.0624
26	0.40	0.0102	3.240	0.1592	1.3460	0.6611	0.4910	10.52	1980	0.1279	0.0628
27	0.42	0.0107	3.221	0.1516	1.2720	0.6068	0.4772	10.55	1980	0.1206	0.0575
28	0.44	0.0112	3.225	0.1538	1.2860	0.6202	0.4821	10.56	1990	0.1218	0.0587
29	0.46	0.0117	3.256	0.1518	1.4160	0.6514	0.4601	10.48	1970	0.1351	0.0622

Appendix III, Table 1: Data for Fully Developed Boundary Layer

N	Y (in)	Y (m)	Ebar (volts)	Erms (volts)	Ubar (m/s)	Urms (m/s)	Turb. Int.	Uwall (m/s)	RPM	Ubar/Uwall	Urms/Uwall
30	0.48	0.0122	3.210	0.1499	1.2260	0.5856	0.4778	10.52	1980	0.1165	0.0557
31	0.50	0.0127	3.207	0.1548	1.2140	0.6012	0.4953	10.49	1970	0.1157	0.0573
32	0.52	0.0132	3.201	0.1529	1.1910	0.5864	0.4923	10.51	1980	0.1133	0.0558
33	0.54	0.0137	3.193	0.1557	1.1620	0.5876	0.5058	10.51	1980	0.1106	0.0559
34	0.56	0.0142	3.201	0.1354	1.1900	0.5189	0.4361	10.51	1980	0.1132	0.0494
35	0.58	0.0147	3.200	0.1512	1.1860	0.5783	0.4875	10.55	1980	0.1124	0.0548
36	0.60	0.0152	3.170	0.1494	1.0770	0.5369	0.4984	10.52	1980	0.1024	0.0510
37	0.65	0.0165	3.194	0.1457	1.1630	0.5505	0.4732	10.52	1980	0.1106	0.0523
38	0.70	0.0178	3.167	0.1527	1.0670	0.5458	0.5113	10.56	1990	0.1010	0.0517
39	0.75	0.0191	3.178	0.1532	1.1060	0.5601	0.5063	10.53	1980	0.1050	0.0532
40	0.80	0.0203	3.182	0.1365	1.1190	0.5030	0.4494	10.54	1980	0.1062	0.0477
41	0.85	0.0216	3.183	0.1515	1.1240	0.5598	0.4980	10.57	1990	0.1063	0.0530
42	0.90	0.0229	3.166	0.1473	1.0620	0.5244	0.4939	10.55	1980	0.1007	0.0497
43	0.95	0.0241	3.126	0.1518	0.9252	0.4949	0.5349	10.55	1980	0.0877	0.0469
44	1.00	0.0254	3.118	0.1467	0.8997	0.4697	0.5220	10.54	1980	0.0854	0.0446
45	1.10	0.0279	3.139	0.1516	0.9704	0.5095	0.5250	10.57	1990	0.0918	0.0482
46	1.20	0.0305	3.105	0.1320	0.8604	0.4107	0.4773	10.56	1990	0.0815	0.0389
47	1.30	0.0330	3.154	0.1477	1.0190	0.5122	0.5029	10.56	1990	0.0965	0.0485
48	1.40	0.0356	3.141	0.1398	0.9769	0.4720	0.4831	10.55	1980	0.0926	0.0447

Appendix III, Figure 1: Velocity Profiles for Fully Developed Flow



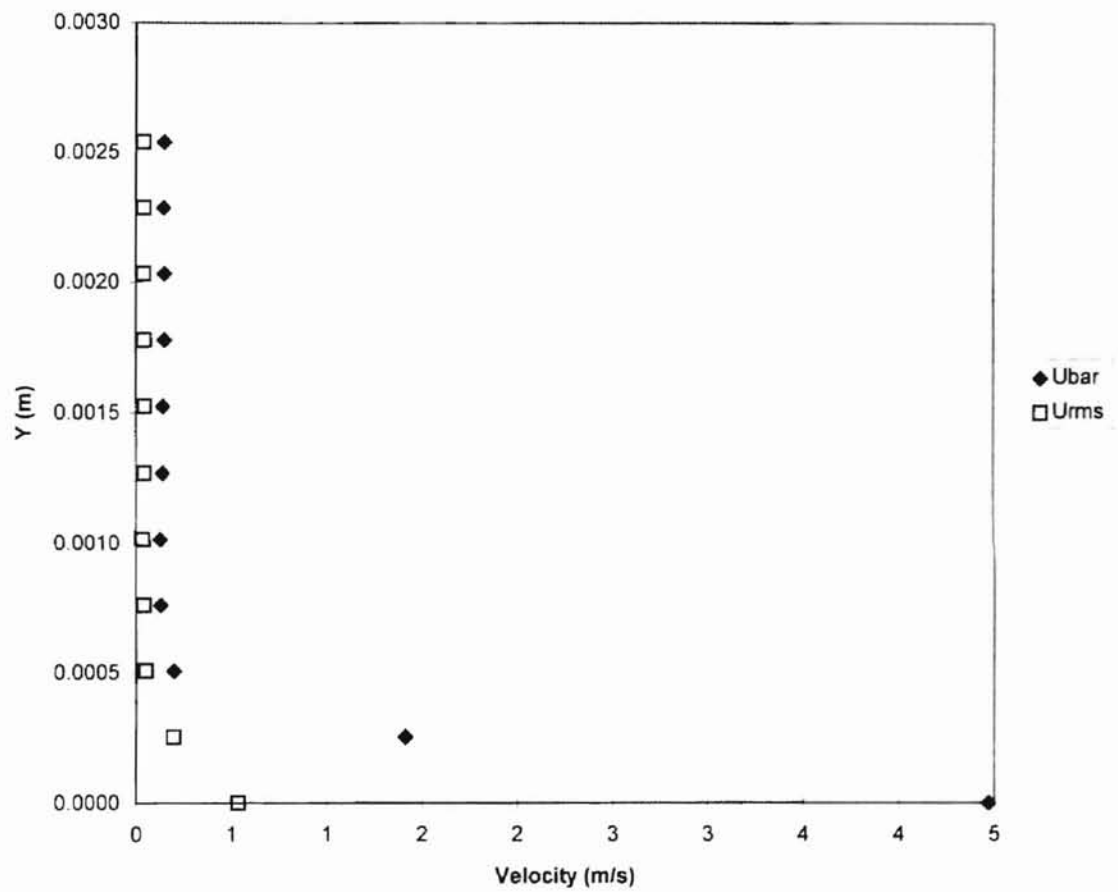
APPENDIX IV

Boundary Layer Data Behind Doctor Blade .

Appendix IV, Table 1: Boundary Layer Data 17 Degrees Behind Doctor Blade

N	Y (in)	Y (m)	Ebar (volts)	Erms (volts)	Ubar (m/s)	Urms (m/s)	Turb. Int.	Uwall (m/s)	RPM	(Uw-U)/Uw
1	0.00	0.00000	3.875	0.060	4.471	0.534	0.120	10.43	1961	0.571
2	0.01	0.00025	3.391	0.047	1.412	0.195	0.138	10.53	1980	0.866
3	0.02	0.00051	2.910	0.042	0.199	0.051	0.254	10.60	1992	0.981
4	0.03	0.00076	2.844	0.044	0.129	0.041	0.319	10.64	1999	0.988
5	0.04	0.00102	2.840	0.037	0.125	0.034	0.272	10.67	2006	0.988
6	0.05	0.00127	2.853	0.042	0.137	0.040	0.295	10.76	2023	0.987
7	0.06	0.00152	2.855	0.044	0.140	0.043	0.306	10.79	2027	0.987
8	0.07	0.00178	2.865	0.042	0.150	0.042	0.283	10.81	2031	0.986
9	0.08	0.00203	2.866	0.041	0.150	0.041	0.274	10.83	2037	0.986
10	0.09	0.00229	2.862	0.043	0.146	0.043	0.291	10.85	2040	0.987
11	0.10	0.00254	2.865	0.041	0.149	0.041	0.274	10.84	2038	0.986
12	1.00	0.02540	2.753	0.049	0.060	0.029	0.481	10.85	2040	0.994

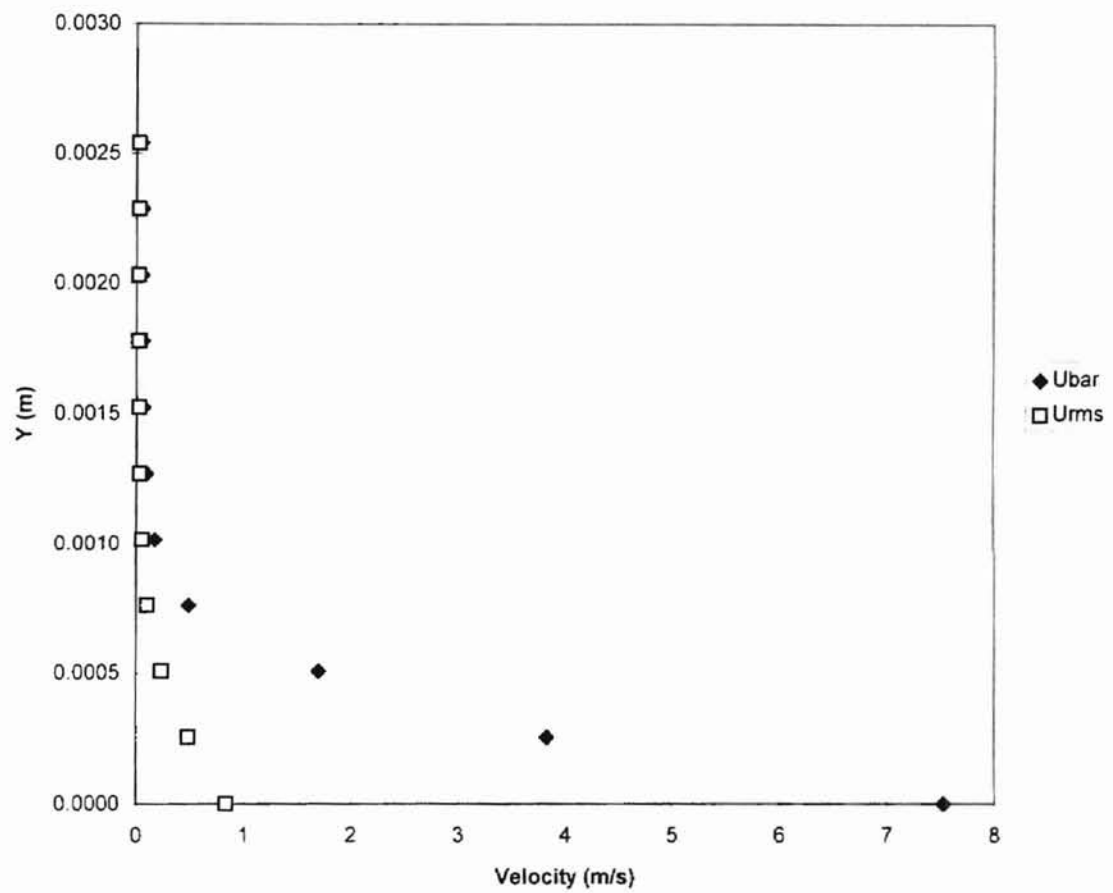
Appendix IV, Figure 1: Velocity Profiles 17 Degrees from Doctor Blade



Appendix IV, Table 2. Boundary Layer Data 36 Degrees Behind Doctor Blade

N	Y (in)	Y (m)	Ebar (volts)	Erms (volts)	Ubar (m/s)	Urms (m/s)	Turb. Int.	Uwall (m/s)	RPM	(Uw-U)/Uw
1	0.00	0.00000	4.157	0.064	7.529	0.841	0.112	10.62	1996	0.2911
2	0.01	0.00025	3.810	0.058	3.828	0.486	0.127	10.73	2017	0.6432
3	0.02	0.00051	3.485	0.048	1.700	0.236	0.139	10.82	2034	0.8429
4	0.03	0.00076	3.134	0.045	0.488	0.100	0.205	10.90	2049	0.9552
5	0.04	0.00102	2.946	0.046	0.173	0.053	0.309	10.96	2061	0.9842
6	0.05	0.00127	2.863	0.041	0.091	0.033	0.361	11.02	2071	0.9917
7	0.06	0.00152	2.827	0.038	0.065	0.025	0.389	11.07	2081	0.9941
8	0.07	0.00178	2.816	0.040	0.058	0.025	0.422	11.12	2091	0.9948
9	0.08	0.00203	2.809	0.041	0.054	0.024	0.454	11.15	2096	0.9952
10	0.09	0.00229	2.819	0.043	0.060	0.027	0.450	11.15	2096	0.9947
11	0.10	0.00254	2.801	0.042	0.049	0.024	0.479	11.19	2104	0.9956
12	1.00	0.02540	2.807	0.049	0.052	0.028	0.541	11.21	2107	0.9953

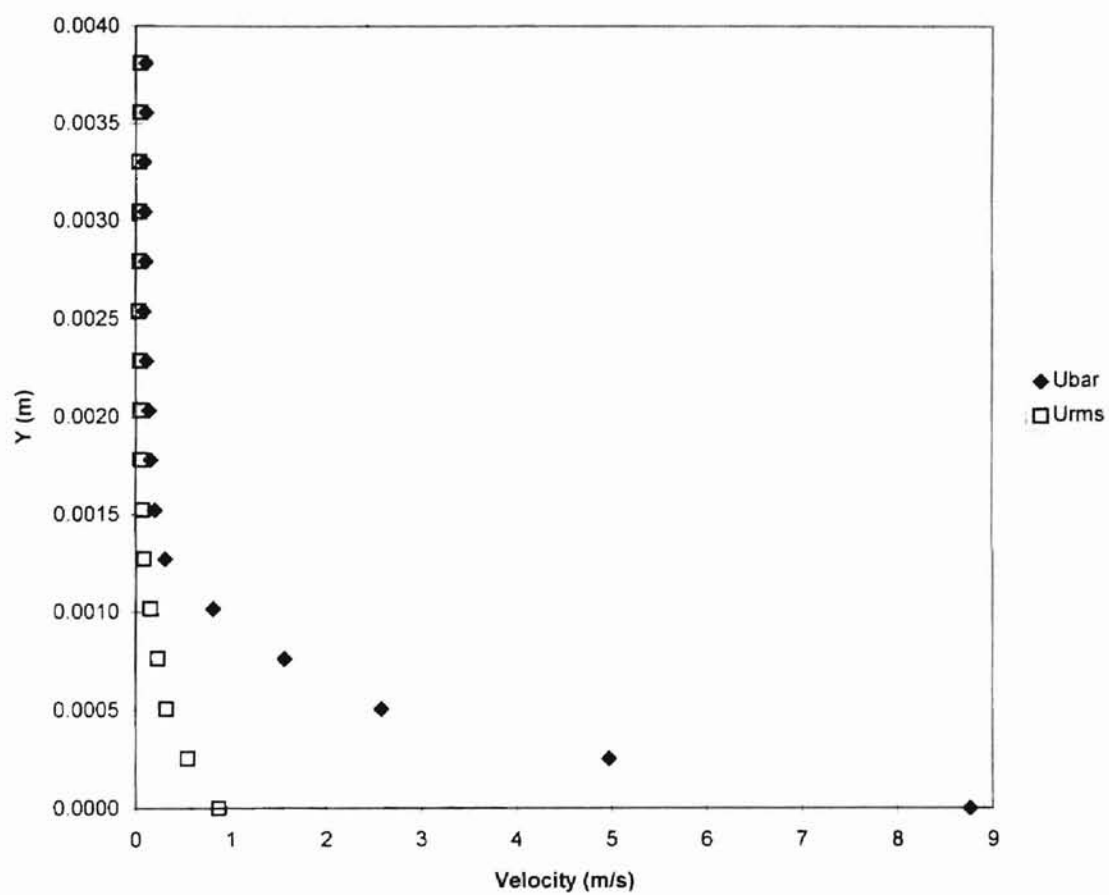
Appendix IV, Figure 2: Velocity Profiles 36 Degrees from Doctor Blade



Appendix IV, Table 3: Boundary Layer Data 69 Degrees Behind Doctor Blade

N	Y (in)	Y (m)	Ebar (volts)	Erms (volts)	Ubar (m/s)	Urms (m/s)	Turb. Int.	Uwall (m/s)	RPM	(Uw-U)/Uw
1	0.00	0.00000	4.2350	0.0591	8.7660	0.8705	0.0993	10.41	1957	0.1579
2	0.01	0.00025	3.9260	0.0545	4.9780	0.5449	0.1095	10.75	2021	0.5369
3	0.02	0.00051	3.6320	0.0495	2.5790	0.3189	0.1236	10.89	2048	0.7632
4	0.03	0.00076	3.4470	0.0501	1.5590	0.2323	0.1490	11.02	2071	0.8585
5	0.04	0.00102	3.2510	0.0508	0.8106	0.1552	0.1915	11.11	2089	0.9270
6	0.05	0.00127	3.0350	0.0515	0.3065	0.0859	0.2803	11.12	2091	0.9724
7	0.06	0.00152	2.9630	0.0557	0.2008	0.0720	0.3586	11.18	2101	0.9820
8	0.07	0.00178	2.9230	0.0456	0.1526	0.0500	0.3277	11.21	2108	0.9864
9	0.08	0.00203	2.9100	0.0507	0.1388	0.0525	0.3783	11.26	2117	0.9877
10	0.09	0.00229	2.8840	0.0488	0.1136	0.0448	0.3945	11.28	2121	0.9899
11	0.10	0.00254	2.8520	0.0417	0.0861	0.0326	0.3779	11.28	2120	0.9924
12	0.11	0.00279	2.8760	0.0448	0.1059	0.0395	0.3734	11.27	2119	0.9906
13	0.12	0.00305	2.8620	0.0440	0.0944	0.0363	0.3839	11.29	2122	0.9916
14	0.13	0.00330	2.8530	0.0424	0.0872	0.0334	0.3827	11.29	2122	0.9923
15	0.14	0.00356	2.8800	0.0486	0.1100	0.0438	0.3982	11.33	2130	0.9903
16	0.15	0.00381	2.8740	0.0488	0.1042	0.0426	0.4092	11.30	2124	0.9908
17	1.00	0.02540	2.8690	0.0531	0.1003	0.0453	0.4519	11.29	2123	0.9911

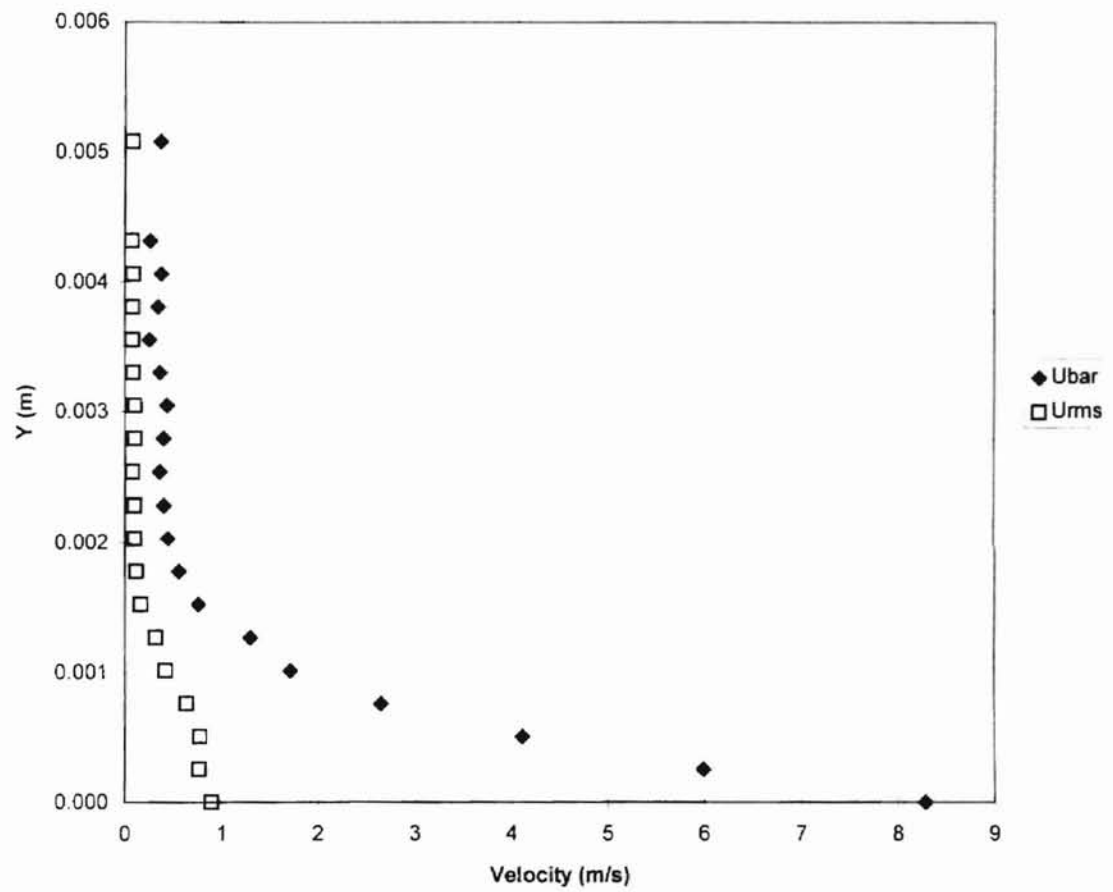
Appendix IV, Figure 3: Velocity Profiles 69 Degrees from Doctor Blade



Appendix IV, Table 4: Boundary Layer Data 93 Degrees Behind Doctor Blade

N	Y (in)	Y (m)	Ebar (volts)	Erms (volts)	Ubar (m/s)	Urms (m/s)	Turb. Int.	Uwall (m/s)	RPM	(Uw-U)/Uw
1	0.00	0.0000	4.171	0.0666	8.2900	0.9001	0.1086	10.20	1917	0.1873
2	0.01	0.0003	3.981	0.0715	5.9920	0.7725	0.1289	10.40	1955	0.4238
3	0.02	0.0005	3.784	0.0931	4.1130	0.7774	0.1890	10.43	1961	0.6057
4	0.03	0.0008	3.582	0.1026	2.6490	0.6366	0.2404	10.50	1974	0.7477
5	0.04	0.0010	3.408	0.0903	1.7090	0.4187	0.2450	10.54	1981	0.8379
6	0.05	0.0013	3.311	0.0820	1.2950	0.3172	0.2449	10.56	1985	0.8774
7	0.06	0.0015	3.147	0.0604	0.7568	0.1652	0.2183	10.64	2001	0.9289
8	0.07	0.0018	3.067	0.0512	0.5569	0.1154	0.2072	10.64	2000	0.9477
9	0.08	0.0020	3.013	0.0514	0.4436	0.1003	0.2261	10.65	2001	0.9583
10	0.09	0.0023	2.991	0.0528	0.4027	0.0971	0.2411	10.68	2007	0.9623
11	0.10	0.0025	2.966	0.0492	0.3576	0.0840	0.2349	10.69	2010	0.9665
12	0.11	0.0028	2.989	0.0558	0.3989	0.1019	0.2553	10.71	2013	0.9628
13	0.12	0.0030	3.009	0.0528	0.4365	0.1021	0.2338	10.73	2017	0.9593
14	0.13	0.0033	2.969	0.0486	0.3634	0.0838	0.2307	10.76	2023	0.9662
15	0.14	0.0036	2.899	0.0558	0.2553	0.0774	0.3030	10.76	2022	0.9763
16	0.15	0.0038	2.959	0.0479	0.3460	0.0801	0.2314	10.75	2020	0.9678
17	0.16	0.0041	2.979	0.0492	0.3805	0.0873	0.2296	10.78	2026	0.9647
18	0.17	0.0043	2.906	0.0513	0.2648	0.0728	0.2748	10.77	2025	0.9754
19	0.20	0.0051	2.975	0.0452	0.3730	0.0792	0.2122	10.79	2029	0.9654
20	1.00	0.0254	2.914	0.0557	0.2765	0.0811	0.2932	10.84	2037	0.9745

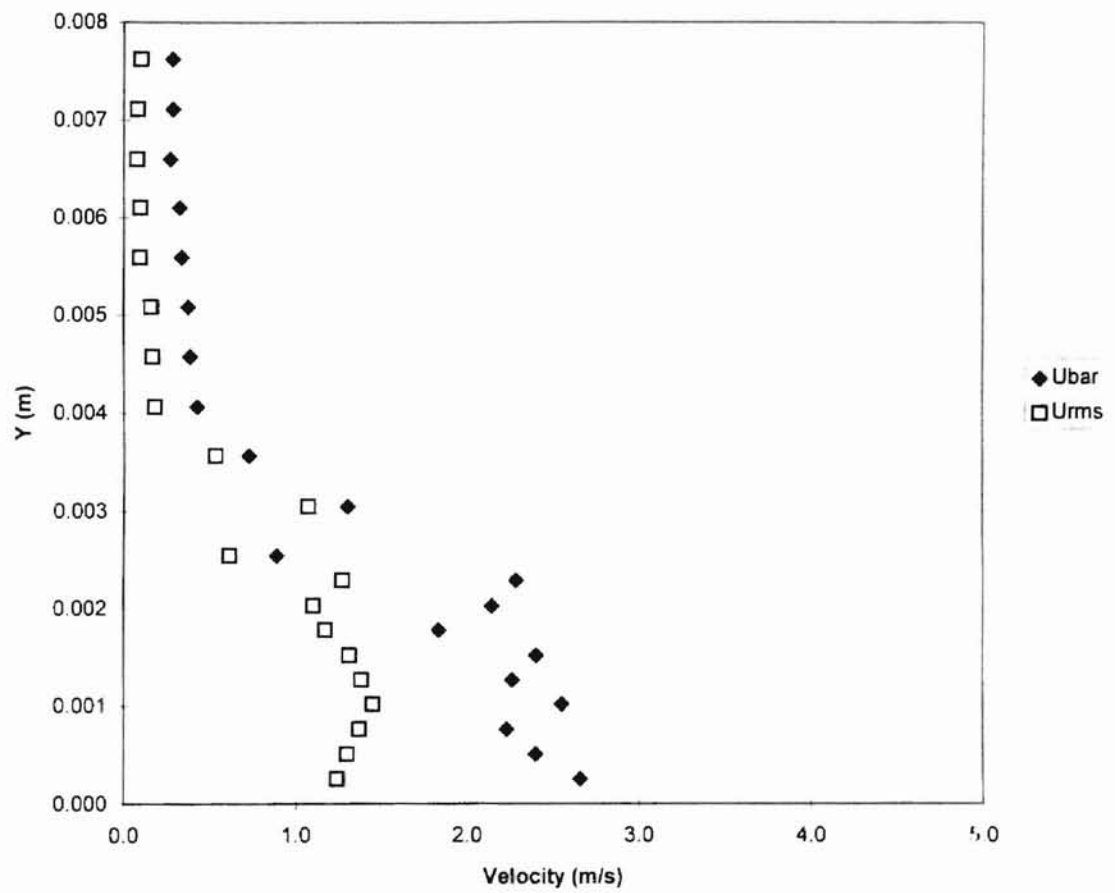
Appendix IV, Figure 4: Velocity Profiles 93 Degrees from Doctor Blade



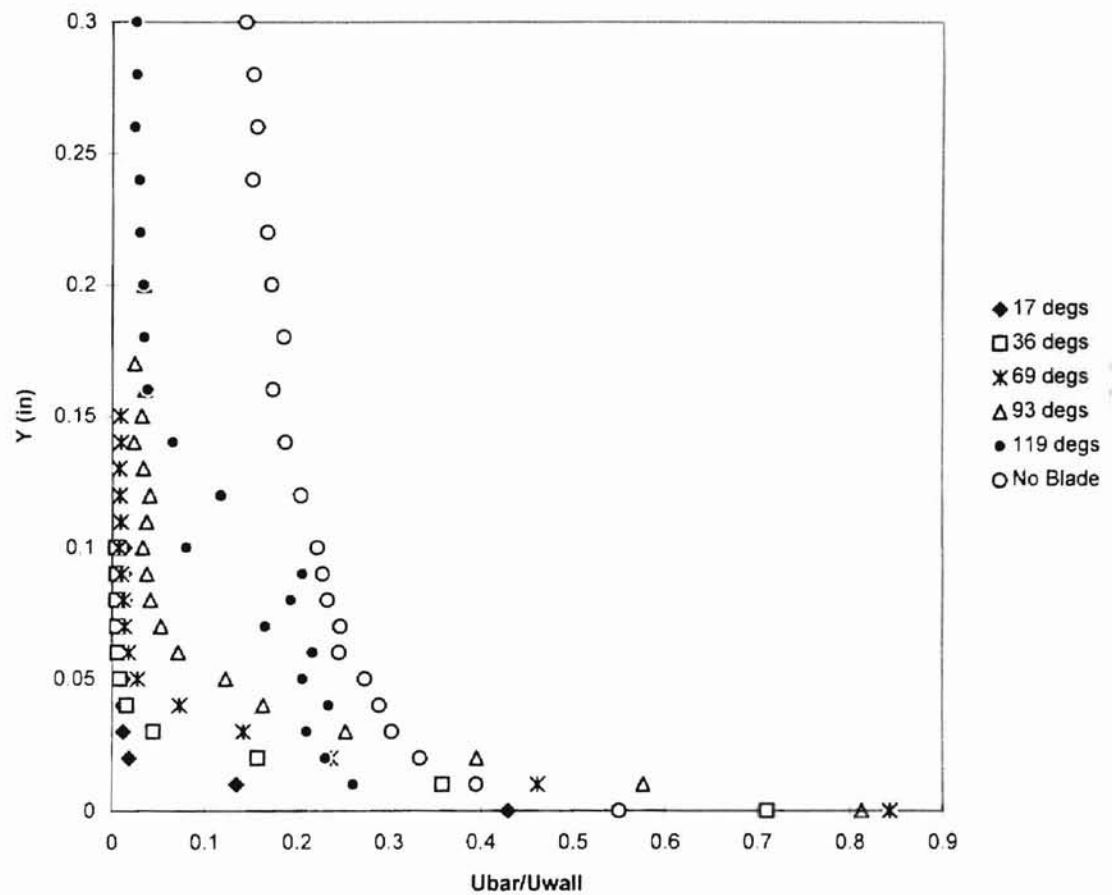
Appendix IV, Table 5: Boundary Layer Data 119 Degrees Behind Doctor Blade

N	Y (in)	Y (m)	Ebar (volts)	Erms (volts)	Ubar (m/s)	Urms (m/s)	Turb. Int.	Uwall (m/s)	RPM	(Uw-U)/Uw
1	0.01	0.00025	3.73	0.1920	2.660	1.2400	0.467	10.20	1910	0.7392
2	0.02	0.00051	3.69	0.2150	2.400	1.3000	0.542	10.40	1950	0.7692
3	0.03	0.00076	3.66	0.2370	2.230	1.3700	0.613	10.60	1990	0.7896
4	0.04	0.00102	3.71	0.2310	2.550	1.4500	0.570	10.90	2040	0.7661
5	0.05	0.00127	3.67	0.2370	2.260	1.3800	0.608	11.00	2070	0.7945
6	0.06	0.00152	3.69	0.2160	2.400	1.3100	0.545	11.10	2080	0.7838
7	0.07	0.00178	3.59	0.2320	1.830	1.1700	0.640	11.10	2080	0.8351
8	0.08	0.00203	3.64	0.1960	2.140	1.1000	0.514	11.10	2090	0.8072
9	0.09	0.00229	3.67	0.2170	2.280	1.2700	0.556	11.10	2090	0.7946
10	0.10	0.00254	3.36	0.1930	0.888	0.6130	0.691	11.10	2090	0.9200
11	0.12	0.00305	3.47	0.2640	1.300	1.0700	0.824	11.10	2090	0.8829
12	0.14	0.00356	3.30	0.1900	0.727	0.5330	0.733	11.10	2080	0.9345
13	0.16	0.00406	3.18	0.0907	0.428	0.1830	0.427	11.10	2080	0.9614
14	0.18	0.00457	3.16	0.0895	0.387	0.1700	0.438	11.10	2080	0.9651
15	0.20	0.00508	3.15	0.0865	0.376	0.1610	0.428	11.10	2090	0.9661
16	0.22	0.00559	3.13	0.0546	0.340	0.0957	0.281	11.10	2080	0.9694
17	0.24	0.00610	3.12	0.0580	0.327	0.0989	0.303	11.10	2080	0.9705
18	0.26	0.00660	3.09	0.0507	0.274	0.0778	0.284	11.10	2080	0.9753
19	0.28	0.00711	3.10	0.0512	0.288	0.0809	0.281	11.00	2080	0.9738
20	0.30	0.00762	3.10	0.0649	0.287	0.1020	0.356	11.10	2080	0.9741
21	1.00	0.02540	3.00	0.0422	0.159	0.0465	0.294	11.10	2080	0.9857

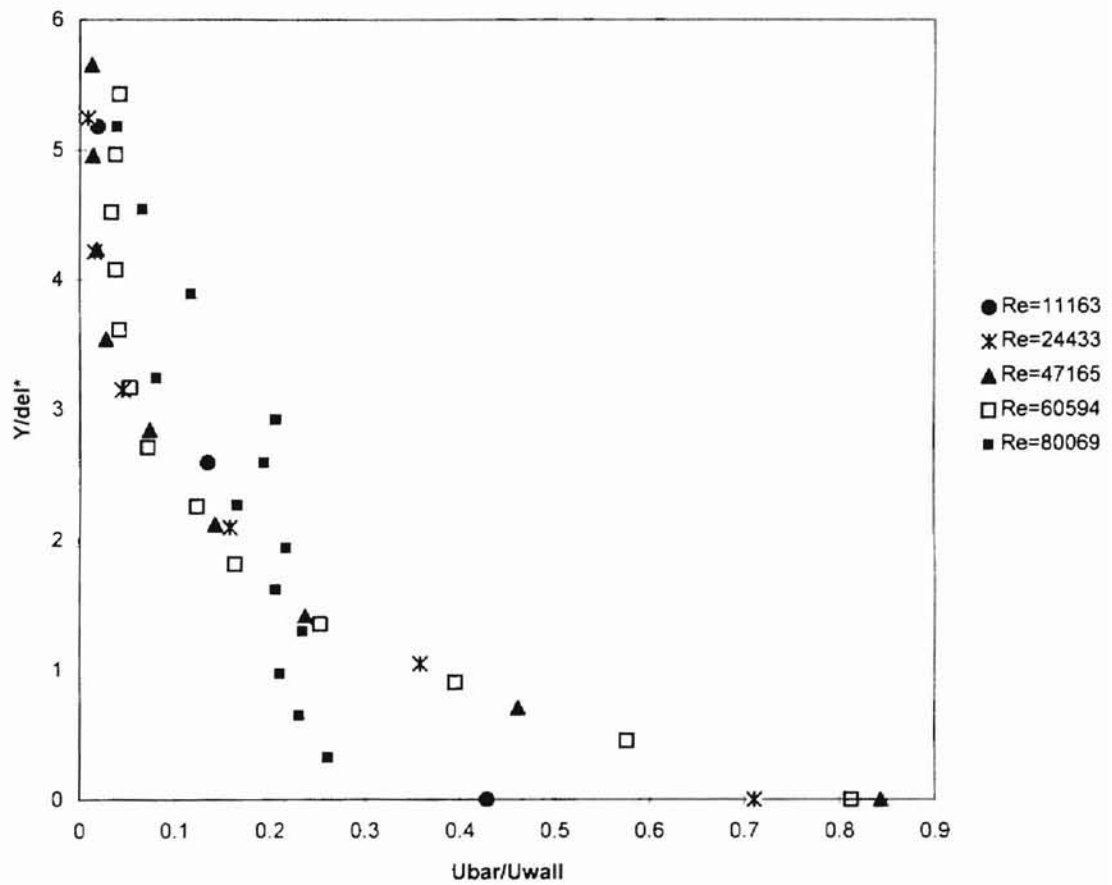
Appendix IV, Figure 5: Velocity Profiles 119 Degrees from Doctor Blade



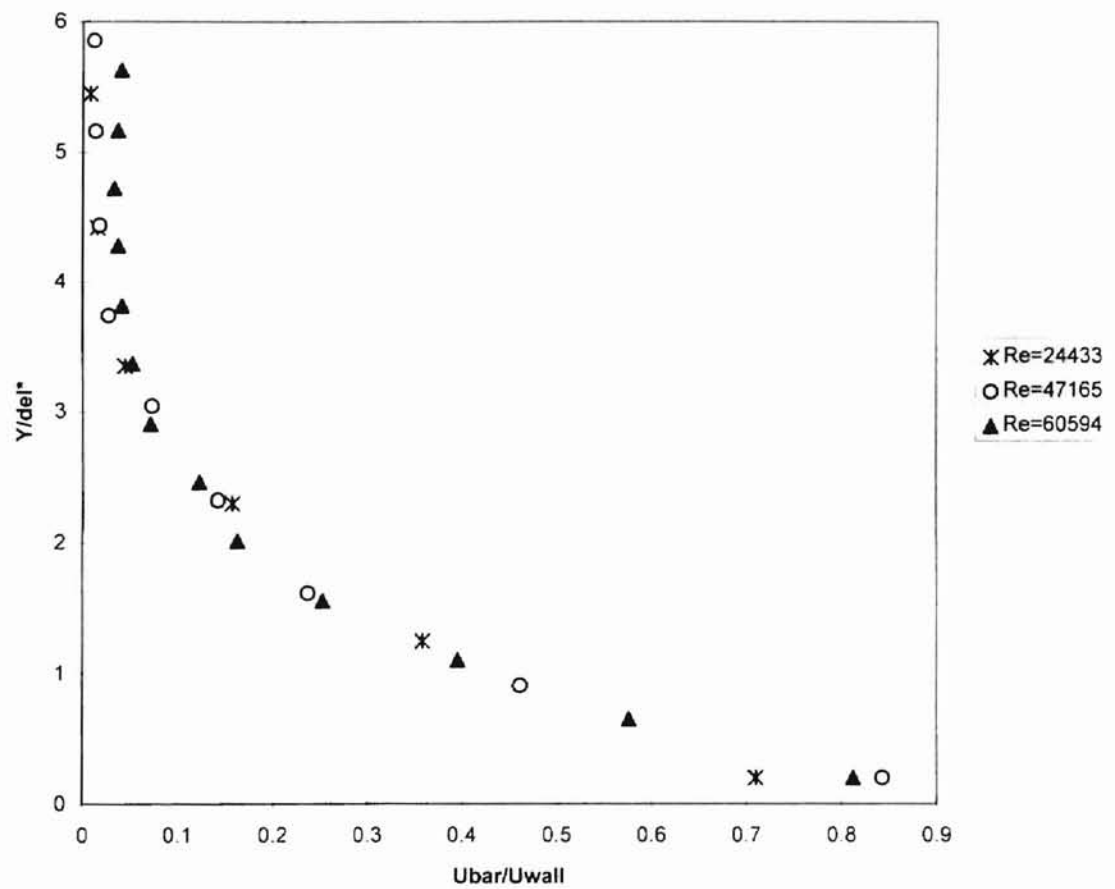
Appendix IV, Figure 6: Velocity Profiles For All Experiments



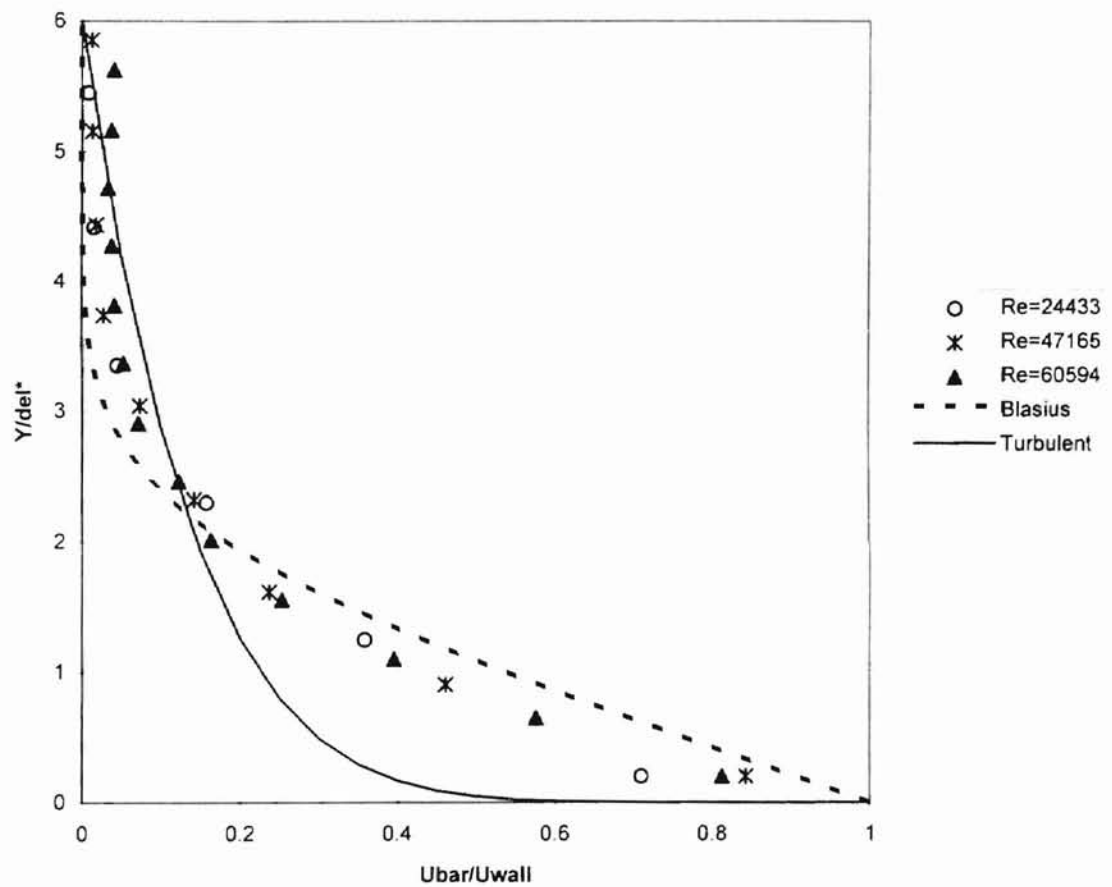
Appendix IV, Figure 7: Dimensionless Velocity Profiles Behind Doctor Blade



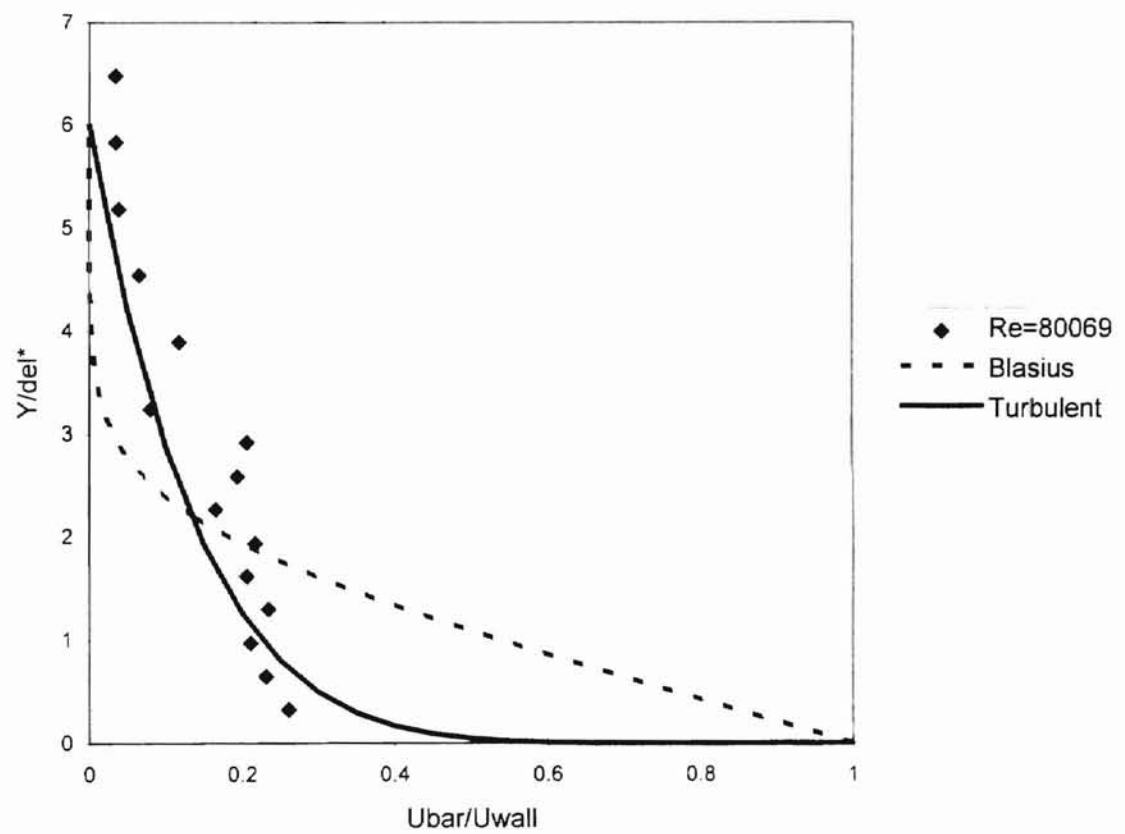
Appendix IV, Figure 8: Dimensionless Velocity Profiles for Laminar Region



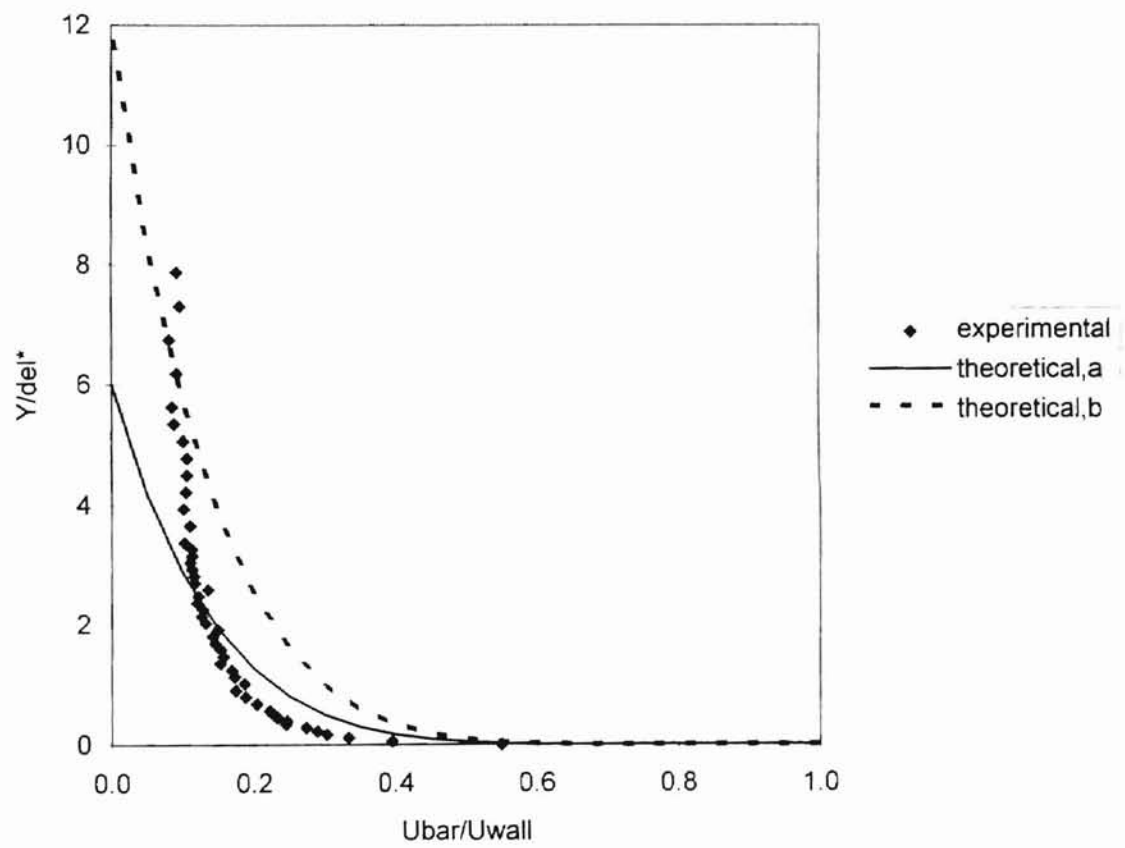
Appendix IV, Figure 9: Comparison With Theoretical Estimates of Velocity Profiles in Laminar Region



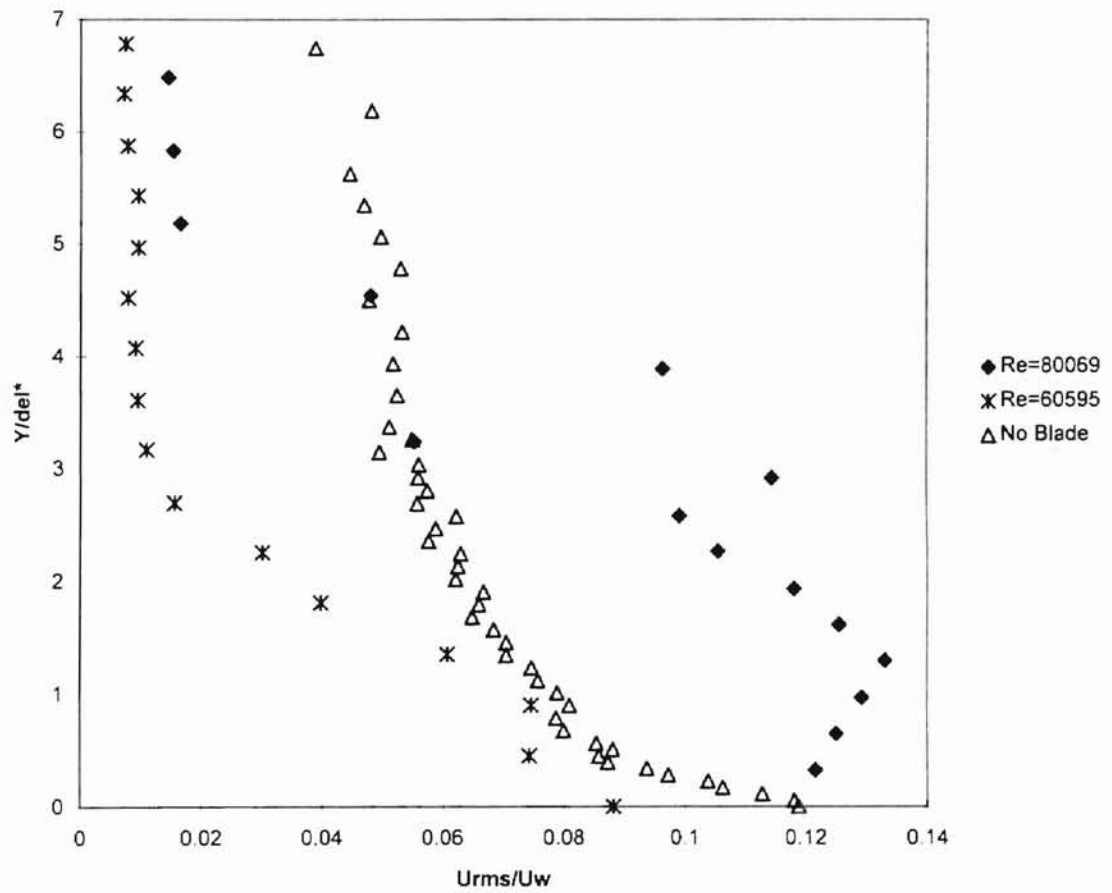
Appendix IV, Figure 10: Comparison Between Experimental Transition Region and Flat Plate Laminar and Turbulent Velocity Profiles



Appendix IV, Figure 11: Comparison Between Fully Developed Experimental and 1/7 Power Law Turbulent Profiles



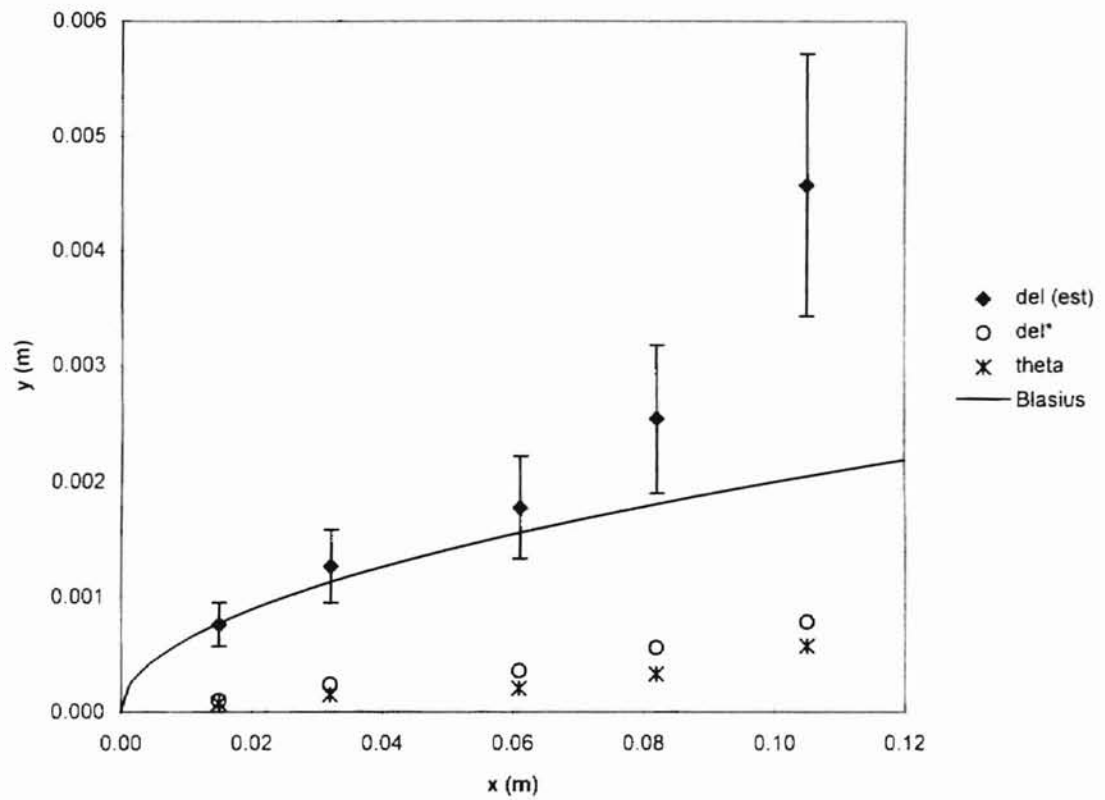
Appendix IV, Figure 12: Turbulent Intensity Profiles Before, During and After Transition



Appendix IV, Table 6: Boundary Layer Characteristics For All Experiments

N	Angle (degrees)	x (m)	Re(x)	δ (estimate) (m)	δ^* (m)	θ (m)	Q (m ² /s)	H
1	17	0.02	11163	0.000762	0.0000981	0.0000763	0.00124	1.29
2	36	0.03	24433	0.001270	0.0002420	0.0001500	0.00262	1.61
3	69	0.06	47165	0.001778	0.0003590	0.0002070	0.00401	1.73
4	93	0.08	60595	0.002540	0.0005620	0.0003310	0.00629	1.70
5	119	0.11	80069	0.004572	0.0007840	0.0005750	0.00924	1.36
6	-	-	-	-	0.00452	0.00383	-	1.18

Appendix IV, Figure 13: Boundary Layer Characteristics Behind Doctor Blade



APPENDIX V

Boundary Layer Data Over Width of Roller.

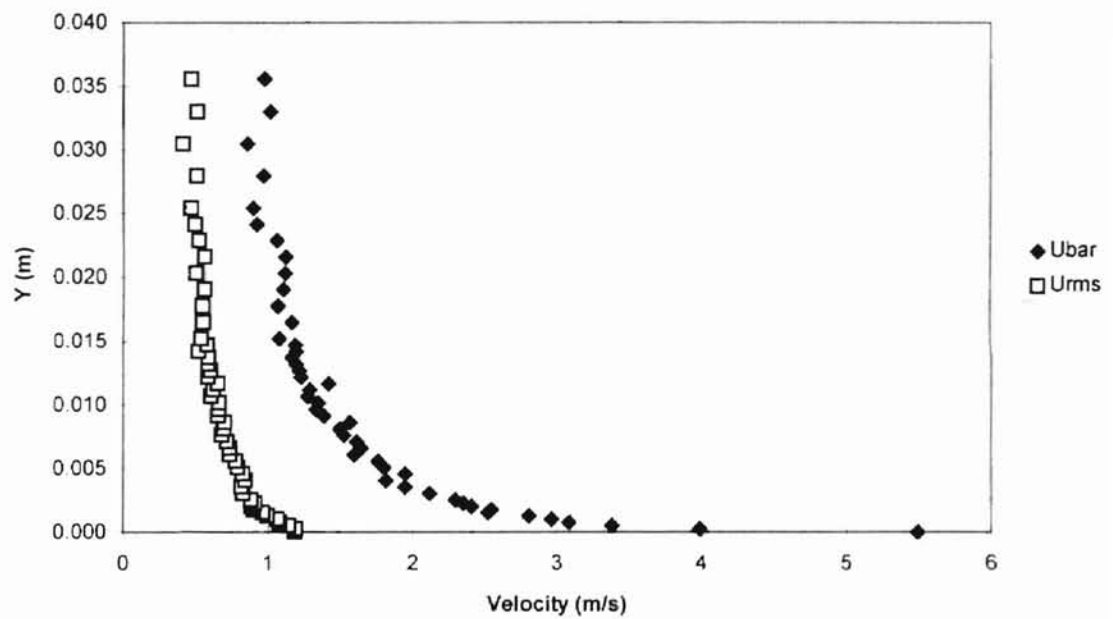
Appendix V, Table 1: Boundary Layer Data for Central Position

N	Y (in)	Y (m)	Ebar (volts)	Erms (volts)	Ubar (m/s)	Urms (m/s)	Turb. Int.	Uwall (m/s)	RPM	Ubar/Uwall	Urms/Uwall
1	0.00	0.0000	3.823	0.1117	5.4960	1.1870	0.2160	9.99	1880	0.5502	0.1188
2	0.01	0.0003	3.666	0.1397	3.9900	1.1930	0.2991	10.10	1900	0.3950	0.1181
3	0.02	0.0005	3.591	0.1498	3.3810	1.1440	0.3384	10.14	1910	0.3334	0.1128
4	0.03	0.0008	3.551	0.1508	3.0840	1.0830	0.3511	10.19	1920	0.3026	0.1063
5	0.04	0.0010	3.533	0.1525	2.9620	1.0650	0.3596	10.25	1930	0.2890	0.1039
6	0.05	0.0013	3.511	0.1483	2.8060	0.9992	0.3561	10.27	1930	0.2732	0.0973
7	0.06	0.0015	3.467	0.1538	2.5230	0.9655	0.3827	10.30	1940	0.2450	0.0937
8	0.07	0.0018	3.471	0.1428	2.5460	0.9018	0.3542	10.33	1940	0.2465	0.0873
9	0.08	0.0020	3.449	0.1460	2.4090	0.8888	0.3689	10.36	1950	0.2325	0.0858
10	0.09	0.0023	3.439	0.1522	2.3510	0.9116	0.3877	10.35	1950	0.2271	0.0881
11	0.10	0.0025	3.430	0.1501	2.2960	0.8851	0.3856	10.37	1950	0.2214	0.0854
12	0.12	0.0030	3.399	0.1487	2.1170	0.8309	0.3925	10.39	1950	0.2038	0.0800
13	0.14	0.0036	3.368	0.1545	1.9490	0.8174	0.4194	10.39	1950	0.1876	0.0787
14	0.16	0.0041	3.342	0.1671	1.8170	0.8442	0.4646	10.44	1960	0.1740	0.0809
15	0.18	0.0046	3.368	0.1560	1.9500	0.8256	0.4234	10.47	1970	0.1862	0.0789
16	0.20	0.0051	3.339	0.1571	1.8030	0.7896	0.4380	10.44	1960	0.1727	0.0756
17	0.22	0.0056	3.331	0.1573	1.7620	0.7790	0.4421	10.45	1960	0.1686	0.0745
18	0.24	0.0061	3.297	0.1590	1.5960	0.7380	0.4623	10.48	1970	0.1523	0.0704
19	0.26	0.0066	3.307	0.1558	1.6460	0.7374	0.4480	10.47	1970	0.1572	0.0704
20	0.28	0.0071	3.300	0.1537	1.6110	0.7173	0.4453	10.50	1970	0.1534	0.0683
21	0.30	0.0076	3.281	0.1513	1.5250	0.6814	0.4469	10.52	1980	0.1450	0.0648
22	0.32	0.0081	3.274	0.1559	1.4950	0.6932	0.4636	10.52	1980	0.1421	0.0659
23	0.34	0.0086	3.290	0.1532	1.5650	0.7015	0.4483	10.53	1980	0.1486	0.0666
24	0.36	0.0091	3.249	0.1543	1.3850	0.6527	0.4713	10.52	1980	0.1317	0.0620
25	0.38	0.0097	3.236	0.1594	1.3320	0.6575	0.4935	10.54	1980	0.1264	0.0624
26	0.40	0.0102	3.240	0.1592	1.3460	0.6611	0.4910	10.52	1980	0.1279	0.0628
27	0.42	0.0107	3.221	0.1516	1.2720	0.6068	0.4772	10.55	1980	0.1206	0.0575
28	0.44	0.0112	3.225	0.1538	1.2860	0.6202	0.4821	10.56	1990	0.1218	0.0587
29	0.46	0.0117	3.256	0.1518	1.4160	0.6514	0.4601	10.48	1970	0.1351	0.0622

Appendix V, Table 1: Boundary Layer Data for Central Position

N	Y (in)	Y (m)	Ebar (volts)	Erms (volts)	Ubar (m/s)	Urms (m/s)	Turb. Int.	Uwall (m/s)	RPM	Ubar/Uwall	Urms/Uwall
30	0.48	0.0122	3.210	0.1499	1.2260	0.5856	0.4778	10.52	1980	0.1165	0.0557
31	0.50	0.0127	3.207	0.1548	1.2140	0.6012	0.4953	10.49	1970	0.1157	0.0573
32	0.52	0.0132	3.201	0.1529	1.1910	0.5864	0.4923	10.51	1980	0.1133	0.0558
33	0.54	0.0137	3.193	0.1557	1.1620	0.5876	0.5058	10.51	1980	0.1106	0.0559
34	0.56	0.0142	3.201	0.1354	1.1900	0.5189	0.4361	10.51	1980	0.1132	0.0494
35	0.58	0.0147	3.200	0.1512	1.1860	0.5783	0.4875	10.55	1980	0.1124	0.0548
36	0.60	0.0152	3.170	0.1494	1.0770	0.5369	0.4984	10.52	1980	0.1024	0.0510
37	0.65	0.0165	3.194	0.1457	1.1630	0.5505	0.4732	10.52	1980	0.1106	0.0523
38	0.70	0.0178	3.167	0.1527	1.0670	0.5458	0.5113	10.56	1990	0.1010	0.0517
39	0.75	0.0191	3.178	0.1532	1.1060	0.5601	0.5063	10.53	1980	0.1050	0.0532
40	0.80	0.0203	3.182	0.1365	1.1190	0.5030	0.4494	10.54	1980	0.1062	0.0477
41	0.85	0.0216	3.183	0.1515	1.1240	0.5598	0.4980	10.57	1990	0.1063	0.0530
42	0.90	0.0229	3.166	0.1473	1.0620	0.5244	0.4939	10.55	1980	0.1007	0.0497
43	0.95	0.0241	3.126	0.1518	0.9252	0.4949	0.5349	10.55	1980	0.0877	0.0469
44	1.00	0.0254	3.118	0.1467	0.8997	0.4697	0.5220	10.54	1980	0.0854	0.0446
45	1.10	0.0279	3.139	0.1516	0.9704	0.5095	0.5250	10.57	1990	0.0918	0.0482
46	1.20	0.0305	3.105	0.1320	0.8604	0.4107	0.4773	10.56	1990	0.0815	0.0389
47	1.30	0.0330	3.154	0.1477	1.0190	0.5122	0.5029	10.56	1990	0.0965	0.0485
48	1.40	0.0356	3.141	0.1398	0.9769	0.4720	0.4831	10.55	1980	0.0926	0.0447

Appendix V, Figure 1: Velocity Profiles for Central Position



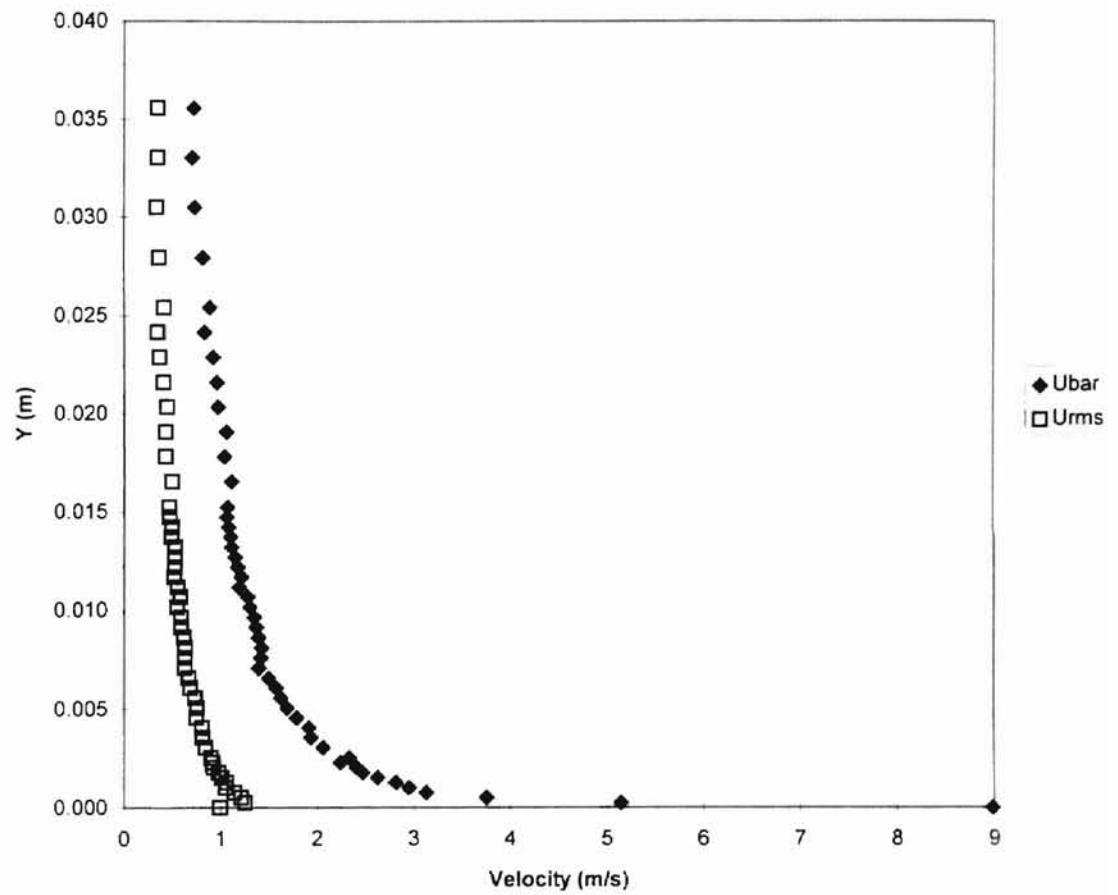
Appendix V, Table 2: Boundary Layer Data for Left Position

N	Y (in)	Y (m)	Ebar (volts)	Erms (volts)	Ubar (m/s)	Urms (m/s)	Turb. Int.	Uwall (m/s)	RPM	Ubar/Uwall	Urms/Uwall
1	0.00	0.00000	4.260	0.066	8.991	0.997	0.111	10.11	1900	0.8893	0.0986
2	0.01	0.00025	3.954	0.122	5.148	1.253	0.243	10.26	1928	0.5018	0.1221
3	0.02	0.00051	3.803	0.146	3.753	1.213	0.323	10.36	1947	0.3623	0.1171
4	0.03	0.00076	3.724	0.156	3.131	1.145	0.366	10.48	1969	0.2988	0.1093
5	0.04	0.00102	3.699	0.149	2.952	1.054	0.357	10.54	1982	0.2801	0.1000
6	0.05	0.00127	3.680	0.155	2.818	1.064	0.378	10.54	1981	0.2674	0.1009
7	0.06	0.00152	3.651	0.155	2.626	1.014	0.386	10.63	1998	0.2470	0.0954
8	0.07	0.00178	3.627	0.156	2.473	0.981	0.397	10.70	2011	0.2311	0.0917
9	0.08	0.00203	3.617	0.150	2.409	0.925	0.384	10.67	2006	0.2258	0.0867
10	0.09	0.00229	3.589	0.156	2.240	0.918	0.410	10.70	2012	0.2093	0.0858
11	0.10	0.00254	3.605	0.149	2.332	0.900	0.386	10.72	2015	0.2175	0.0840
12	0.12	0.00305	3.558	0.151	2.059	0.842	0.409	10.75	2022	0.1915	0.0783
13	0.14	0.00356	3.534	0.152	1.931	0.811	0.420	10.73	2017	0.1800	0.0756
14	0.16	0.00406	3.530	0.152	1.912	0.806	0.422	10.78	2026	0.1774	0.0748
15	0.18	0.00457	3.506	0.147	1.785	0.749	0.420	10.77	2024	0.1657	0.0695
16	0.20	0.00508	3.486	0.154	1.685	0.756	0.449	10.76	2022	0.1566	0.0703
17	0.22	0.00559	3.473	0.153	1.620	0.732	0.452	10.78	2027	0.1503	0.0679
18	0.24	0.00610	3.462	0.146	1.570	0.683	0.435	10.75	2021	0.1460	0.0635
19	0.26	0.00660	3.445	0.147	1.494	0.667	0.446	10.74	2019	0.1391	0.0621
20	0.28	0.00711	3.423	0.145	1.393	0.627	0.450	10.76	2023	0.1295	0.0583
21	0.30	0.00762	3.427	0.144	1.412	0.629	0.445	10.77	2024	0.1311	0.0584
22	0.32	0.00813	3.429	0.144	1.420	0.632	0.445	10.77	2025	0.1318	0.0587
23	0.34	0.00864	3.422	0.143	1.390	0.617	0.444	10.76	2023	0.1292	0.0573
24	0.36	0.00914	3.416	0.138	1.363	0.589	0.432	10.77	2024	0.1266	0.0547
25	0.38	0.00965	3.411	0.139	1.342	0.587	0.437	10.77	2025	0.1246	0.0545
26	0.40	0.01016	3.400	0.132	1.297	0.547	0.421	10.77	2024	0.1204	0.0508
27	0.42	0.01067	3.395	0.142	1.276	0.581	0.455	10.77	2024	0.1185	0.0540
28	0.44	0.01118	3.373	0.141	1.188	0.553	0.465	10.78	2026	0.1102	0.0513
29	0.46	0.01168	3.378	0.131	1.209	0.518	0.429	10.80	2031	0.1119	0.0480

Appendix V, Table 2: Boundary Layer Data for Left Position

N	Y (in)	Y (m)	Ebar (volts)	Erms (volts)	Ubar (m/s)	Urms (m/s)	Turb. Int.	Uwall (m/s)	RPM	Ubar/Uwall	Urms/Uwall
30	0.48	0.01219	3.369	0.135	1.172	0.523	0.446	10.77	2025	0.1088	0.0485
31	0.50	0.01270	3.362	0.138	1.145	0.527	0.461	10.79	2028	0.1061	0.0489
32	0.52	0.01321	3.352	0.141	1.107	0.528	0.477	10.81	2032	0.1024	0.0488
33	0.54	0.01372	3.349	0.132	1.097	0.488	0.445	10.79	2027	0.1017	0.0453
34	0.56	0.01422	3.344	0.136	1.077	0.498	0.462	10.82	2034	0.0995	0.0460
35	0.58	0.01473	3.339	0.131	1.059	0.474	0.448	10.78	2026	0.0982	0.0440
36	0.60	0.01524	3.341	0.128	1.067	0.466	0.437	10.81	2031	0.0987	0.0431
37	0.65	0.01651	3.352	0.133	1.107	0.497	0.449	10.78	2027	0.1027	0.0461
38	0.70	0.01778	3.333	0.119	1.038	0.428	0.412	10.78	2027	0.0963	0.0397
39	0.75	0.01905	3.339	0.118	1.059	0.428	0.404	10.80	2029	0.0981	0.0396
40	0.80	0.02032	3.314	0.131	0.972	0.449	0.462	10.82	2034	0.0898	0.0415
41	0.85	0.02159	3.312	0.120	0.964	0.410	0.425	10.81	2032	0.0892	0.0379
42	0.90	0.02286	3.300	0.111	0.924	0.370	0.400	10.79	2028	0.0856	0.0343
43	0.95	0.02413	3.272	0.112	0.835	0.350	0.419	10.81	2032	0.0773	0.0324
44	1.00	0.02540	3.289	0.128	0.890	0.416	0.467	10.79	2028	0.0824	0.0385
45	1.10	0.02794	3.267	0.117	0.817	0.361	0.442	10.84	2038	0.0754	0.0333
46	1.20	0.03048	3.238	0.118	0.733	0.339	0.462	10.80	2030	0.0679	0.0314
47	1.30	0.03302	3.229	0.125	0.707	0.351	0.497	10.78	2026	0.0656	0.0326
48	1.40	0.03556	3.235	0.123	0.724	0.351	0.485	10.81	2031	0.0670	0.0325

Appendix V, Figure 2: Velocity Profiles for Left Position



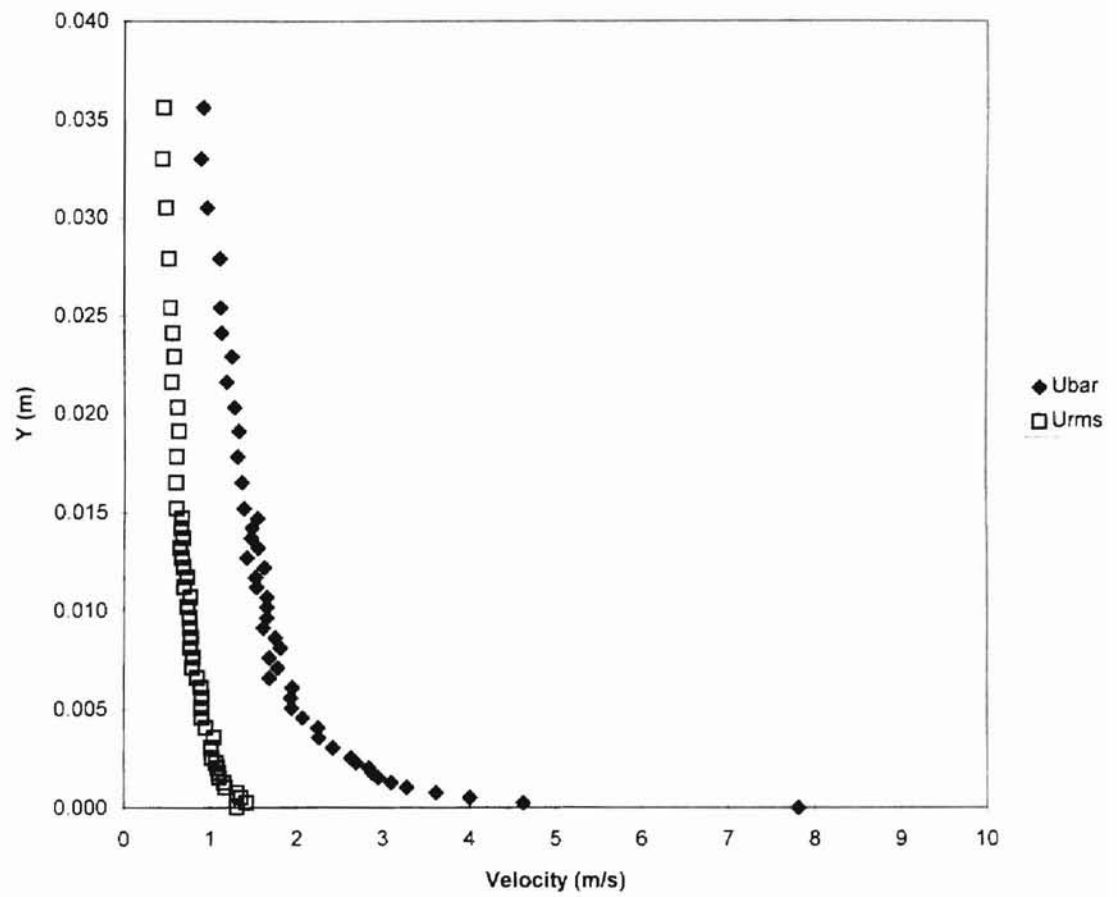
Appendix V, Table 3: Boundary Layer Data for Right Position

N	Y (in)	Y (m)	Ebar (volts)	Erms (volts)	Ubar (m/s)	Urms (m/s)	Turb. Int.	Uwall (m/s)	RPM	Ubar/Uwall	Urms/Uwall
1	0.00	0.00000	4.120	0.095	7.810	1.310	0.168	10.5	1970	0.7438	0.1248
2	0.01	0.00025	3.850	0.148	4.630	1.420	0.306	10.6	1990	0.4368	0.1340
3	0.02	0.00051	3.780	0.156	4.010	1.360	0.339	10.7	2010	0.3748	0.1271
4	0.03	0.00076	3.730	0.161	3.620	1.310	0.363	10.8	2020	0.3352	0.1213
5	0.04	0.00102	3.690	0.154	3.280	1.180	0.358	10.8	2030	0.3037	0.1093
6	0.05	0.00127	3.670	0.159	3.100	1.160	0.376	10.8	2040	0.2870	0.1074
7	0.06	0.00152	3.640	0.157	2.950	1.110	0.378	10.9	2040	0.2706	0.1018
8	0.07	0.00178	3.630	0.157	2.880	1.100	0.381	10.9	2050	0.2642	0.1009
9	0.08	0.00203	3.630	0.156	2.840	1.080	0.380	11.0	2060	0.2582	0.0982
10	0.09	0.00229	3.610	0.160	2.690	1.070	0.397	11.0	2060	0.2445	0.0973
11	0.10	0.00254	3.600	0.155	2.630	1.020	0.388	10.9	2060	0.2413	0.0936
12	0.12	0.00305	3.570	0.162	2.420	1.010	0.417	11.0	2060	0.2200	0.0918
13	0.14	0.00356	3.540	0.174	2.260	1.040	0.457	11.0	2070	0.2055	0.0945
14	0.16	0.00406	3.540	0.160	2.250	0.949	0.422	11.0	2070	0.2045	0.0863
15	0.18	0.00457	3.510	0.161	2.070	0.901	0.437	11.0	2070	0.1882	0.0819
16	0.20	0.00508	3.480	0.167	1.940	0.898	0.462	11.0	2070	0.1764	0.0816
17	0.22	0.00559	3.480	0.168	1.930	0.901	0.467	11.0	2070	0.1755	0.0819
18	0.24	0.00610	3.480	0.165	1.950	0.894	0.458	11.1	2080	0.1757	0.0805
19	0.26	0.00660	3.430	0.173	1.680	0.848	0.507	11.1	2080	0.1514	0.0764
20	0.28	0.00711	3.450	0.154	1.780	0.787	0.442	11.0	2080	0.1618	0.0715
21	0.30	0.00762	3.430	0.163	1.680	0.799	0.475	11.0	2070	0.1527	0.0726
22	0.32	0.00813	3.460	0.150	1.810	0.771	0.426	11.0	2080	0.1645	0.0701
23	0.34	0.00864	3.450	0.155	1.750	0.778	0.445	11.0	2080	0.1591	0.0707
24	0.36	0.00914	3.420	0.160	1.610	0.764	0.473	11.1	2080	0.1450	0.0688
25	0.38	0.00965	3.430	0.156	1.650	0.759	0.459	11.1	2080	0.1486	0.0684
26	0.40	0.01020	3.430	0.152	1.650	0.738	0.447	11.1	2080	0.1486	0.0665
27	0.42	0.01070	3.430	0.158	1.650	0.768	0.466	11.1	2080	0.1486	0.0692
28	0.44	0.01120	3.400	0.151	1.530	0.697	0.457	11.1	2080	0.1378	0.0628
29	0.46	0.01170	3.400	0.160	1.520	0.732	0.483	11.1	2080	0.1369	0.0659

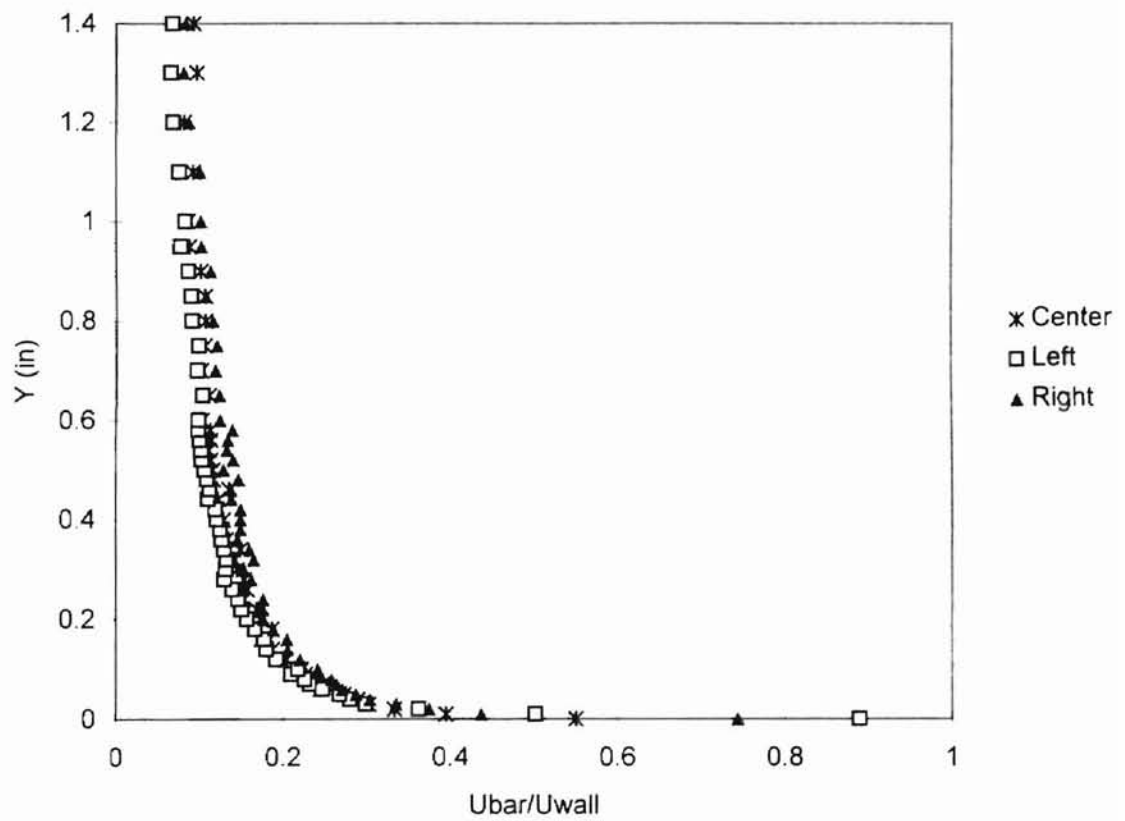
Appendix V, Table 3: Boundary Layer Data for Right Position

N	Y (in)	Y (m)	Ebar (volts)	Erms (volts)	Ubar (m/s)	Urms (m/s)	Turb. Int.	Uwall (m/s)	RPM	Ubar/Uwall	Urms/Uwall
30	0.48	0.01220	3.420	0.144	1.620	0.690	0.427	11.1	2090	0.1459	0.0622
31	0.50	0.01270	3.380	0.154	1.420	0.677	0.475	11.1	2080	0.1279	0.0610
32	0.52	0.01320	3.400	0.139	1.550	0.648	0.419	11.1	2090	0.1396	0.0584
33	0.54	0.01370	3.390	0.152	1.470	0.683	0.466	11.1	2090	0.1324	0.0615
34	0.56	0.01420	3.390	0.147	1.480	0.665	0.448	11.1	2090	0.1333	0.0599
35	0.58	0.01470	3.400	0.144	1.540	0.667	0.432	11.1	2090	0.1387	0.0601
36	0.60	0.01520	3.370	0.139	1.380	0.600	0.435	11.1	2080	0.1243	0.0541
37	0.65	0.01650	3.360	0.139	1.360	0.594	0.435	11.1	2080	0.1225	0.0535
38	0.70	0.01780	3.350	0.144	1.310	0.601	0.458	11.1	2090	0.1180	0.0541
39	0.75	0.01910	3.360	0.149	1.330	0.630	0.474	11.1	2080	0.1198	0.0568
40	0.80	0.02030	3.340	0.150	1.280	0.617	0.482	11.1	2090	0.1153	0.0556
41	0.85	0.02160	3.320	0.141	1.190	0.552	0.465	11.1	2080	0.1072	0.0497
42	0.90	0.02290	3.340	0.142	1.250	0.575	0.459	11.1	2090	0.1126	0.0518
43	0.95	0.02410	3.310	0.148	1.130	0.564	0.498	11.1	2090	0.1018	0.0508
44	1.00	0.02540	3.300	0.142	1.120	0.538	0.481	11.1	2090	0.1009	0.0485
45	1.10	0.02790	3.300	0.138	1.110	0.517	0.467	11.1	2090	0.1000	0.0466
46	1.20	0.03050	3.260	0.141	0.965	0.483	0.500	11.1	2080	0.0869	0.0435
47	1.30	0.03300	3.240	0.135	0.895	0.442	0.494	11.1	2080	0.0806	0.0398
48	1.40	0.03560	3.250	0.138	0.921	0.459	0.498	11.1	2080	0.0830	0.0414

Appendix V, Figure 3: Velocity Profiles for Right Position



Appendix V, Figure 4: Velocity Profiles over Width of Roller



VITA

William Gary Dewar

Candidate for the Degree of

Master of Science

Thesis: BOUNDARY LAYER DEVELOPMENT BEHIND A DOCTOR BLADE
RESTING ON THE SURFACE OF A CYLINDER ROTATING IN
STILL AIR

Major Field: Mechanical Engineering

Biographical:

Education: Received Bachelor of Engineering degree in Aerospace
Engineering from the University of Glasgow, Glasgow, Scotland in
July 1994.

Completed the requirements for the Master of Science Degree with
a major in Mechanical & Aerospace Engineering at Oklahoma
State University in May 1996.

Professional Memberships: Royal Aeronautical Society.